An Enhanced Multicarrier Modulation System for Mobile Communications

Mohammed AL-Attraqchi

Newcastle University

Newcastle upon Tyne, U.K.

A thesis submitted for the degree of

Doctor of Philosophy

October 2012

To my beloved ones… Thank you for being there for me all the time, I would have never succeeded without your support.

Thank you

Acknowledgment

Without any doubt, I would not be able to achieve this research project without the help and the support of many people, so it would be selfish not to acknowledge them and their efforts. First, I would like to express my sincere gratitude to my first supervisor Prof. Said Boussakta who accepted me as his Ph.D. student. Without his constant encouragement, patience, and immense knowledge, I would not have been able to complete this project. I would like to thank my second supervisor Dr. Stephane Le Goff, from him I learnt many things, and his support was greatly needed and deeply appreciated. It is a pleasure to thank the lovely postgraduate research coordinator, Mrs. Gill Webber, and the school receptionist, Mrs. Deborah Alexander, for their assistance in numerous ways. I thank the staff and the technical team of the School of Electrical and Electronics Engineering and Newcastle University for their aids and their role in developing my skills.

I would like to acknowledge the financial support of Ministry of Higher Education and Scientific Research (MOHSR) of Iraq through their scholarship. I offer my regards and blessings to all those who supported me in any respect during the completion of the project; I would especially like to all my friend, their friendship and company made life enjoyable at the university.

I would also like to show my gratitude to my precious wife who I cannot find enough words to express my appreciation for what she has done to support and help me during this long journey.

Finally, to my parents who dedicate their lives to protect, encourage, advice, and support me throughout my life, I would like to thank you from the bottom of my heart, without you, I would not be the person who I am now. I thank the mighty God for all the positive things that have happened to me in my life.

Abstract

The recent revolution in mobile communications and the increased demand on more efficient transmission systems influence the research to enhance and invent new modulation techniques. Orthogonal frequency division multiplexing with offset quadrature amplitude modulation (OFDM/OQAM) is one of the multicarrier modulations techniques that overcomes some of the weaknesses of the conventional OFDM in term of bandwidth and power efficiencies. This thesis presents a novel multicarrier modulation scheme with improved performance in mobile communications context.

Initially, the theoretical principles behind OFDM and OFDM/OQAM are discussed and the advantages of OFDM/OQAM over OFDM are highlighted. The time-frequency localization of pulse shapes is examined over different types of pulses. The effect of the localization and the pulse choice on OFDM/OQAM performance is demonstrated.

The first contribution is introducing a new variant of multicarrier modulation system based on the integration of the Walsh-Hadamard transform with the OFDM/OQAM modulator. The full analytical transmission model of the system is derived over flat fading and frequency selective channels. Next, because of the critical requirement of low implementation complexity in mobile systems, a new fast algorithm transform is developed to reduce the implementation complexity of the system. The introduced fast algorithm has demonstrated a remarkable 60 percent decrease in the hardware requirement compared to the cascaded configuration.

Although, the problem of high peak to average power ratio (PAPR) is one of the main drawbacks that associated with most multicarrier modulation techniques, the new system achieved lower values compared to the conventional systems. Subsequently, three new algorithms to reduce PAPR named Walsh overlapped selective mapping (WOSLM) for a high PAPR reduction, simplified selective mapping (SSLM) for a very low implementation complexity and Walsh partial transmit sequence (WPTS), are developed.

Finally, in order to assess the reliability of the presented system in this thesis at imperfect environments, the performance of the system is investigated in the presence

of high power amplifier, channel estimation errors, and carrier frequency offset (CFO). Two channel estimations algorithms named enhanced pair of pilots (EPOP) and averaged enhanced pair of pilots (AEPOP), and one CFO estimator technique called frequency domain (FD) CFO estimator, are suggested to provide reliable performance.

Contents

List of Figures

List of Tables

Nomenclature

1G	First Generation
2G	Second Generation
3G	Third Generation
4G	Forth Generation
Ac	Autocorrelation
ADSL	Asymmetric Digital Subscriber Line
AEPOP	Averaged Enhanced Pair of Pilots
AM/AM	Amplitude/Amplitude Conversion
AM/PM	Amplitude/Phase Conversion
AWGN	Additive White Gaussian Noise
BER	Bit Error Rate
BLT	Balian-Low Theorem
BPSK	Binary Phase Shift Keying
B-QAM	B-order Quadrature Amplitude Modulation
C2R	Complex to Real
CCDF	Complementary Cumulative Distribution Function
CE	Channel Estimation
CFO	Carrier Frequency Offset
CIR	Channel Impulse Response
CP	Cyclic Prefix
CP-OFDM	Orthogonal Frequency Division Multiplexing with Cyclic Prefix
DFT	Discrete Fourier Transform
EGF	Enhanced Gaussian Function
EPOP	Enhanced Pair of Pilots
EQ	Equalizer
FD	Frequency Domain
FDM	Frequency Division Multiplexing
FFT	Fast Fourier Transform

FMT	Filtered Multitone
FPGA	Field Programmable Gate Array
HPA	High Power Amplifier
IAM	Interference Approximation Method
IBO	Input Back-Off
ICI	Inter-Carrier Interference
IDFT	Inverse Discrete Fourier Transform
IFFT	Inverse Fast Fourier Transform
IOTA	Isotopic Orthogonal Transform Algorithm
ISI	Inter-Symbol Interference
ITU	International Telecommunication Union
LS	Least Square
LTE	Long Term Evolution
MC-CDMA	Multicarrier Coded Division Multiple Access
MCM	Multicarrier Modulation
MDFT	Modified Discrete Fourier Transform Filterbank
MIA	Minimized Interference Algorithm
MIMO	Multiple-Input Multiple-Output
ML	Maximum Likelihood
MMSE	Minimum Mean Square Error
NPR	Nearly Perfect Reconstruction
OFDM	Orthogonal Frequency Division Multiplexing
OFDMA	Orthogonal Frequency Division Multiple Access
OQAM	Offset Quadrature Amplitude Modulation
OSLM	Overlapped Selective Mapping
PAPR	Peak to Average Power Ratio
PM	Phase Mapping
POP	Pair of Pilots
PPN	Polyphase Network
PR	Perfect Reconstruction
PSD	Power Spectral Density

PSK	Phase Shift Keying
PTS	Partial Transmit Sequence
R2C	Real to Complex
RMSE	Root Mean Square Error
RTG	Receive Time / Transition Gap
Rx	Receiver
SC-FDMA	Single Carrier Frequency Division Multiple Access
SLM	Selective Mapping
SRRC	Square Root Raised Cosine
SSLM	Simplified Selective Mapping
SSPA	Solid-State Power Amplifier
SUI	Stanford University Interim
TD	Time Domain
TF	Time Frequency
TFL	Time-Frequency Localisation Filter
TMUX	Transmultiplexer
TWT	Travelling Wave Tube
Tx	Transmitter
WHT	Walsh-Hadamard Transform
WiMAX	Worldwide Interoperability for Microwave Access
WLAN	Wireless Local Area Network
WOSLM	Walsh Overlapped Selective Mapping
WPTS	Walsh Partial Transmit Sequence
ZF	Zero Forcing

List of Symbols

M	Number of subcarriers
K	Overlapping factor
L	Prototype filter length
$g(t)$	Prototype pulse shape filter
$a_{m,n}$	Real data coefficient
m	Subcarrier index
n	Time or block index
$h(t)$	Channel impulse response
$H(f)$	Channel frequency response
$WH_{m,n}$	Walsh-Hadamard matrix element
$\mathbb{R}$	Real vector field
$\mathbb{C}$	Complex vector field
$\mathbb{Z}$	Integer vector field
$\langle \cdot, \cdot \rangle$	Vectors inner product
$\|\cdot\|$	Norm of a vector
$\ell^2(\mathbb{Z})$	Vector space of square summable sequences
$\mathcal{L}^2(\mathbb{R})$	Vector space of square integrable functions
$\mathcal{H}$	Hilbert vector space
ρ_G	Gabor system density or lattice size
ξ	Time-frequency localisation factor
m_2	Modified second moment in time
M_2	Modified second moment in frequency
$s[k]$	Discrete time-domain transmitted signal
$s(t)$	Continuous time-domain transmitted signal
$c_{m,n}$	Complex transmitted coefficient
$\hat{c}_{m,n}$	Complex estimated coefficient
F_o	Subcarrier spacing
T_o	Symbol duration

$\prod$	Rectangular pulse
$(\cdot)^*$	Complex conjugate operation
$\delta_{m,n}$	Kronecker delta $\left(\delta_{m,n} = 1 \; if \; m = n, othwise \; \delta_{m,n} = 0\right)$
$A_g(\tau, v)$	Ambiguity function of $g(t)$
$[\cdot]^H$	Hermitian transposition operation
$[\cdot]^T$	Transposition operation
L_{CP}	Cyclic prefix length
L_h	Length of the channel impulse response
mod	Modulo operation
$a_{m,n}$	Real transmitted coefficient
$\hat{a}_{m,n}$	Real estimated coefficient
$g_\lambda(t)$	Gaussian function
$Re\{\cdot\}$	Real part of a complex variable
Im$\{\cdot\}$	Imaginary part of a complex variable
WHT_M	Walsh-Hadamard matrix of order $M \times M$
$\boldsymbol{I}_M$	Identity matrix of order $M \times M$
$x_{i,n}$	Real coefficients at the input of WHT matrix
$\hat{x}_{i,n}$	Estimated real coefficients at the WHT matrix output
$\theta_{m,n}$	Phase mapping coefficient
$Tx(z)$	Synthesis filterbank
$Rx(z)$	Analysis filterbank
$\otimes$	Convolution operation
$E\{\cdot\}$	Expected value
τ_o	Delay factor between real OQAM symbols
h_d	Channel complex path gain
τ_d	Channel path delay
$r(t)$	Received signal
$y_{m,n}$	Subcarrier demodulated signal
η	Noise vector
I_{m_o,n_o}	Residual interference caused by the surrounding subcarriers
ψ_{m_o,n_o}	Equalized noise term

σ_x^2	Real symbol variance
SNR	Signal to noise ratio
$\mathcal{P}^{AWGN}$	Theoretical bit error rate over AWGN
$\mathcal{P}^{f-select}$	Theoretical bit error rate over frequency selective channel
$\emptyset$	Time dependant phase matrix
C_{Add}	Number of complex addition operations of V- transform
C_{Multi}	Number of complex multiplication operations of V-transform
R_{Add}	Number of real addition operations of V- transform
R_{Multi}	Number of real multiplication operations of V-transform
RTx_{Add}	Number of real additions for WHT/OQAM with V- transform
RTx_{Multi}	Number of real multiplications for WHT/OQAM with V-transform
DTx_{Add}	Number of real additions for WHT/OQAM in cascaded mode
DTx_{Multi}	Number of real multiplications for WHT/OQAM in cascaded mode
$PSD_s(f)$	Power spectral density of the signal s
$\mathcal{F}\{\cdot\}$	Fourier transform of a variable
ζ	PAPR threshold value
$G(A)$	Amplitude transfer function of the high power amplifier
Q	ratio between real and imaginary parts of a channel coefficient
$\lvert\cdot\rvert$	Absolute value of a complex variable
ε	Normalised carrier frequency offset
$\hat{\varepsilon}$	Estimated normalised carrier frequency offset

Chapter 1. Introduction

1.1. Mobile Communication Revolution

Mobile broadband is becoming a reality as people now can browse the internet, watch TV on the move, send and receive videos or music on their handheld devices wherever they go without the need to be in their office or at home. This bloom in mobile communication increases the demand on more efficient systems to cope with this growing industry, which is now part of everyone's life.

The story started back in 1946 with the invention of the first mobile phone. However, early 1980s is when mobile phones were first introduced for commercial use. The first generation (1G) of mobile phones was designed to work on analogue transmission technique. The capacity was limited and the phones were bulky and expensive and regarded as luxury items. Later on with the advances in digital communication, the second generation (2G) emerged mid 1990s. This generation was capable of transmitting digitally voice and data but with very limited rate. This accompanied with reduction of the cost, which made this service become widely popular. Data services ranged from text messaging to accessing email and basic browsing for the internet.

The third generation (3G) was deployed first in 2001 in Japan. It was designed to boast the data rate to support the requirement of wider range of applications. 3G can provide users with reliable voice, data, video calls, graphical and multimedia services regardless of their location in the network. Although 3G delivered incredible transformation to the way people think of the mobile devices capabilities, the fourth generation (4G) has already set off towards better experience and much higher data rate.

The fourth generation of mobile communications relies on multicarrier modulation technique (MCM) to deliver its reliable mobile broadband to everywhere. However, the standard for 4G is still under development and not matured enough. Therefore, different proposals have already been in practice such as the long-term evolution (LTE) and the world interoperability for microwave access (WiMAX). Both of these techniques depends on the orthogonal frequency division multiple access (OFDMA) which is a multiuser version of the orthogonal frequency division multiplexing (OFDM) as part of their systems.

The dependence on multicarrier modulation technique is originated from its capability, over single carrier system, to mitigate the influence of the multipath fading channels. This is accomplished by splitting a high symbol rate serial data stream into a large group of lower rate parallel streams as illustrated in Figure 1.1. The fading over each subcarrier can be considered as flat fading as demonstrated in Figure 1.2. Thus, it can be compensated at the receiver by simple one tap equalizer.

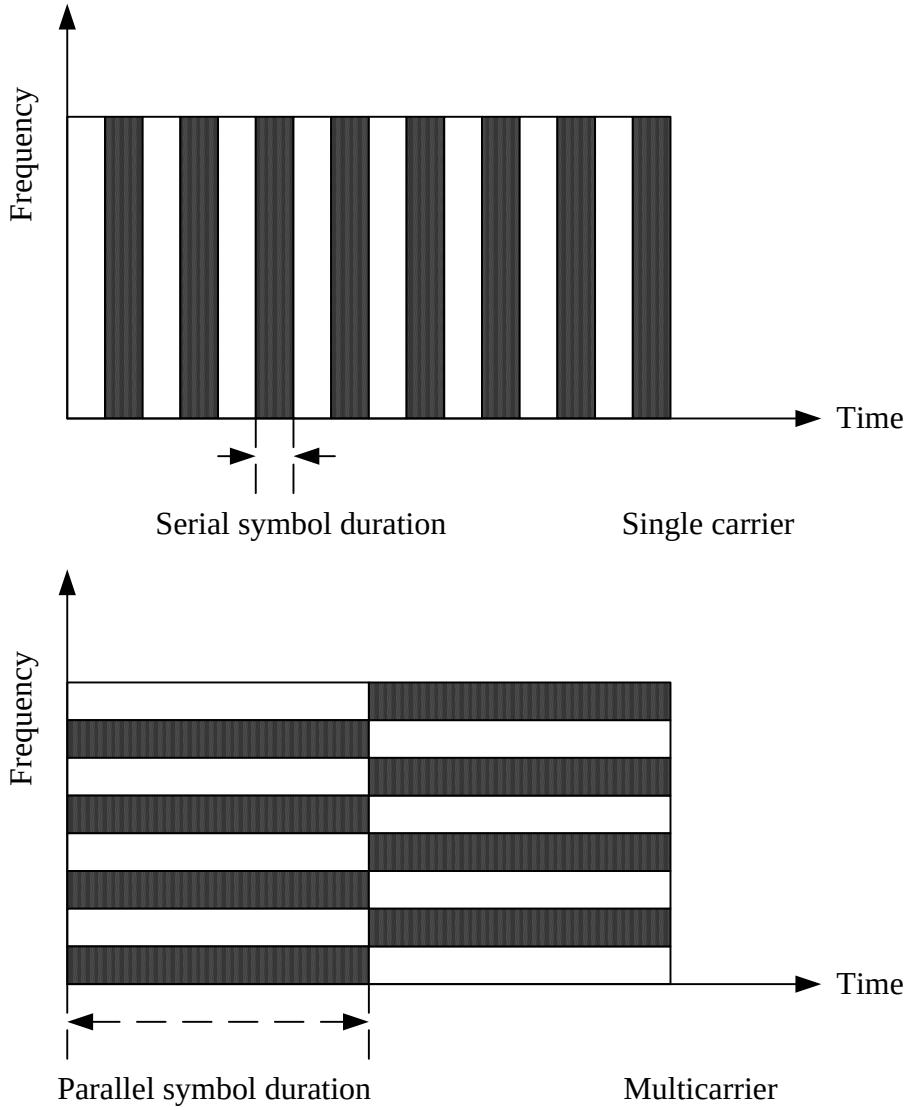

Figure 1.1 Multicarrier modulation concept

The flagship of multicarrier modulation technique is the OFDM system, which can be considered as the optimised version of the frequency division multiplexing (FDM). This system was initially proposed in mid 1960s, but the high complexity, at that time, to generate banks of sinusoidal generators and precise demodulators made it expensive and limited its success. At the early 1970s, the discrete Fourier transform (DFT) was

considered as an alternative to the sinusoidal generators banks. This was a step in the right direction to bring this system to the circle of interest and open the possibility of implementing it digitally. Now, this system is regarded as part of many standards for different applications over wired and wireless networks. For instance, it has been exploited for wired-broadband communication in the asymmetric digital subscriber lines (ADSL), and for the wireless local area networks (WLAN) under the IEEE standards 802.11 a / g / n.

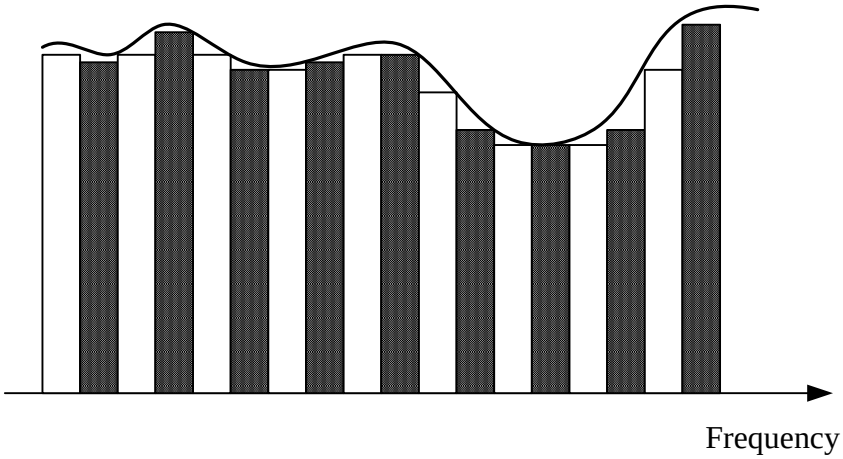

Figure 1.2 Nearly flat fading per subcarrier in MCM

Although OFDM system has better performance over frequency selective channels than single carrier transmission, it has some drawbacks such as:

- OFDM system requires an overhead of redundant data called cyclic prefix (CP) to be transmitted in order to combat the effect of multipath channels that produce inter-symbol interference (ISI). The cyclic prefix might cause a loss in the data throughput by 25% depending on the delay spread of the channel impulse response.
- OFDM suffers from high spectral leakage due to the low attenuation in the stopband. This is because OFDM employs rectangular pulses in time domain, which results in *sinc* pulses in frequency domain that have attenuation of only 13 dB at the first side lobe.
- OFDM signal envelop has large variations which might results in high peaks to the average power. High power amplifiers lack this wide dynamic range in their amplification characteristics, which might result in a clipping for the signals that exceed the saturation range of the amplifier.

On the other hand, an alternative multicarrier modulation system, known as OFDM with offset quadrature amplitude modulation (OFDM/OQAM), has some distinctive properties over the OFDM. This system is based on filterbanks for modulation and demodulation. This means the possibility to attain better frequency response and reduction in the spectral leakage. The other important facility of this system, is omitting the need for the CP. Therefore, OFDM/OQAM can benefit from 100% of the rate for data transmission. This thesis focuses on a variant of this system and its properties.

1.2. Aims and Contributions

This thesis aims to develop an alternative multicarrier modulator that have better performance over frequency selective channels and lower peak to average power ratio (PAPR). The new system should maintain the full bandwidth for data transmission plus the ability to cut the level of spectral leakage. The complexity of this novel system has to be minimized and the energy consumption needs to be kept to minimum so that it can suit mobile applications and hand-held devices. Then, the objective of this work is to evaluate the performance of the developed system and highlight strength and weakness points.

Therefore, this thesis presents a novel system featuring a combination of the OFDM/OQAM as modulator/demodulator and the Walsh-Hadamard transform (WHT) as data uniform distributor to create a novel system called WHT/OFDM/OQAM. The proposed system demonstrates significant improvement in bit error rate (BER) over multipath fading channels and reasonable reduction in PAPR. Besides that, the system benefits from filterbanks to attain higher containment for the spectrum. As with the OFDM/OQAM, this system does not require a redundant data like the OFDM, hence the full spectral efficiency is dedicated for the data transmission. The analytical model of the system is provided and the theoretic bit error rate is derived to provide closed from equations for different channel models.

In addition, the computational complexity of the proposed system is addressed. A new fast transform is developed and the computational complexity is derived and formulated. This transform offers a considerable reduction in the number of mathematical operations conducted for each transmitted symbol.

Moreover, the power spectral density (PSD) of the system is analysed and derived. The PSD of the WHT/OFDM/OQAM is compared, by means of computer simulations, with

different systems and different prototype filters to demonstrate the control attained over the spectrum.

WHT/OFDM/OQAM is a multicarrier modulation system, which means the system is affected by the PAPR issue. However, the analysis and computer simulations indicate a reasonable reduction in the PAPR value compared to its rivals. Three PAPR reduction algorithms based on state of art method are presented in this thesis. The Walsh overlapped selective mapping (WOSLM) offers a very high reduction in PAPR, while the simplified selective mapping (SSLM) proved less improvement in term of PAPR but it has very low implementation complexity. The Walsh partial transmit sequence (WPTS) has less improvement with moderate complexity level, so each method can be dedicated for certain purposes or application. Additionally, system performance is evaluated in the presence of high power amplifier (HPA) nonlinear distortion. The provided algorithms for PAPR reduction are combined with HPA to verify their efficiency.

Furthermore, two algorithms based on preamble pilots are presented for channel estimation. The enhanced pair of pilots (EPOP) is designed to limit the number of symbols incorporated in the estimation process while the averaged EPOP is considered for better accuracy.

Finally, the effect of carrier frequency offset (CFO) on the system performance is investigated. System sensitivity to the residual CFO is analysed and evaluated by computer simulations. A robust and simple approach to estimate CFO is proposed. The preamble algorithms are utilised for the estimation in the frequency domain.

In summary, the following points restate the contribution of this thesis:

1. A novel system is presented featuring high resilience to frequency selective channels, lower PAPR level, and elimination of CP.
2. Analytical model of the system with theoretical BER are provided.
3. New fast algorithm is developed to reduce the computational complexity.
4. PSD of the system is derived and evaluated.
5. Three different algorithms are presented to reduce PAPR levels.
6. High power amplifiers nonlinearity effect on the performance is demonstrated.
7. Two preamble pilots schemas are proposed for the channel estimation.

8. New CFO estimation technique is presented. The sensitivity of the system to the residual CFO is introduced.
9. All the proposed methods, derivations, and algorithms are verified by computer simulations.

1.3. Publications Arising From This Research

- M. Al-Attraqchi, S. Boussakta, and S. Le Goff, "An Enhanced OFDM/OQAM System Exploiting Walsh-Hadamard Transform," in *Vehicular Technology Conference (VTC Spring), 2011 IEEE 73rd*, 2011, pp. 1-5.

1.4. Thesis Outline

The thesis is organised as follows:

Chapter 2 provides some preliminaries and definitions. It also covers the basics of the OFDM system. Moreover, it demonstrates and explains the principles of OFDM/OQAM. In addition, it illustrates some of the prototype filters and their associated characteristics.

Chapter 3 which is the first main chapter in this thesis, presents some of the related work and the concepts of the WHT/OFDM/OQAM. The analytical model and the theoretical BER derivation are introduced. The evaluation of the system performance using computer simulation is also provided. Additionally, this chapter includes the fast algorithm development and the computational complexity formulation and calculations.

Chapter 4 begins with the analysis of PSD of the system accompanied with some examples. Then, PAPR of the WHT/OFDM/OQAM is introduced followed by PAPR reduction algorithms. Furthermore, the implications of HPA are demonstrated and corrected by the proposed algorithms.

Chapter 5 focuses on the channel and CFO estimations. It presents two preamble pilots schemas for channel estimation with their evaluations. Then, this chapter deals with the CFO effect on the performance of the system specifically for residual CFO case. In addition, the proposed CFO estimation method is demonstrated and evaluated.

Finally, conclusions are drawn in Chapter 6 and the thesis ends with a possible line of further work.

Chapter 2. Principles of OFDM/OQAM

2.1. Introduction

In multicarrier modulation (MCM) systems, the well-known technique is the OFDM. The simplicity of this technique for implementation and the ease of equalization made it quite popular and part of many of the current standards in wire and wireless communications. However, this technique requires sacrificing some of the transmission bandwidth for some redundant data named cyclic prefix (CP) to maintain orthogonality between subcarriers. This CP can cause a reduction of up to 25% of the transmission bandwidth over some channels that have long delay spread.

On the other hand, another multicarrier modulation technique based on filterbank seems to be the new candidate for the future communication known as OFDM/OQAM. This system can achieve 100% transmission bandwidth as it maintains the orthogonality between subcarriers without the necessity for the CP. This is because the system relies on well-localised pulses that can achieve Nyquist criteria[1] for ISI free transmission [1]. This improvement comes with a bonus of having higher attenuation in the stopband to cut the level of energy leak. The sacrifice in this case is the computational complexity compared with the OFDM.

This chapter aims to study the principles of multicarrier transmission exploiting OFDM and OFDM/OQAM. In addition, it aims to reveal the differences between these two techniques and the key points to allow the possibility of preserving the transmission bandwidth. Moreover, the prototype filters' specifications to attain Nyquist principle are also to be considered.

The outline of this chapter is as follows. Section 2.2 provides preliminaries and definitions of some fundamentals. In addition, Section 2.3 explains the principles of the OFDM system. Moreover, the OFDM/OQAM is presented in Section 2.4. Furthermore,

[1] Nyquist criterion for ISI avoidance: if the channel impulse response is denoted by $h(t)$, the condition for ISI free transmission can be expressed as

$$h(nT) = \begin{cases} 1 & for\ n = 0 \\ 0 & for\ n \neq 0 \end{cases}$$

for all integer *n*, with *T* is the symbol period. Letting $H(f)$ represent the Fourier transform of $h(t)$, then the preceding condition can be written equivalently as

$$\frac{1}{T}\sum_{k=-\infty}^{\infty} H\left(f - \frac{k}{T}\right) = 1$$

in another word, the frequency shifted replicas of $H(f)$ must add up to a constant value.

some of the well-localised prototype filters are demonstrated in Section 2.5. Finally, Section 2.6 provides conclusion and summary.

2.2. Preliminary

In this section, some of the important definitions and fundamental notations are presented. Further reading is possible at many references such as [2-4].

2.2.1. Vector spaces

The basic element that constructs any vector space is the vector, which can be defined as:

Definition 1. Vector

A vector is a group of *n* elements in the field of $\mathbb{Q}$ (examples of $\mathbb{Q}$: real $\mathbb{R}$ or complex $\mathbb{C}$ or integer $\mathbb{Z}$ fields) [2]:

$$x = [x_1, \dots x_i, \dots x_n] \tag{2.1}$$

These vectors can be associated with each other, as in Figure 2.1, to form a vector space that is defined as

Definition 2. Vector space

A vector space *V* is a set of vectors on the field of $\mathbb{Q}$ together with two operators (addition and scalar multiplication) defined over the elements of the set and satisfy certain properties for all vectors $x, y, z \in V$:

- Commutative law: $x + y = y + x \in V$
- Associative law: $(x + y) + z = x + (y + z)$
- Zero vector: there exists an element $0 \in V$ such that $x + 0 = x$
- Additive inverse: there exists an element $\tilde{x}$ such that $x + \tilde{x} = 0$

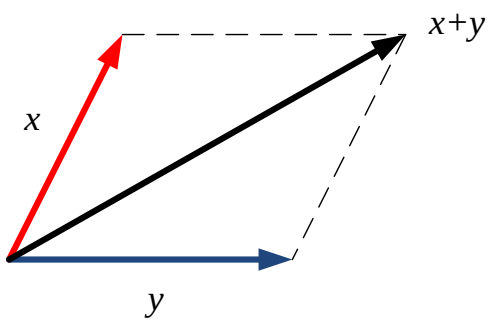

Figure 2.1 Vector space of the sum of two vectors

Another important definition for a relation that formulates the relationship between vectors known as the inner product, that can be defined as:

Definition 3. Inner product

An inner product (can be called dot product or scalar product) represents element by element multiplication between two vectors in the field of $\mathbb{Q}$ and the result being scalar. Given two vectors $x = [x_1, \dots, x_n]$ and $y = [y_1, \dots, y_n]$, the inner product is indicated by $\langle x, y \rangle$ which equals to [3-4]:

$$\langle x, y \rangle = \sum_{i=0}^{n-1} x_i \, y_i^* \tag{2.2}$$

with * represents the complex conjugate of the complex number. It has the following properties:

- $\langle x, y \rangle^* = \langle y, x \rangle$
- Bilinearity: $\langle \lambda x + \mu y, z \rangle = \lambda \langle x, z \rangle + \mu \langle y, z \rangle$
- Positive definitive: $\langle x, x \rangle > 0$ if $x \neq 0$

Any two vectors *x* and *y* is said to be orthogonal if $\langle x, y \rangle = 0$. In addition, the inner product provokes the norm of *x* noted $\|x\|$ such that:

$$\|x\|^2 = \langle x, x \rangle \tag{2.3}$$

Moreover, the inner product holds these properties over the vector space:

- Cauchy-Schwarz inequality

$$|\langle x, y \rangle| \leq \|x\| \|y\| \tag{2.4}$$

with equality if and only if $x = \alpha y$, where α is positive real constant.

- Triangle inequality

$$\|x + y\| \leq \|x\| + \|y\| \tag{2.5}$$

with equality if and only if $x = \alpha y$.

- Parallelogram law

$$\|x + y\|^2 + \|x - y\|^2 \leq 2(\|x\|^2 + \|y\|^2) \tag{2.6}$$

A sequence of vectors $\{x_n\}$ is known as Cauchy sequence in *V* if $\|x_n - x_m\| \to 0$, when $n, m \to \infty$. If all the Cauchy sequences in the space *V* converge to a vector in *V*, then *V*

is called complete. Furthermore, an inner product added to a vector space *V* is known as inner product space. This space is called Hilbert space if the inner product is complete.

In signal processing, the majority of sequences $x[n]$ to be dealt with have finite energy, with $x[n]$ is complex valued sequence and $n \in \mathbb{Z}$. This sequence can be considered as a vector in a space known as space of square summable sequences $\ell^2(\mathbb{Z})$, which is a Hilbert space. The inner product can be written as

$$\langle x, y \rangle = \sum_{n=-\infty}^{\infty} x^*[n]y[n] \tag{2.7}$$

At the same time, the real value of the above equation is defined as the Euclidian inner product:

$$\langle x, y \rangle = Re\left\{ \sum_{n=-\infty}^{\infty} x^*[n]y[n] \right\} \tag{2.8}$$

The Euclidian inner product and $\ell^2(\mathbb{Z})$ is considered as Hilbert space. The norm of both cases can be expressed as

$$\|x\| = \sqrt{\langle x, x \rangle} = \sqrt{\sum_{n=-\infty}^{\infty} |x[n]|^2} \tag{2.9}$$

Another frequently used space is called space of square integrable functions $\mathcal{L}^2(\mathbb{R})$, this is related to a function $f(t)$ defined over the field of $\mathbb{R}$ that can be in Hilbert space if the square of the magnitude $|f(t)|^2$ is integrable i.e.:

$$\sqrt{\int_{t\in\mathbb{R}} |f(t)|^2 dt} < \infty \tag{2.10}$$

The inner product on the space $\mathcal{L}^2(\mathbb{R})$ can be written as

$$\langle f, g \rangle = \int_{t\in\mathbb{R}} f^*(t)g(t)dt \tag{2.11}$$

Equally, taking the real value of (2.11):

$$\langle f, g \rangle = Re\left\{ \int_{t\in\mathbb{R}} f^*(t)g(t)dt \right\} \tag{2.12}$$

is defined as the Euclidian inner product and by combining it with $\mathcal{L}^2(\mathbb{R})$ the result is also Hilbert space. For both cases, the norm equals to

$$\|f\| = \sqrt{\langle f, f \rangle} = \sqrt{\int_{t \in \mathbb{R}} |f(t)|^2 dt} \tag{2.13}$$

2.2.2. Bases and frames

Definition 4. Basis

Let $\mathcal{H}$ denotes a separable Hilbert space such as $\mathcal{L}^2(\mathbb{R})$ a companied with inner product $\langle f, g \rangle$ and norm $\|f\| = \sqrt{\langle f, f \rangle}$. A sequence $\{e_n\}$ with $n \in \mathbb{Z}$ is a basis for $\mathcal{H}$ if there exists unique scalar c_n dependant on f for all $f \in \mathcal{H}$ such that

$$f = \sum c_n e_n \tag{2.14}$$

If the series expansion is converged to f in the norm irrelevant to the order of the sequence $\{e_n\}$, then the basis is called unconditional [3].

Definition 5. Orthonormal basis

A basis $\{e_n\} \subseteq \mathcal{H}$ is an orthonormal basis if and only if:

- $\langle e_n e_m \rangle = \delta_{n,m}$ with $\delta_{n,m}$ represents Kronecker delta ($\delta_{m,n} = 1 \; if \; m = n$, otherwise $\delta_{m,n} = 0$).
- For all $f \in \mathcal{H}, f = \sum_{n \in \mathbb{Z}} \langle f, e_n \rangle e_n$
- Parseval's equality: for all $f \in \mathcal{H}, \|f\|^2 = \sum_{n \in \mathbb{Z}} |\langle f, e_n \rangle|^2$

In the consideration of Hilbert space $\mathcal{H}$, an orthonormal basis is similar to a Hilbertian basis.

Definition 6. Riesz basis

A basis $\{f_n\}$ is described as Riesz basis, if a biorthogonal family $\{\check{f}_n\}$ exists satisfying $\langle f_k \check{f}_n \rangle = \delta_{k,n}$ that produces ℓ^2 coefficients $c_n = \langle f, \check{f}_n \rangle \; \forall f \in \mathcal{H}$.

Definition 7. Frame

A sequence $\{f_n\}$ in $\mathcal{H}$ is a frame for $\mathcal{H}$ if there exist constants $0 < A \leq B < +\infty$ such that $\forall f \in \mathcal{H}$

$$A\|f\|^2 \leq \sum_n \|\langle f, f_n \rangle\|^2 \leq B\|f\|^2 \tag{2.15}$$

The constants *A* and *B* are defined as the frame bounds. The frame is described as tight if *A*=*B*, and it is called exact if it is not a frame anymore, this is when any one of its elements is removed. Bessel sequence is a sequence that satisfies the upper frame bound (which may or may not satisfy the lower frame bound) [3, 5].

If the frame bounding constants are equal to 1, then the frame is an orthonormal basis and an orthonormal basis must be a tight frame. In addition, any Riesz basis for $\mathcal{H}$ is considered a frame, in contrast, a frame is a Riesz basis if and only if it is exact. Moreover, if $\{f_n\}$ in $\mathcal{H}$ represents a frame, then there exists a dual frame $\{\check{f}_n\}$ $\forall f \in \mathcal{H}$ with 1/*B* and 1/*A* are the frame bounds, such that

$$f = \sum_n \langle f, f_n \rangle \check{f}_n = \sum_n \langle f, \check{f}_n \rangle f_n \tag{2.16}$$

Furthermore, in every frame $\{f_n\}$ in $\mathcal{H}$ there exists a sequence of square summable coefficients c_n, which provides an arbitrary elements $f \in \mathcal{H}$ formed in a series so that $f = \sum_n c_n f_n$. If the frame is not exact then these coefficients are not unique. However, it is always possible to find a computable sequence.

2.2.3. Gabor systems, Gabor frames and density

In 1946, Dennis Gabor introduced a method to express one-dimensional signal in two-dimensional representation, with time and frequency as co-ordinates [6]. He called this two-dimensional interpretation as information diagram, as this diagram area is proportional to the number of independent data that can be conveyed. He focused in his research on how to represent the information of a signal $g(t)$ by a finite number of data as good as possible. Gabor proposed utilizing a series of elementary functions $\{g_{m,n}\}$ that are formulated from a single building block by translation and modulation to represent a function g.

Definition 8. Gabor system

Given $g \in \mathcal{L}^2(\mathbb{R})$ and fixed $T_o, F_o > 0$, the Gabor system corresponding to g, T_o and F_o verifies for all $t \in \mathbb{R}$

$$g_{m,n}(t) = g(t - nT_o)e^{j2\pi mF_o t} \tag{2.17}$$

where the function g is called a prototype function, and the functions $g_{m,n}$ are the resulting functions of the prototype function translations with parameters T_o and F_o.

Gabor system is sometimes called as Weyl-Heisenberg system. Gabor frame is a Gabor system that constructs a frame for $\mathcal{L}^2(\mathbb{R})$. The density, or sometimes called lattice size, of Gabor system is defined as $\rho_G = \frac{1}{T_o F_o}$. A Gabor system $\{g_{m,n}\}_{m,n \in \mathbb{Z}}$ is said to be

frame only when $\rho_G \geq 1$, and it will be an exact frame when $\rho_G = 1$, and it turn to be incomplete if $\rho_G < 1$ [7-10].

2.2.4. Gabor system and Balian-Low theorem

The Balian-Low theorem (BLT) is a key result in time-frequency analysis. it was originally stated by Balian [11] and, then independently, by Low [12].

Theorem 1. If a Gabor system $\{g_{m,n}\}_{m,n \in \mathbb{Z}}$ with density $\rho_G = 1$ forms an orthonormal basis for $\mathcal{L}^2(\mathbb{R})$ then

$$\left(\int_{-\infty}^{\infty} |tg(t)|^2 dt\right)\left(\int_{-\infty}^{\infty} |\gamma \hat{g}(\gamma)|^2 d\gamma\right) = +\infty \tag{2.18}$$

where $\hat{g}(\gamma) = \int_{-\infty}^{\infty} g(t)e^{-j2\pi\gamma t}dt$ is the Fourier transform of g.

The BLT was extended later from orthonormal bases to exact frames [7, 13-14]. BLT gives the relation between Gabor density and signal localisation as

- $\rho_G > 1$: Frames with excellent time-frequency localisation properties exist (a particular example; a frame with g as Gaussian function with appropriate density).
- $\rho_G = 1$: Frames and orthonormal bases are possible, but without good time-frequency localisation.
- $\rho_G < 1$: Gabor system is incomplete.

Gabor systems can be utilised in many practical signal-processing techniques to decompose and reconstruct signals. For example, sub-band coding, or signal synthesis followed by signal analysis as in a transmission system. In the first example, Gabor frame is required to reconstruct the signal perfectly so the density has to be $\rho_G \geq 1$. In the second one, in order to recover the transmitted information, the Gabor set $\{g_{m,n}\}$ has to satisfy a linear independence condition, i.e. corresponds to Riesz bases with $\rho_G \leq 1$.

Consequently, for the purpose of multicarrier modulation, there are three distinctive cases [15]:

- Under-critical time-frequency lattice grid ($TF > 1$): Incomplete Riesz bases exist with well-localised prototypes' functions.
- Critical time-frequency lattice grid ($TF = 1$): Complete Gabor bases exist but they are associated with bad time-frequency localisation.

- Over-critical time-frequency lattice grid ($TF < 1$): Riesz bases do not exist and if frames with well-localised prototypes may exist, they do not permit to recover the information from the received signal.

2.2.5. Time-Frequency localisation

The localisation of a signal in the time-frequency plane or phase space represents the distribution of the signal energy in that space. This localisation feature can be utilised as a measurement to distinguish between different signals based on how well their energy are centred at the origin of the phase space. Signals that are well localised in time and frequency, have higher resistance against ISI and ICI [15-16]. Therefore, this parameter is important in the quest for the best shape for the signal to attain highest efficiency.

A measure of the time-frequency localisation for a discrete time sequence $x[n]$ is given by [17-18]:

$$\xi = \frac{1}{4\pi\sqrt{m_2 M_2}} \tag{2.19}$$

where m_2 is the modified second moment in time and can be expressed as

$$m_2(x) = \frac{1}{\|x\|^2} \sum_{n=-\infty}^{\infty} \left(n - \frac{1}{2} - T(x)\right)^2 \left|\frac{x[n] + x[n-1]e^{j2\pi F(x)}}{2}\right|^2 \tag{2.20}$$

and M_2 is the modified second moment in frequency which can be written as

$$M_2(x) = \frac{1}{(2\pi)^2\|x\|^2} \sum_{n=-\infty}^{\infty} \left|x[n] - x[n-1]e^{j2\pi F(x)}\right|^2 \tag{2.21}$$

where $F(x)$ is the gravity centre in frequency as follows:

$$F(x) = \frac{1}{2\pi} \frac{Im\{\sum_{n=-\infty}^{\infty} x[n]x^*[n-1]\}}{Re\{\sum_{n=-\infty}^{\infty} x[n]x^*[n-1]\}} \qquad \left(mod\ \frac{1}{2}\right) \tag{2.22}$$

with *mod* stand for the modulo operation. While $T(x)$ is the gravity centre in time that is described by

$$T(x) = \frac{\sum_{n=-\infty}^{\infty} \left(n - \frac{1}{2}\right) \left|\frac{x[n] + x[n-1]e^{j2\pi F(x)}}{2}\right|^2}{\sum_{n=-\infty}^{\infty} \left|\frac{x[n] + x[n-1]e^{j2\pi F(x)}}{2}\right|^2} \tag{2.23}$$

Theorem 2. The time-frequency localisation of a discrete time signal is bounded in $0 \leq \xi \leq 1$ with optimum value equals to 1.

This important factor will be recalled back later in this chapter.

2.2.6. Gabor theory and MCM systems

The Balian-LOW theorem revealed an important fact for the MCM systems, in which a compromise between the localisation and the maximum spectral efficiency is inevitable, and it is impossible to have both orthogonality and good localisation in a critically sampled Gabor system. Consequently, to attain maximum spectral efficiency, *TF* must equal to one (*TF*=1) so the system operates in the critical sampling, hence, it is impossible to utilise well-localised pulses. The resulting system is sensitive to the dispersion in transmission channel. By sacrificing the transmission efficiency and permitting the system to work below critical sampling, *TF* can take any value more than one, such as *TF*=2. The system gains the possibility to employ well-localised pulses that can suppress the effect of the channel easily. The former approach is chosen for the standard OFDM system, while the later one is considered for the filtered multitone (FMT) systems [15, 19].

OFDM system is a basic member of the Gabor systems and it dated back to 1966 by Chang [20]. It has been studied thoroughly and evolved over the past decades as result of its desirable properties [21-22]. In OFDM, square pulses are utilised as the transmission signals and these pulses have bad localisation in time and frequency. This system succeed to maintain the orthogonality over distortionless channels, however it suffers from loss of orthogonality over dispersive channels that produce ISI and ICI. In order to counteract channel interference [23] suggested, then acknowledged by [24], employing guard time that is governed by the delay spread of the channel. This can be achieved by appending some redundancy to the transmitted signal such as a duplication part of the OFDM symbol and it is called cyclic prefix (CP). Thus, CP is capable of eliminating ISI and ICI effects resulting from channel desperation. The CP redundancy is the compromise in the transmission efficiency to restore the orthogonality. The efficient implementation of the OFDM system via IFFT/FFT blocks came to practice since 1971 [23].

FMT systems relax the Gabor density by utilizing under critical time-frequency sampling (TF >1) to gain more freedom in the employment of well-localised pulses. The price, again, is the spectral efficiency. Since this thesis focuses only on the critical time-frequency lattice grid (TF=1), FMT is out of the thesis scope. For the interested readers in this topic, they can refer to the related reference such as [4, 19, 25-27].

On the other hand, another MCM system that is based on Gabor system, the so-called OFDM/OQAM, or for short OQAM, was firstly proposed by Saltzberg in 1967 [28] in which he extended the work of Chang [20]. Later on, Hirosaki [29] submitted further enhancements to the OQAM by introducing the DFT to the modulation of the system. Although the simplified implementation of the transmultiplexer based on the polyphase network and DFT has already been proposed in [30], the concept took a while to be applied to the OQAM to attain an efficient implementation [18].

OQAM system depends on critical sampling in Gabor system to achieve maximum spectral efficiency besides having well-localised pulses in time and frequency to eliminate ISI and ICI distortions. At first, this system seems to contradict with the Balian-Low theorem of having critical sampling beside well-localised pulses. The key idea behind that is the relaxation of the orthogonality condition from complex-valued field to real-valued field. This opens the possibility to employ pulses with Nyquist characteristics and maintain the full spectral efficiency. In the forthcoming sections, more details of how OQAM works are demonstrated.

2.3. OFDM Modulation

Orthogonal frequency division multiplexing is a very popular modulation technique because of two main advantages: the efficient implementation by IFFT/FFT blocks and the simple equalization stage at the receiver. In this section, the modulator of the OFDM is firstly presented, and then the properties of the rectangular pulse are reviewed. Finally, the efficient implementation is overviewed.

2.3.1. OFDM modulator and demodulator

In OFDM, a block of M complex data coefficients is transmitted over M parallel subcarriers via M modulation filters, as illustrated in Figure 2.2. This structure is a typical filterbank in a transmultiplexer (TMUX) arrangement in which a synthesis filterbank $Tx(z)$ followed by analysis filterbank $Rx(z)$. The complex data coefficients $c_{m,n}$ are generated by a mapping block (not shown in the figure) such as PSK or QAM, with $m = 0,1, \dots, M-1$ indicates the subcarrier index and n stands for the time index.

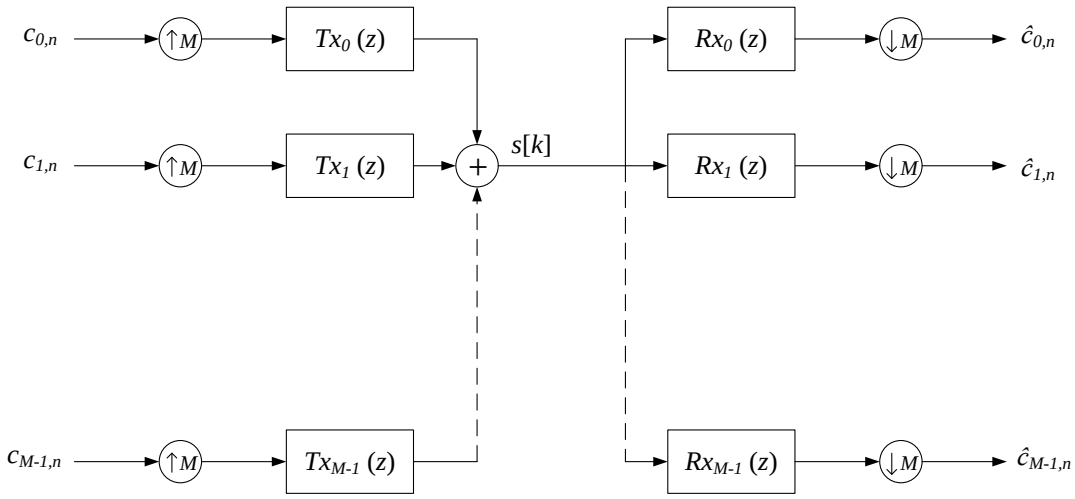

Figure 2.2 Block diagram of the OFDM system

The discrete baseband transmitted signal $s[k]$, which represents the sum of all the transmitter filters, can be expressed as the following [4, 19, 31-33]:

$$s[k] = \frac{1}{\sqrt{M}} \sum_{m=0}^{M-1} \sum_{n=-\infty}^{\infty} c_{m,n} \prod [k - nT_o] e^{j2\pi m F_o \left(k - \frac{D}{2}\right)} \tag{2.24}$$

with F_o is the subcarrier spacing that equals to $F_o = {}^{1}/_{M}$. T_o is the symbol duration with $T_o = M$. D is the required delay to maintain the causality of the system with $D = M - 1$. The number of subcarriers M is assumed an even number. The transmitter employs rectangular filter indicated by $\prod$ with length equals to M and can be defined as

$$\prod[k] = \begin{cases} 1 & k \in \left[-\frac{M}{2}, \frac{M}{2}\right] \\ 0 & otherwise \end{cases} \tag{2.25}$$

By comparing equation (2.24) with (2.17), it is easy to find the similarity between the two equations. In fact, the filterbank function represents Gabor function in which it performs modulation in frequency and translation in time, so the basis function can be written as

$$\prod_{m,n}[k] = \frac{1}{\sqrt{M}} \prod [k - nT_o] e^{j2\pi m F_o \left(k - \frac{D}{2}\right)} \tag{2.26}$$

Consequently, the orthonormal basis can be constructed from the basis function to produce:

$$\langle \prod_{m,n}, \prod_{p,q} \rangle = \sum_{k \in \mathbb{Z}} \prod_{m,n}[k] \prod_{p,q}^{*}[k] = \delta_{m,p} \delta_{n,q} \tag{2.27}$$

The last equality is also known as the orthogonality condition. In the following section, the implications of utilizing the rectangular pulse are discussed.

2.3.2. Rectangular pulses

OFDM system employs basic pulse shaping in the modulation, which is the rectangular pulse. Rectangular pulses have sharp edges in the time domain that cause long trails in the frequency domain, which can have bad implications on the neighbouring subcarriers. The *sin* (*x*)/*x* frequency response also leads to lower attenuation in the side lobes with only 13 dB for the first side lobe as demonstrated in Figure 2.3.

As stated in the Balian-Low theorem, for the critical Gabor system, no basis function that can exist has orthogonality and good localisation in time and frequency simultaneously. Therefore, to investigate the localisation of rectangular pulse, the localisation factor ξ is calculated to confirm the theorem with $\xi = 0.1549$ which is far below the optimal value of one.

To grasp thorough understanding of the energy distribution in the time-frequency plane (phase plane), the ambiguity function can be used here [16, 34]. The ambiguity function can be described as the Fourier transform of the instantaneous autocorrelation function of the signal along the time axis *t*, which can be expressed as

$$A_g(\tau, v) = \int_{-\infty}^{\infty} g\left(t + \frac{\tau}{2}\right) g^*\left(t - \frac{\tau}{2}\right) e^{j2\pi v t} dt \tag{2.28}$$

If the prototype function has unity energy i.e. normalised, then the maximum value for the ambiguity function is one: $max\left(A_g(\tau, v)\right) = A_g(0,0) = 1$. The ambiguity function of the rectangular pulse is demonstrated in Figure 2.4 in which $T_o = M = 16$. It can be noticed from the ambiguity function plot that the energy of the rectangular pulse extends in the frequency domain more than the time domain. This wide spread in the frequency domain makes the system with these pulses more sensitive to frequency selective channels and narrowband noise. As a result, the OFDM system is sensitive to ICI and narrowband noise.

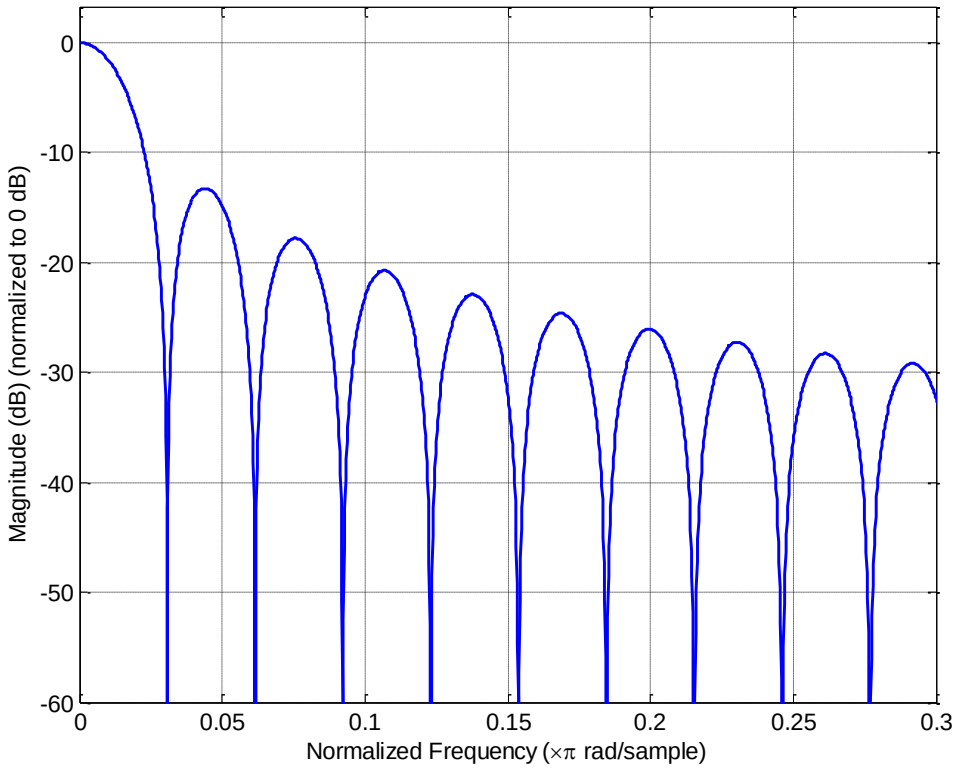

Figure 2.3 Frequency response of the rectangular pulse

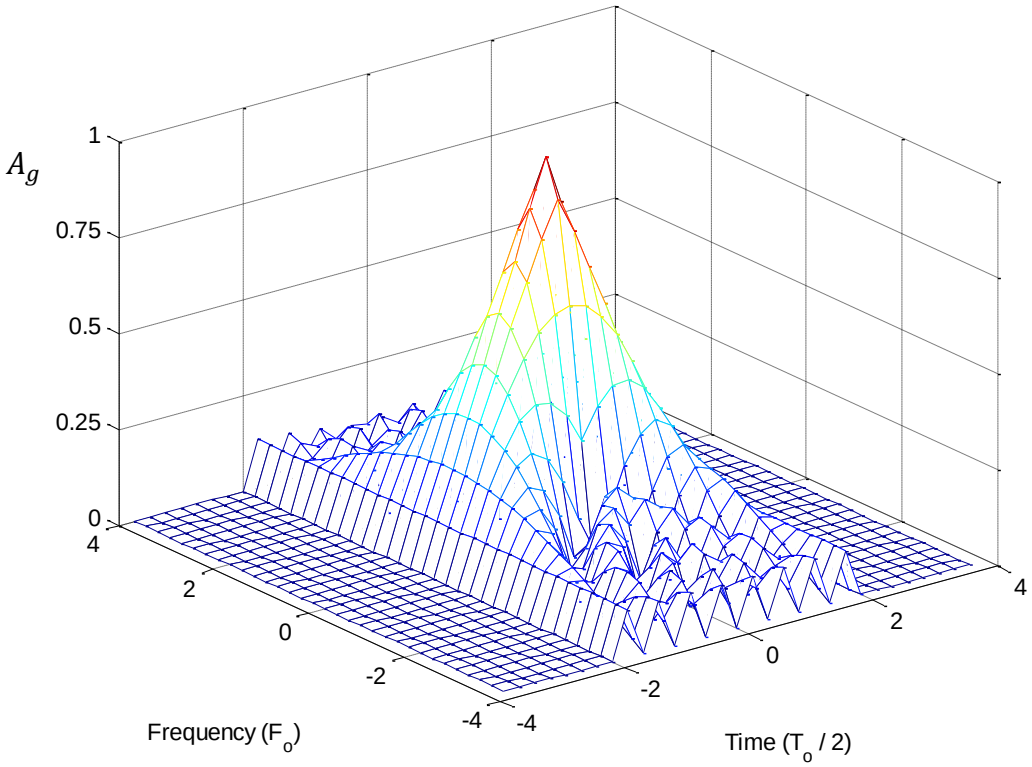

Figure 2.4 Ambiguity function of the rectangular pulse

2.3.3. OFDM efficient implementation

For large number of subcarriers M, the direct implementation of the OFDM system as illustrated in Figure 2.2 would require high computational complexity because all the filtering processes are performed at high rate of $\frac{M}{T_o}$. The efficient implementation of the OFDM is dated back to 1971 [23] which benefited from the Cooley-Tukey fast algorithm for calculating the discrete Fourier transform (DFT) which is known as fast Fourier transform (FFT) [35]. The system then is constructed of inverse FFT (IFFT) block at the transmitter and FFT block at the receiver as depicted in Figure 2.5.

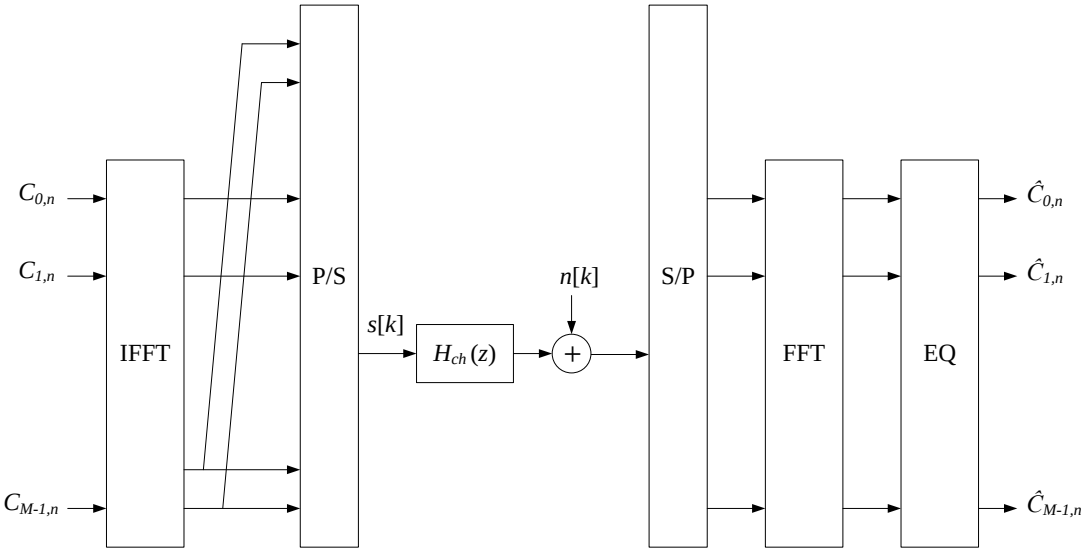

Figure 2.5 OFDM efficient implementation block diagram

To combat ISI and ICI resulting for the transmission over realistic channels, the CP is introduced. The CP is an extension to the OFDM symbol created by inserting a duplicated section of the end part of the symbol right at the start of the symbol. This will increase the duration of the symbol to become T_s as demonstrated in Figure 2.6. The length of the CP is supposed to be longer than the channel impulse response (CIR) length.

2.3.4. OFDM mathematical model

The *n*-th block of complex data coefficients $\boldsymbol{c}_n = \left[c_{0,n}, c_{1,n}, \dots, c_{M-1,n}\right]^T$ ($[\cdot]^T$ indicates a transpose operation) is firstly processed by the IDFT to produce the time domain vector as [33]

$$\boldsymbol{s}_n = \boldsymbol{F}^H \boldsymbol{c}_n \tag{2.29}$$

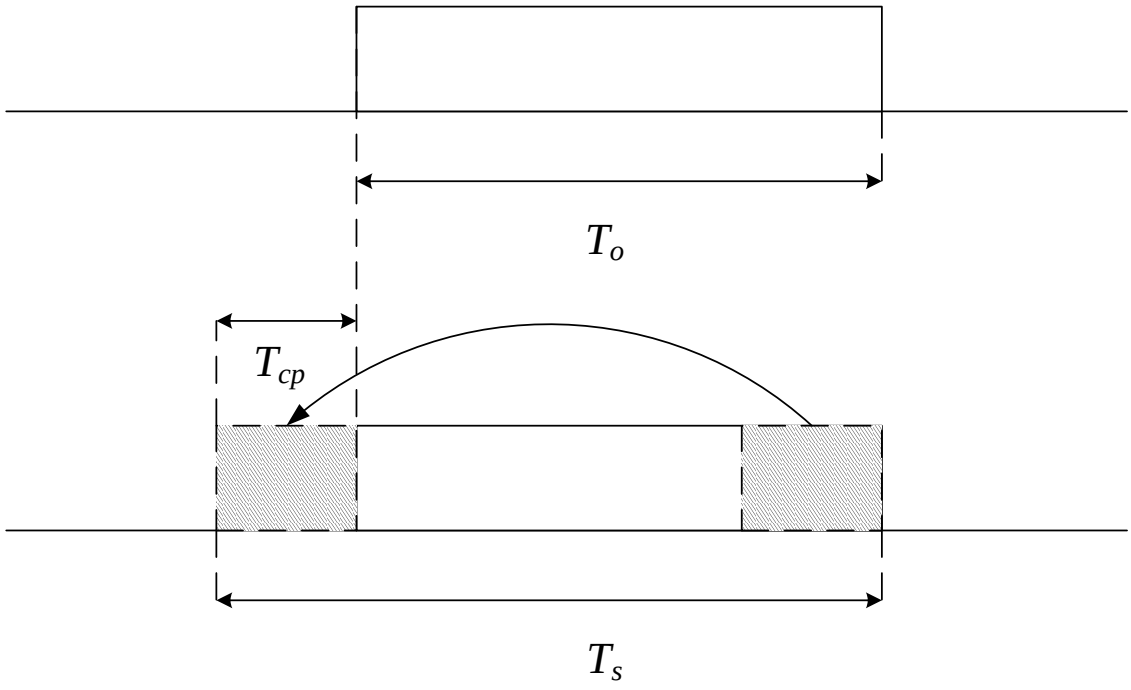

Figure 2.6 Introducing a guard time

where $[\cdot]^H$ represents Hermitian transposition, and $\boldsymbol{F}$ is the M point DFT matrix with entries can be written as

$$[\boldsymbol{F}]_{m,k} = \frac{1}{\sqrt{M}} e^{-j\frac{2\pi mk}{M}} \tag{2.30}$$

Then the vector $\boldsymbol{s}_n$ is converted from parallel to serial and a CP of length L_{cp} is inserted by copying the last L_{cp} elements to the front to generate $\boldsymbol{s}_n^{CP}$. This vector can be modelled as

$$\boldsymbol{s}_n^{CP} = \boldsymbol{T}^{CP}\boldsymbol{s}_n \tag{2.31}$$

where

$$\boldsymbol{T}^{CP} = \begin{bmatrix} \boldsymbol{P}_{CP} \\ \boldsymbol{I}_M \end{bmatrix} \tag{2.32}$$

with $\boldsymbol{P}_{CP}$ is the matrix that collect the last part of the symbol with dimensions of $CP \times M$. While the $\boldsymbol{I}_M$ represents an identity matrix sized $M \times M$.Therefore, the total number of time domain samples per transmitted block is $M_{CP} = M + L_{cp}$.

The frequency selective channel can be modelled as a finite impulse response (FIR) filter with CIR vector $\boldsymbol{h} = \left[h_0, h_1, \dots, h_{L_h-1}\right]^T$ with L_h represents the channel length expressed in signalling intervals. Then, by assuming $L_{CP} \geq L_h$ and taking out the effect

of the additive white Gaussian noise (AWGN) for simplicity, the *n*-th received symbol is expressed as the convolution between the transmitted symbol $\boldsymbol{s}_n^{CP}$ and the channel $\boldsymbol{h}$ such as:

$$\boldsymbol{r}_n^{CP} = \boldsymbol{H}^0 \boldsymbol{s}_n^{CP} + \boldsymbol{H}^1 \boldsymbol{s}_{n-1}^{CP} \tag{2.33}$$

where $\boldsymbol{H}^0$ and $\boldsymbol{H}^1$ are Toeplitz filtering matrices with size $M_{CP} \times M_{CP}$:

$$\boldsymbol{H}^0 = \begin{bmatrix} h_0 & 0 & 0 & \cdots & 0 \\ \vdots & h_0 & 0 & \cdots & 0 \\ h_{L_h-1} & \vdots & \ddots & \ddots & \vdots \\ \vdots & \ddots & \vdots & \ddots & 0 \\ 0 & \cdots & h_{L_h-1} & \cdots & h_0 \end{bmatrix} \tag{2.34}$$

and

$$\boldsymbol{H}^1 = \begin{bmatrix} 0 & \cdots & h_{L_h-1} & \cdots & h_0 \\ \vdots & \ddots & 0 & \cdots & \vdots \\ 0 & \cdots & 0 & \ddots & h_{L_h-1} \\ \vdots & \vdots & \vdots & \ddots & \vdots \\ 0 & \cdots & 0 & \cdots & 0 \end{bmatrix} \tag{2.35}$$

The second term in equation (2.33) represents ISI interference, which is suppressed by discarding the CP section. This can be done by multiplying the received vector by CP removal matrix $\boldsymbol{R}^{CP} = \left[\boldsymbol{0}_{M \times L_{CP}} \, \boldsymbol{I}_M\right]$ and using the identity $\boldsymbol{R}^{CP}\boldsymbol{H}^1 = \boldsymbol{0}_{M \times M_{CP}}$, to produce:

$$\boldsymbol{r}_n^{CP} = \boldsymbol{R}^{CP}\boldsymbol{r}_n^{CP} = \boldsymbol{H}^C \boldsymbol{F}^H \boldsymbol{c}_n \tag{2.36}$$

where $\boldsymbol{H}^C = \boldsymbol{R}^{CP}\boldsymbol{H}^0\boldsymbol{T}^{CP}$ is a circulant matrix of size $M \times M$ with first column is $\left[\boldsymbol{h}\, \boldsymbol{0}_{M-L_h}\right]^T$.

After converting the received vector to parallel from serial and demodulate it with the DFT matrix, the frequency domain received signal can be expressed as

$$\boldsymbol{R}_n = \boldsymbol{F}\boldsymbol{H}^C \boldsymbol{F}^H \boldsymbol{c}_n \tag{2.37}$$

By recalling the well known property that every circulant matrix can be diagonalized when multiplied by IFFT/FFT matrix [36], this results in:

$$\boldsymbol{D}_H = \boldsymbol{F}\boldsymbol{H}^C \boldsymbol{F}^H \tag{2.38}$$

where $\boldsymbol{D}_H$ is a diagonal matrix with diagonal elements results from $\boldsymbol{H} = \sqrt{M}\boldsymbol{F}\boldsymbol{h}$.

Therefore, the frequency domain received symbol can be rewritten as

$$\boldsymbol{R}_n = \boldsymbol{D}_H \boldsymbol{c}_n \tag{2.39}$$

or the scalar form as

$$R_n(m) = H(m)c_{m,n} \tag{2.40}$$

with $m = 0,1,\dots,M-1$. $H(m)$ denotes the channel transfer function over the m-th subcarrier which can be written as

$$H(m) = \sum_{l=0}^{L_h-1} h(l)e^{-j\frac{2\pi ml}{M}} \tag{2.41}$$

Based on the result of equation (2.40), OFDM transmission can be thought of as a parallel transmission of M non interfering subcarriers set attenuated by different complex valued factors $H(m)$. Therefore, to restore and recover the transmitted data, the received symbol required to be multiplied by the inverse of the $\boldsymbol{D}_H$ such as

$$\hat{\boldsymbol{c}}_n = \boldsymbol{D}_H^{-1}\boldsymbol{R}_n \tag{2.42}$$

or the scalar form of that:

$$\hat{c}_{m,n} = \frac{R_n(m)}{H(m)} \tag{2.43}$$

The last equation reveals the simplicity of the equalization stage required to neutralise the effect of the channel, which can be accomplished by a bank of one-tap complex multipliers with values set to $1/H(m)$. This type of equalization is called zero-forcing equalizer. However, due to the presence of AWGN in the received signal, the recovered signal is accompanied by amplified noise level that limits the system form attaining error free transmission.

2.4. OFDM/OQAM Modulation

In a previous section, the bad localisation of the rectangular pulse was discussed and the consequence of the loss in the transmission efficiency to conquer that. The urge to have better localisation for the pulses besides having full transmission efficiency seemed far from possible as a result of Balian-Low theorem. So when Saltzberg managed to achieve that [28], it was like a miracle to break the concept of BLT. In the following sections, the fundamentals of the OFDM/OQAM are presented to reveal how this

system is constructed. In addition, the mathematical model and the efficient implementation are also demonstrated.

2.4.1. OFDM/OQAM basics

The constraint with Balian-Low theorem, that for any Gabor function, it is not possible to have well-localised pulse and critical density at the same time. OFDM/OQAM managed to defeat that limitation by relaxing the orthogonality condition to the real field. Consequently, it allows the transmission of the real and imaginary parts of the complex QAM coefficients over successive subcarriers separated in time by $T_o/2$. This principle is demonstrated in Figure 2.7 for the modulation stage and Figure 2.8 for the demodulation.

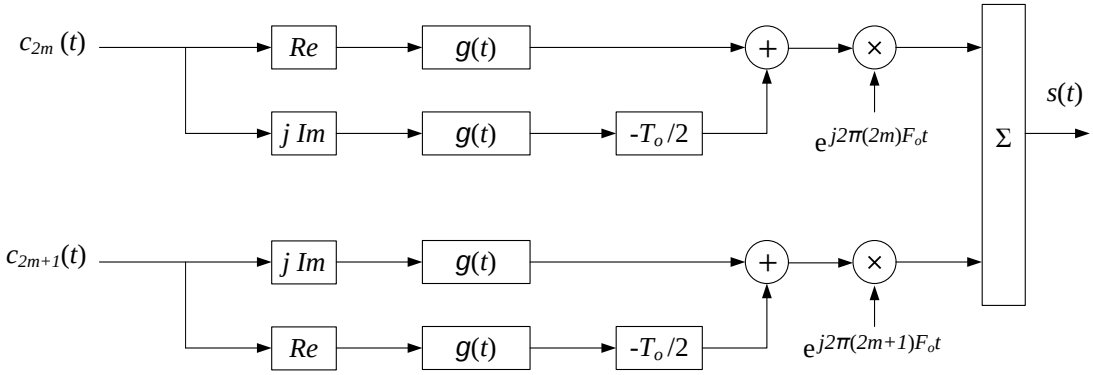

Figure 2.7 A branch of analogue OFDM/OQAM modulator

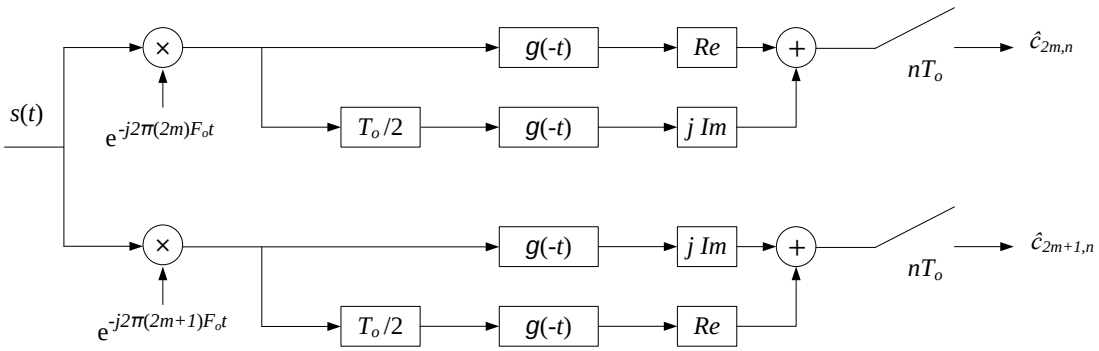

Figure 2.8 A branch of analogue OFDM/OQAM demodulator

Thus OQAM introduces a time offset or delay of $T_o/2$ between real and imaginary parts of the complex QAM coefficients for a specific subcarrier, while the delay is introduced between imaginary and real parts of the following subcarrier. The number of subcarriers is assumed to be even, and the transmitted signal in the continuous time can be expressed as [18]

$$s(t) = \sum_{n=-\infty}^{\infty} \sum_{m=0}^{N-1} \left(c_{2m,n}^{\Re} g(t - nT_o) + j c_{2m,n}^{\Im} g\left(t - \frac{T_o}{2} - nT_o\right) \right) e^{j2\pi(2m)F_o t} + \left(j c_{2m+1,n}^{\Im} g(t - nT_o) + c_{2m+1,n}^{\Re} g\left(t - \frac{T_o}{2} - nT_o\right) \right) e^{j2\pi(2m+1)F_o t} \quad (2.44)$$

where $N = M/2$ and M is the number of subcarriers. T_o indicates the signalling interval and F_o=1/T_o refer to the frequency spacing between neighbour subcarriers. $c_{m,n}^{\Re}$ and $c_{m,n}^{\Im}$ are the real and imaginary parts of the complex QAM coefficient $c_{m,n}$, respectively. $g(t)$ represents a symmetrical real-valued pulse shape.

To have better understanding for the difference between OFDM/QAM and OFDM/OQAM, Figure 2.9 can be exploited in which the phase space of both systems is illustrated. In the conventional OFDM with QAM constellation, the symbols are located at (mF_o, nT_o) points in the phase space grid and indicated by the squares in the figure. This distribution reflects the case of critical sampling with F_oT_o=1. On the other hand, the OQAM real symbols, that produced by staggering the complex QAM coefficients (hence the old name staggered QAM), are located at (mF_o, nT_o/2). It seems that the OQAM raises the density to 2, however this is a virtual increase in the density. Actually, the OQAM has an identical spectral efficiency as in the case of conventional OFDM without CP, this means that the system is still working with critical sampling. Since the transmission process of real-valued symbols on a lattice with density 2 is equivalent to the transmission of symbols with complex values on a lattice of density equal to 1. With this arrangement of transmitting the real and imaginary parts separately, the orthogonality condition is relaxed to the real field, which allows the choice of better localisation for the transmission pulses and gives a room for an improvement in the performance of the system.

The demodulated signals at the receiver side based on Figure 2.8 configuration, can be expressed as

$$\hat{c}_{2m,n}^{\Re} = Re\left\{ \int_{-\infty}^{\infty} s(t) g(t - nT_o) e^{-j2\pi(2m)F_o t}\, dt \right\} \quad (2.45)$$

$$\hat{c}_{2m,n}^{\Im} = \mathrm{Im}\left\{ \int_{-\infty}^{\infty} s(t) g\left(t - \frac{T_o}{2} - nT_o\right) e^{-j2\pi(2m)F_o t}\, dt \right\} \quad (2.46)$$

$$\hat{c}_{2m+1,n}^{\Im} = \mathrm{Im}\left\{\int_{-\infty}^{\infty} s(t)g(t-nT_o)e^{-j2\pi(2m+1)F_o t}\,dt\right\} \tag{2.47}$$

$$\hat{c}_{2m+1,n}^{\Re} = Re\left\{\int_{-\infty}^{\infty} s(t)g\left(t-\frac{T_o}{2}-nT_o\right)e^{-j2\pi(2m+1)F_o t}\,dt\right\} \tag{2.48}$$

The above set of equations shows how the real field is only required to reconstruct the transmitted symbol without the need for the complex orthogonality.

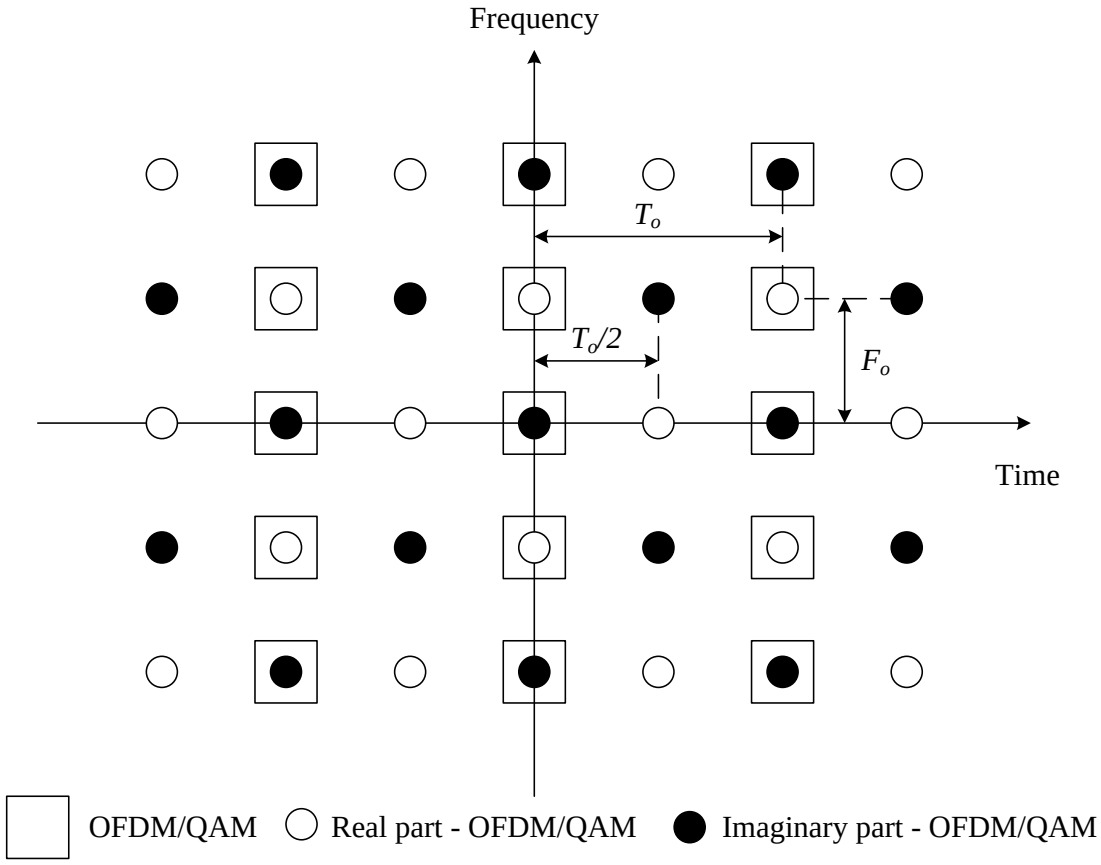

Figure 2.9 Phase space with different lattice point for both OFDM/QAM and OQAM

2.4.2. OFDM/OQAM mathematical model

The previous section demonstrated the principles of the OQAM and the continuous time model of the system. This section focuses on the presentation of the discrete time mathematical model and the orthogonality condition of the OQAM. The staggering of the complex QAM coefficients can be pre-processed prior to the modulation process. Thus, the discrete time OQAM signal can be written as [18, 37]

$$s[k] = \sum_{m=0}^{M-1}\sum_{n=-\infty}^{\infty} a_{m,n}\underbrace{g[k-nN]e^{j\frac{2\pi m}{M}\left(k-\frac{L-1}{2}\right)}e^{j\phi_{m,n}}}_{g_{m,n}[k]} \tag{2.49}$$

with

$$\phi_{m,n} = \phi_0 + \frac{\pi}{2}(m+n) \qquad (mod\ \pi) \tag{2.50}$$

where $N = M/2$ represents discrete time offset with M has to be even number, while $\phi_{m,n}$ is an additional phase term in which ϕ_0 can be arbitrarily chosen. The real-valued coefficient $a_{m,n}$, holds either real or imaginary part of the staggered complex QAM coefficient. L indicates the length of the prototype filter g, that can take an integer multiple of M such as

$$L = KM \tag{2.51}$$

K is called overlapping factor with $K > 0, K \in \mathbb{Z}$.

Assuming that the prototype filters of the OQAM have unity energy (normalised), the subcarrier filters are attained by uniformly frequency shifting single low-pass FIR prototype filter g. Consequently, the synthesis filterbank, as depicted in Figure 2.10, can be expressed as [18, 37]

$$Tx_m[k] = g[k]e^{j\frac{2\pi m}{M}\left(k-\frac{L-1-N}{2}\right)} \tag{2.52}$$

while the analysis filterbank can be written as

$$Rx_m[k] = g[k]e^{j\frac{2\pi m}{M}\left(k-\frac{L-1+N}{2}\right)} = Tx_m^*[L-1-k] \tag{2.53}$$

for all $m = 0,1,\dots,M-1$ and $k = 0,1,\dots,L-1$. If the prototype filter g is assumed to be real and symmetrical, as in the rest of this thesis, then $Rx_m[k] = Tx_m[k]$ for all m and k.

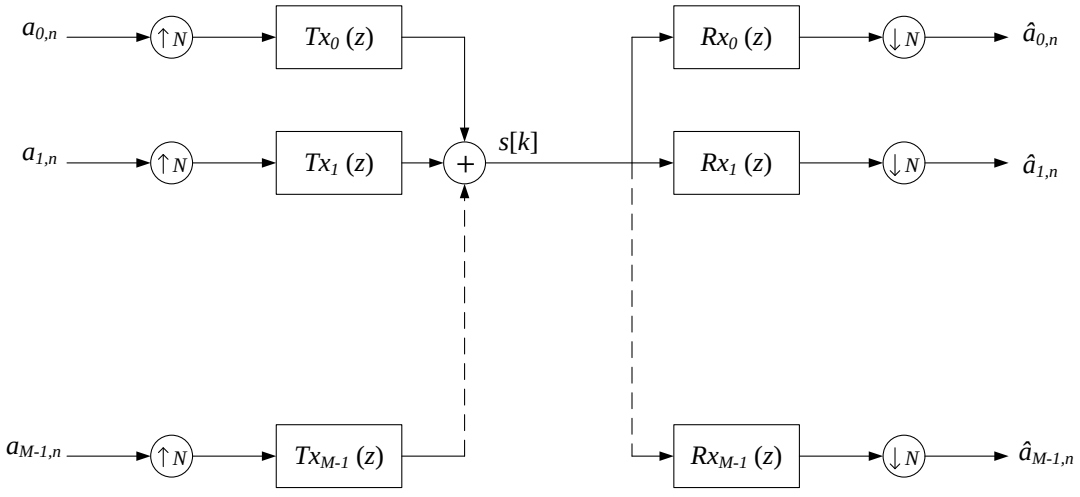

Figure 2.10 Structure of OFDM/OQAM system in discrete time

The Gabor function in this case is the term $g_{m,n}[k]$ in (2.49) from which the orthogonality condition can be calculated such as

$$Re\langle g_{m,n}, g_{p,q}\rangle = Re\left\{\sum_{k=0}^{L-1} g_{m,n}[k]g_{p,q}^{*}[k]\right\} = \delta_{m,p}\delta_{n,q} \tag{2.54}$$

where $\delta_{m,p}$ and $\delta_{n,q}$ are both Kronecker deltas. If $m,n \neq p,q$, then the inner product $\langle g_{m,n}, g_{p,q}\rangle$ is a pure imaginary term.

In theory, the prototype filter g can be designed to produce TMUX configuration that can accomplish perfect reconstruction (PR) of the transmitted data at the receiver side. By assuming a distortion free channel and an ideal transmission process, then the received signal with these PR filters is just delayed version of the transmitted signal. On the other hand, the prototype filter can be designed to produce nearly perfect reconstruction (NPR). As a result, some marginal levels of ISI and ICI are present even in the case of distortion free channel. However, during the design process of the filter, the level of interference can be kept to minimum. These NPR filters offer more freedom in the filter design process to achieve higher level of stop-band attenuation than the PR with the same length [37-38]

2.4.3. Efficient implementation of OFDM/OQAM

The direct implementation of OQAM as in Figure 2.10 for large number of subcarriers would be computationally expensive and far from practical especially with long filters. Therefore, the reduction in the complexity is obtained by opting to the polyphase representation of the filters to construct the discrete Fourier transform (DFT) filterbanks as demonstrated in Figure 2.11and Figure 2.12 [18, 38-39].

The first part in the modulator depicted in Figure 2.11, is the C2R block, which stands for complex to real mapping. This block performs the first process in the OQAM modulation by inserting delay between the real and imaginary parts of the complex QAM that can be expressed as [37]

$$a_{m,2n} = \begin{cases} Re\{c_{m,n}\} & n\ even \\ \mathrm{Im}\{c_{m,n}\} & n\ odd \end{cases} \tag{2.55}$$

and

$$a_{m,2n+1} = \begin{cases} \mathrm{Im}\{c_{m,n}\} & n\ even \\ Re\{c_{m,n}\} & n\ odd \end{cases} \tag{2.56}$$

Therefore, the C2R block ensures that the real and imaginary parts are alternating in their order from subcarrier to another for the consecutive symbols in time. This operation increases the sampling rate of the signal effectively by a factor of two. The output of the C2R then is processed by the phase mapping section which stops any interference between adjacent subcarriers.

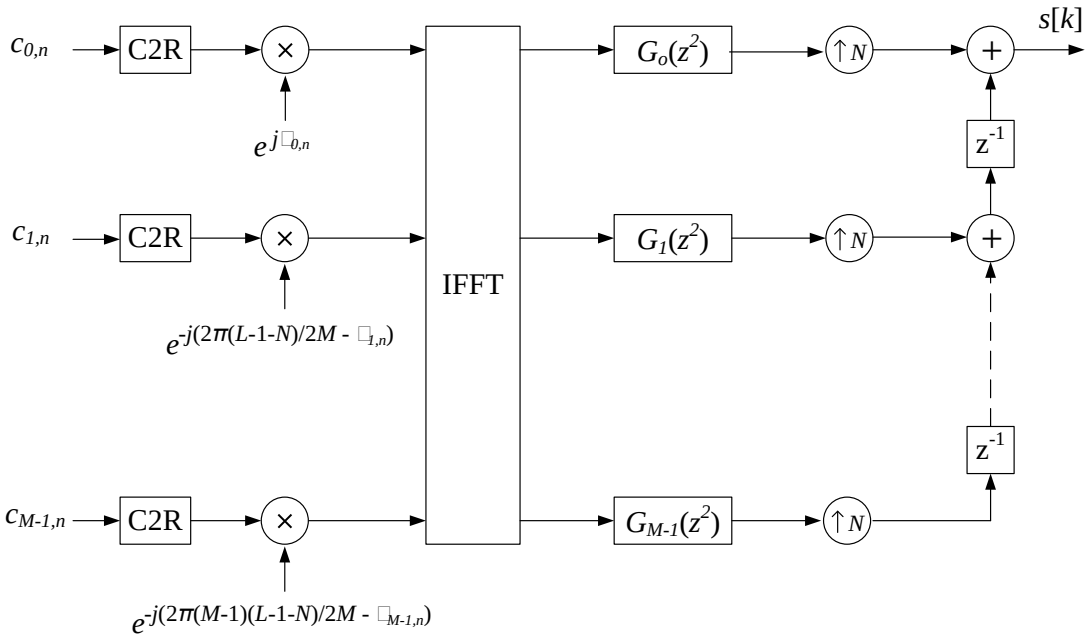

Figure 2.11 Efficient implementation of OFDM/OQAM modulator by polyphase representation

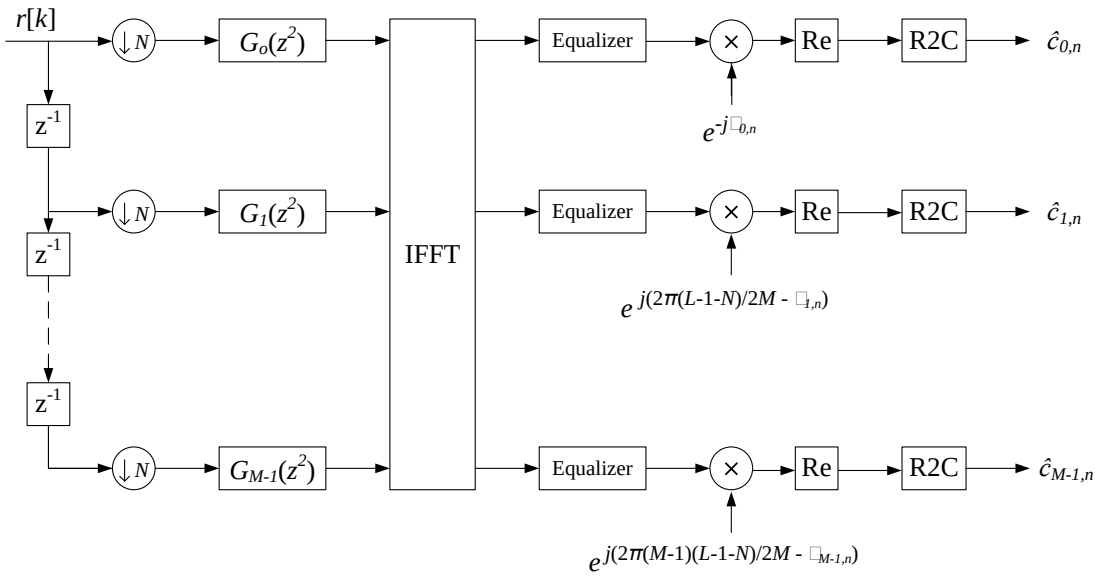

Figure 2.12 Efficient implementation of OFDM/OQAM demodulator by polyphase representation

After the phase mapping process, the combination of the IFFT block and the polyphase network (PPN), which forms the analysis filterbank, complete the modulation process. The IFFT block performs the required modulation for the subcarriers. The polyphase decomposition of the filter based on type 1 can be calculated from the z-transform of the prototype filter as the following [38-39]:

$$G(z) = \sum_{l=0}^{M-1} z^{-l} P_l(z^M) \tag{2.57}$$

with $P_l(z)$ equals to

$$P_l(z) = \sum_{n} g[l + nM] z^{-n} \tag{2.58}$$

It is worth noting that the synthesis filterbank at the demodulator can be constructed by either exploiting polyphase network based on type 1 and IFFT block or opting to the type 2 and FFT block. More details on this topic can be found in [38-39].

2.5. Prototype Filters

The key difference between the OFDM/QAM and OFDM/OQAM is the possibility of exploiting well-localised prototype filters in the later to eliminate the need for the redundant data transmission as in the former to avoid ISI and ICI. Therefore, these prototype filters play important role in the control of the performance of the system, thus, require carful design process and selection criteria to attain the highest possible efficiency depending on the transmission environments. For example, in indoor situations where time dispersion is normally small (low ISI levels), a pulse that has well localisation in frequency is an appropriate choice. While for low frequency dispersion situations (low ICI levels), a well-localised pulse in time is more suitable choice. This possibility of selecting different prototype of filters gives the ability to improve some of the performance aspects such as throughput or robustness to interference. This section reviews some of the pulse shapes and evaluates their localisation factor and their individual properties.

2.5.1. Square root raised cosine filter (SRRC)

One of the well-known filters in digital communication is the square root raised cosine filter. This filter satisfies Nyquist criterion for ISI free transmission if it is utilised in both of the transmitter and receiver filters. Although this filter is still used in many areas of discrete-time digital communication, it cannot satisfy Nyquist criteria perfectly as a

result of the truncation and discretization (Nyquist principle satisfaction is conditioned by infinite length pulses in continuous time). The frequency domain response of the SRRC filter can be expressed as below [18]

$$R_c(v) = \begin{cases} \dfrac{1}{\sqrt{F_o}} & |v| \le (1-\beta)\dfrac{F_o}{2} \\ \dfrac{1}{\sqrt{F_o}} \cos\left(\dfrac{\pi}{2\beta}\left(\dfrac{|v|}{F_o} - \dfrac{1-\beta}{2}\right)\right) & (1-\beta)\dfrac{F_o}{2} < |v| \le (1+\beta)\dfrac{F_o}{2} \\ 0 & (1+\beta)\dfrac{F_o}{2} < |v| \end{cases} \quad (2.59)$$

where $0 \le \beta \le 1$ is the roll-off factor. The continuous-time response of the SRRC filter can be written as the following:

$$r_c(t) = \sqrt{F_o}\,\frac{4\beta F_o t \cos(\pi(1+\beta)F_o t) + \sin(\pi(1-\beta)F_o t)}{(1-(4\beta F_o t)^2)\pi F_o t} \quad (2.60)$$

The time and frequency response of the SRRC filter are depicted in Figure 2.13 for *M* = 64 and filter length of 4*M* with β is set to equal 1. For the comparison purposes, the responses of the rectangular pulse are also included in the same figure.

The SRRC has better frequency response with lower first side lobe than the rectangular pulse, which means better localisation in the frequency domain. However, the filter spreads in time, which affects slightly the time localisation. The time-frequency localisation factor reflects that and equals for this arrangement $\xi = 0.8037$ which is very good compared to the rectangular pulse result previously mentioned ($\xi = 0.1549$).

By inspecting the ambiguity function representation for the SRRC shown in Figure 2.14, it can be noticed the concentration of the pulse energy in frequency domain is better than time domain. This can be translated to the practical environment as: a system that employ the SRRC filters suffers from the interference in time (ISI) more than from frequency interferences (ICI). Consequently, the SRRC can be considered as the right choice when the transmission suffers from frequency dispersion mostly.

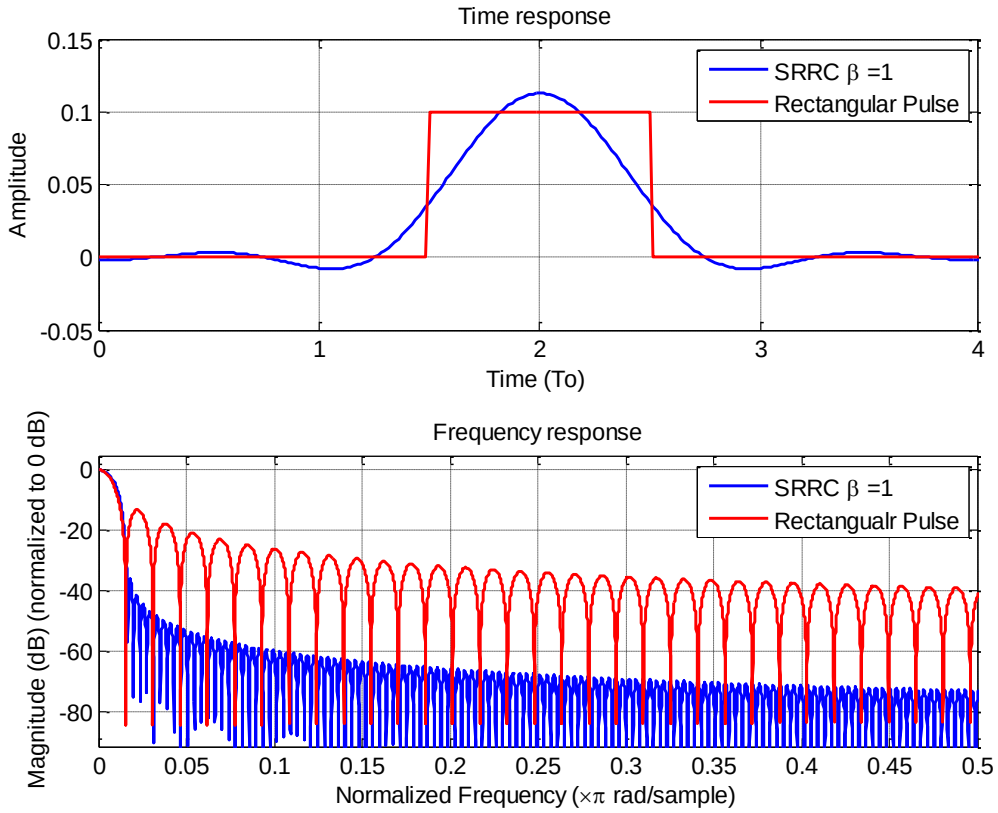

Figure 2.13 Time and frequency response of the SRRC filter with K=4

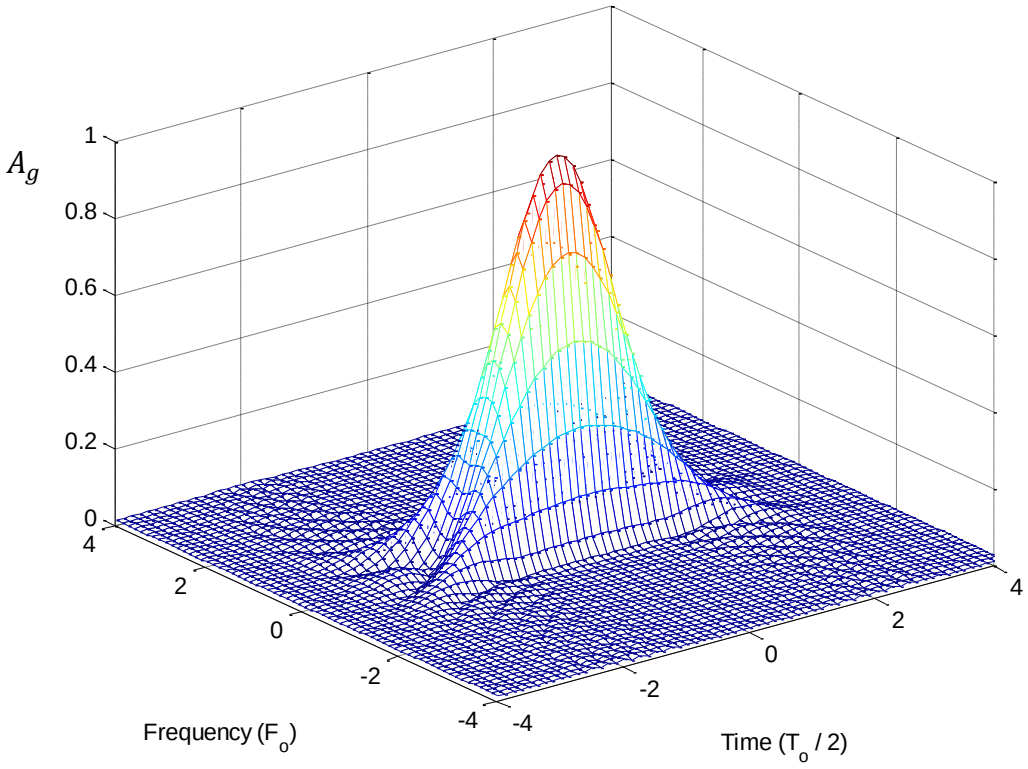

Figure 2.14 Ambiguity function for the SRRC filter

2.5.2. Enhanced Gaussian functions filters (EGF)

The extended Gaussian function (EGF) is a family of filters that is originated from the well-localised non-orthogonal Gaussian function. This function can be approximated by the following closed form expression (valid for $0.528v_o^2 \leq \lambda \leq 1.8939/v_o^2$) [40]:

$$z_{\lambda,v_o,\tau_o}(t) = \frac{1}{2}\sum_{k=0}^{\infty} d_{k,\lambda,v_o}\left[g_\lambda\left(t+\frac{k}{v_o}\right)+g_\lambda\left(t-\frac{k}{v_o}\right)\right]\sum_{l=0}^{\infty} d_{l,\frac{1}{\lambda},v_o}\cos\left(2\pi\frac{t}{\tau_o}\right) \quad (2.61)$$

with g_λ represents the Gaussian function that can be written as

$$g_\lambda(t) = (2\lambda)^{\frac{1}{4}}e^{-\pi\lambda t^2} \quad (2.62)$$

where λ is the spreading parameter, which is a strictly positive real number. d_{k,λ,v_o} are real coefficients whose expression is given in [40]. τ_o and v_o are the time and frequency parameters of the modulation system such as $\tau_o v_o = 1/2$ for the OQAM modulator.

One particular case of the EGF family is $\lambda = 1$, in which this function in time domain is identical to its Fourier transform. That leads to a special filter called isotropic orthogonal transform algorithm (IOTA). The time and frequency response for the IOTA filter is depicted in Figure 2.15 for *M*=64 and *L*=256. From this figure, it is clear that this pulse has better localisation in the frequency domain with first lobe at -34dB, unlike rectangular pulse with only -13dB.

As the name suggests, the energy of this pulse is distributed isotropically in time and frequency as demonstrated in the ambiguity function plot in Figure 2.16. IOTA represents a well-localised pulse, as the localisation factor is equal to 0.9705 for this configuration. In this thesis, the IOTA is the only case of the EGF family to be considered.

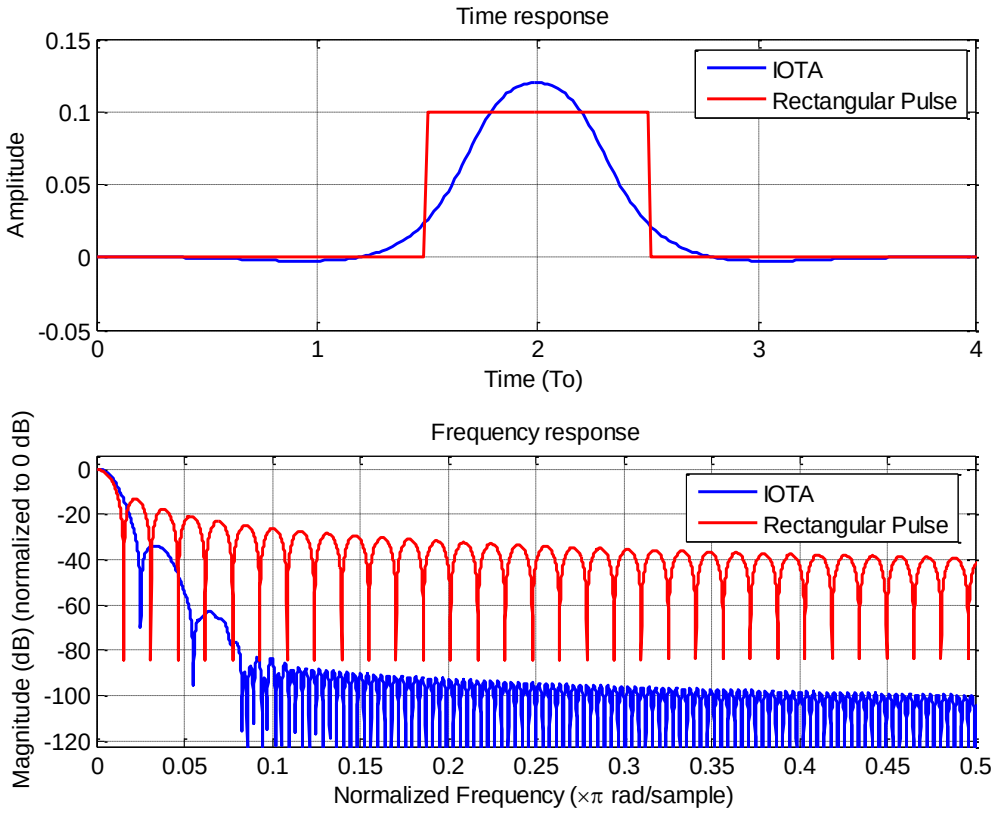

Figure 2.15 Time and frequency response of the IOTA filter with K=4

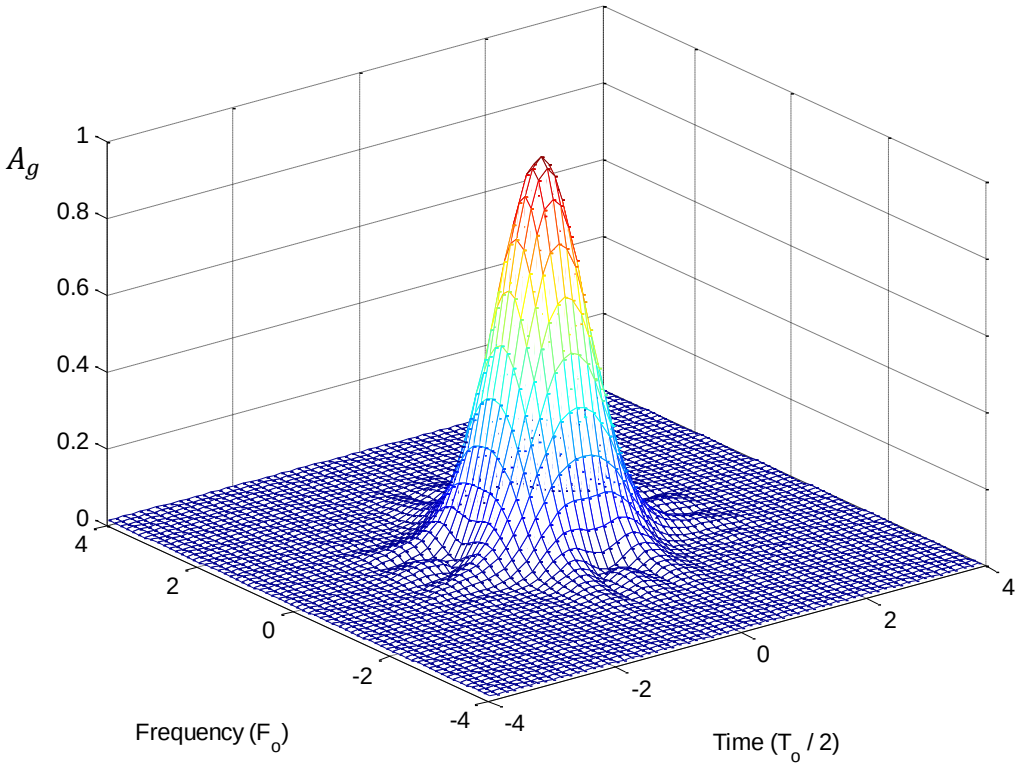

Figure 2.16 Ambiguity function for the IOTA filter

2.5.3. Time-Frequency localisation filter (TFL)

The SRRC and the IOTA filters are both orthogonal in the continuous time domain. However, in digital communication these filters need to be truncated and digitised which lead to a loss in their orthogonality. SRRC suffers more than IOTA of the orthogonality loss for the same truncation length [18]. To avoid this problem, the filter design process is conducted in the discrete domain directly while maintaining orthogonality condition. In addition, the localisation of the filter is an important factor that required to be considered in the design process. Therefore, [41-42] included all these factors in the design criteria to produce filters with high localisation factors that meet the orthogonality condition in the discrete domain named time-frequency localisation filter (TFL).

Figure 2.17 demonstrate the time and frequency response for the TFL filter with M= 64 and K=1. This filter has better localisation for the energy in time over frequency as illustrated by the ambiguity function in Figure 2.18. The localisation factor for TFL1 (as K=1) is equal to 0.9104.

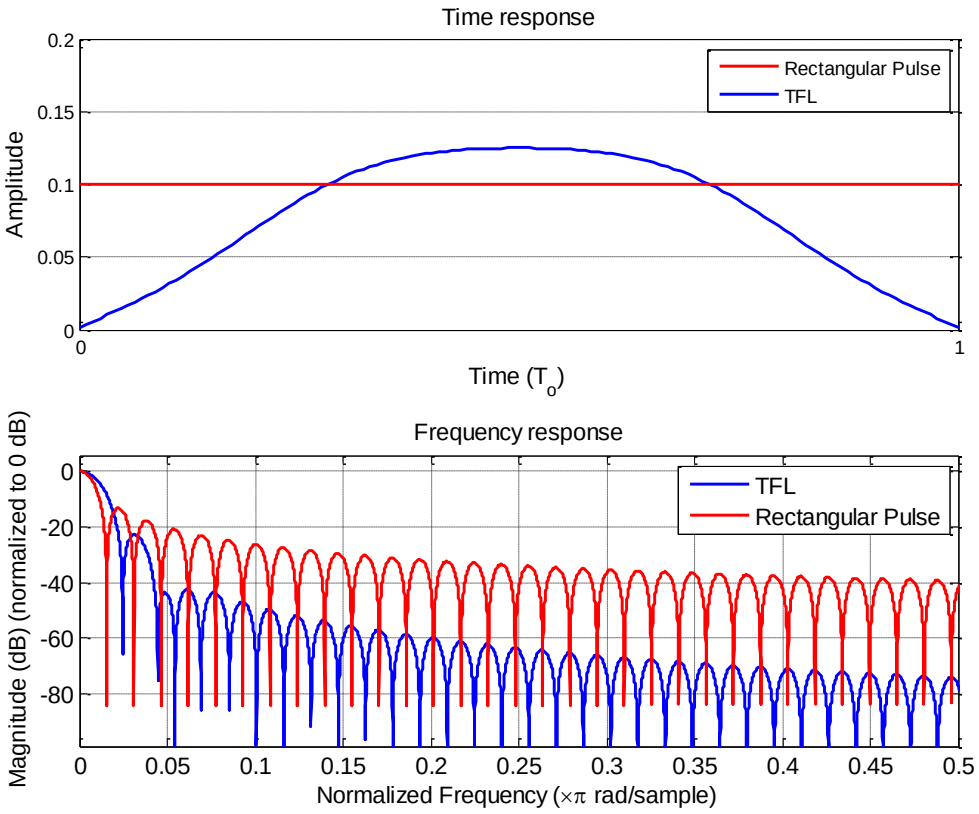

Figure 2.17 Time and frequency response of the TFL filter with K=1

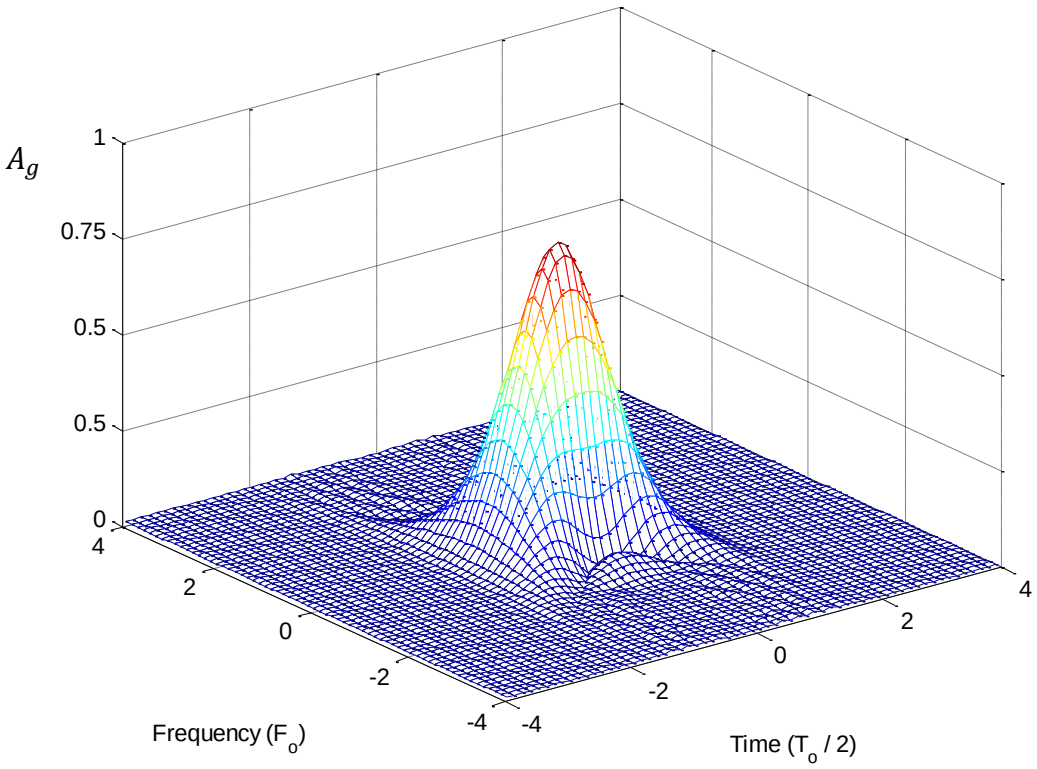

Figure 2.18 Ambiguity function for the TFL filter

2.5.4. Minimized interference algorithm filter (MIA)

There are many methods and algorithms to design the best filter for the specified applications, and the same applied for the filterbanks. The minimized interference algorithm (MIA) [43] is set to minimize the interference generated in the system. This can be achieved by minimizing a cost function that depends on the stopband attenuation and the ISI levels.

The frequency response of this prototype filter, shown in Figure 2.19, indicates higher attenuation compared to the rectangular pulse. This pulse is well localised in time and frequency with $\xi = 0.9536$ for *M*=64 and MIA4 (K=4). This is demonstrated in the energy distribution illustration in Figure 2.20. Ambiguity function reveals better localisation in the frequency side than the time, which can be useful to contradict ICI interference.

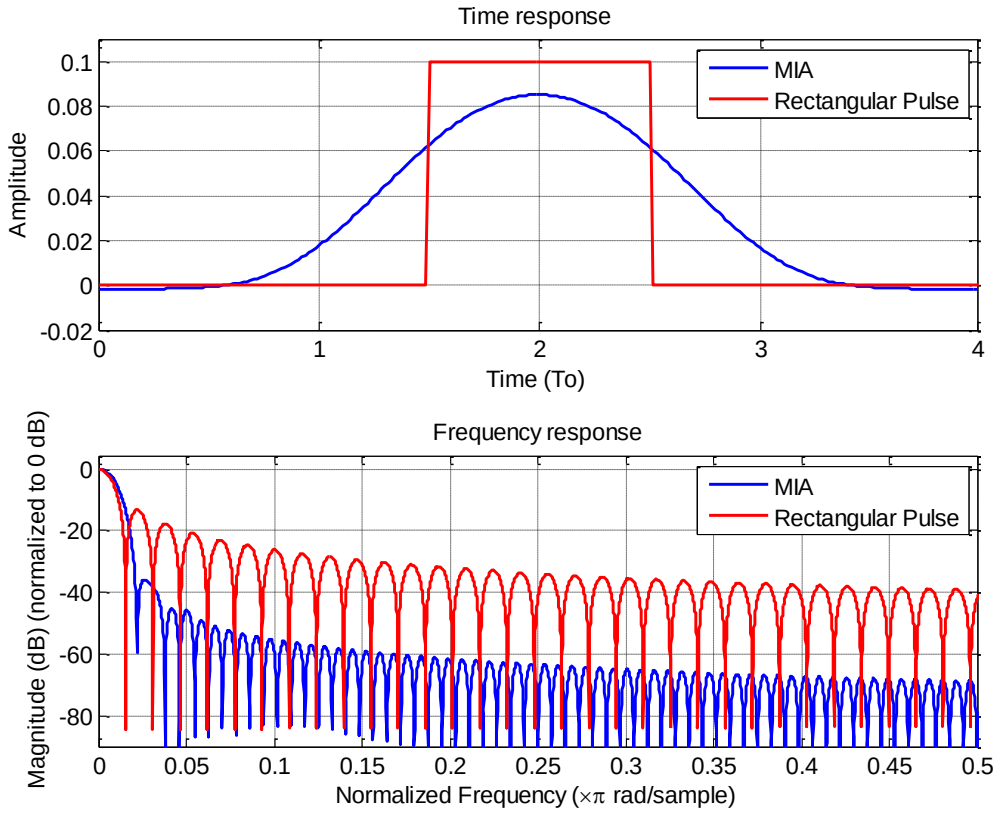

Figure 2.19 Time and frequency response of the MIA filter with K=4

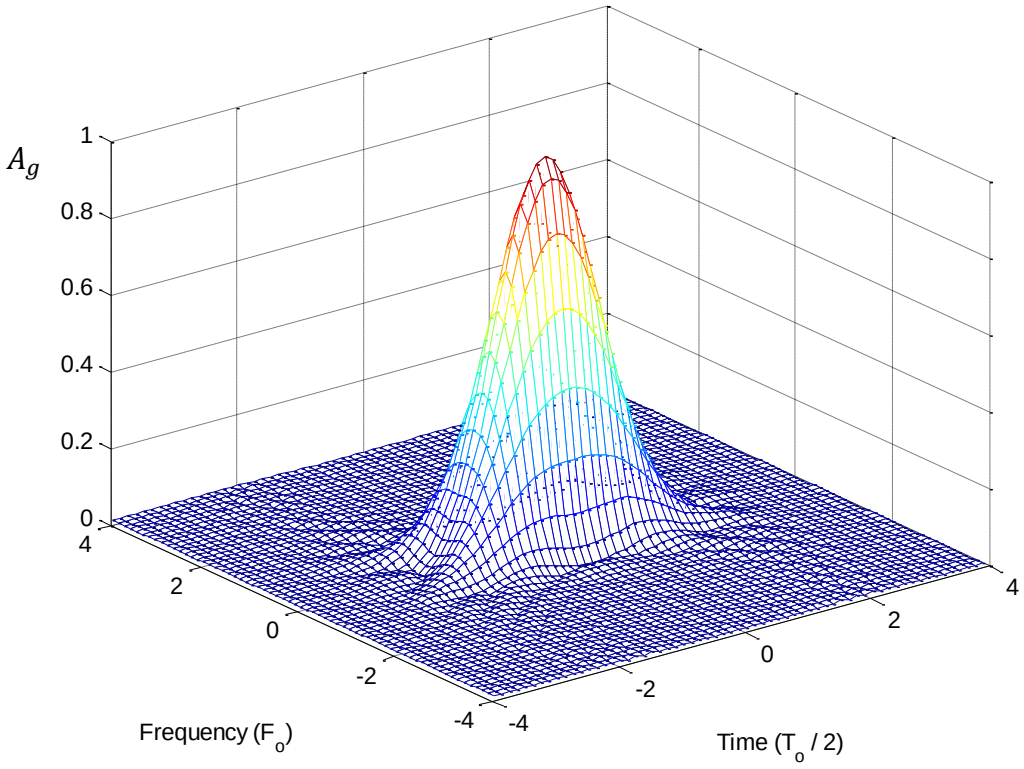

Figure 2.20 Ambiguity function for the MIA filter

The localisation factor for all the considered filters are provided in Table 2.1 for different number of subcarriers and filter lengths.

		L=*M*	*L*=4*M*	*L*=8*M*
M=64	SRRC	0.1931	0.8240	0.8957
	IOTA	0.2063	0.9705	0.9770
	TFL	0.9104	-	-
	MIA	0.2088	0.9536	0.8828
M=128	SRRC	0.1365	0.7129	0.8869
	IOTA	0.1463	0.9572	0.9769
	TFL	0.9087	-	-
	MIA	0.1611	0.9513	0.8819
M=1024	SRRC	0.0483	0.3590	0.7860
	IOTA	0.0519	0.8145	0.9767
	TFL	0.8732	-	-
	MIA	0.0917	0.9495	0.8706

Table 2.1 The localisation factor for the considered filters

From the previous filter characteristics, it can be concluded that the OQAM has higher stopband attenuation and better frequency selectivity compared to the conventional OFDM. This advantage comes beside the removal of the redundant data transmission that allows the system to achieve higher data transmission rate. Furthermore, the discard of the CP part can be considered as method of energy saving or more efficient energy wise, thus the system can have a title of the green OFDM.

2.6. Conclusion and Summary

In this chapter, the principles and aspects of the OFDM and OFDM/OQAM have been presented. The Balian-Low theorem that governs the Gabor system density with the localisation in time and frequency of the prototype function that form the orthonormal basis was studied. This theorem indicates the impossibility to have density equal to one and having a well localisation for the pulses at the same time. A well-localised pulse can achieve ISI free transmission based on Nyquist criterion.

The conventional OFDM system was demonstrated. The weakness of the OFDM as a result of the rectangular pulse utilization was discussed. These pulses suffer from bad

localisation which results in an ISI in the received symbol. This problem can be solved by extending the transmitted symbol with redundant data, which causes a loss in the transmission rate. The efficient implementation and the mathematical model of the system were also presented.

OFDM/OQAM is another multicarrier modulation system that exploits well-localised pulse shapes in conjunction with critical sampling, was also presented in this chapter. This innovative system is able to break the Balian-Low theorem by relaxing the orthogonality condition to the real field by staggering the complex data coefficients. Therefore, this system utilises the full transmission bandwidth and well-localised prototype filters to attain ISI free transmission. The mathematical model and the efficient implementation using polyphase filters were all illustrated. Finally, some of the well-localised prototype filters with their time-frequency analysis were demonstrated.

Chapter 3. The New Walsh OFDM/ OQAM System

3.1. Precoded Multicarrier Modulation Systems

Over the past years, the research has been fuelled to improve the transmission of multicarrier systems over multipath fading channels. This has been achieved by means of forward error correction techniques or by combining orthogonal transforms to the transmitter and receiver matrices to function as precoders for the resulting systems.

The combination of Walsh-Hadamard transform (WHT) and OFDM system has proved to be a promising candidate for the next generation wireless commutation systems. The so-called WHT-OFDM shows an enhancement on the overall OFDM system performance. The main advantage of using WHT with OFDM is to improve the system performance over selective multipath fading channels [44-45]. In addition, a reduction in the peak to average power ratio (PAPR) over the conventional systems [46-48]. The combinational system maintains the same data transmission rate as OFDM that makes it an attractive alternative to the forward error correction.

As mentioned previously, there is superiority for the OFDM/OQAM over the conventional OFDM system in some aspects due to the utilisation of filterbanks in their transceivers. In order to exploit the advantages of both WHT and OFDM/OQAM, a combination of both techniques is proposed to generate a new system that can be called as WHT/OFDM/OQAM or for short WHT/OQAM. This system presents superior performance over the existing systems in the sense of utilising all the advantages of the filterbanks such as the full transmission bandwidth and the lower out of band energy leakage while performing better over multipath channels.

At the same time, the integration of this transform into OFDM/OQAM system means an increase of the whole system complexity. Therefore, the aim is to tackle this problem and find the best way to integrate WHT while maintaining low complexity or even minimizing it. As a result, a fast algorithm is developed for the system, which results in a considerable reduction for the complexity.

The structure of this chapter is as follows. Section 3.2 provides an overview of the related work in the literatures. Section 3.3 review the definition of the WHT. In Section

3.4, the proposed WHT/OQAM system is illustrated. Section 3.53.5.1 introduce the full analysis of the transmission model for the WHT/OQAM. In addition, the inherited interference in the received symbol is discussed and analysed in Section 3.5.2. Moreover, the derivation and calculation of the theoretical bit error rate are provided in Section 3.5.3. Furthermore, Section 3.5.4 presents the results of the system performance over different channel models using simulation programs. Section 3.6.1 explains the derivation of the fast algorithm, while Section 3.6.2 evaluates the complexity of the new transform over the cascaded implementation. Conclusion and summary are presented in Section 3.7.

3.2. Related Work

In the past few years, the principle of using unitary precoders with multicarrier modulators was investigated thoroughly. Different kinds of precoders such as the DFT, DCT, and WHT were suggested for the conventional OFDM system [49]. For example, recently the DFT precoder has been chosen as standard for the Long Term Evolution (LTE) standard in the uplink to form the Single Carrier Frequency Division Multiple Access (SC-FDMA) [50-51].

The utilization of the WHT with the CP- OFDM was proposed firstly in [44]. The system showed a substantial performance enhancement over the conventional system. The effect of the WHT on the received symbol constellation was illustrated to show the effect of the noise averaging. The WHT was considered as an alternative way to the higher complexity of optimal or adaptive receivers. However, the overall complexity of the system was not considered in that work.

The characteristics of the WHT-OFDM system was analysed in [47]. The system showed reduction in the clipping probability therefore a reduction in the spectral re-growth over the conventional system which results in a reduction in the peak to average power ratio. This improvement is discussed further in the next chapter.

To resolve the noise enhancement issue caused by the spreading of the weak subcarrier with WHT, an iterative detector was proposed in [52]. The iterative detector concept is based on replacing the weak subcarrier with an estimated one to achieve error free received signal after number of iterations. Although this technique improves the received signal in term of the bit error rate, it also increases the latency of the detection depending on the number of the iterations.

The reduction of the complexity of the WHT-OFDM was the main interest in [45-46]. A low computational complexity transform was introduced to combine WHT with IFFT. The system achieved higher resilience for the frequency selective channels over the conventional OFDM.

It is worth noting that the WHT was combined with OFDM/OQAM for the purpose of creating multicarrier coded division multiple access (MC-CDMA) in [53-54]. However, the multiuser transmission was the main interest of that work.

3.3. Walsh-Hadamard Transform (WHT)

Walsh-Hadamard is a real, symmetric, orthogonal transform. Its elements are equal to ±1 which make the hardware implementation requires only addition operations[2]. The Walsh-Hadamard matrix can be constructed by its basis function as follows [55]:

$$WH_{ij} = \frac{1}{\sqrt{M}} (-1)^{u} \tag{3.1}$$

$$u = \sum_{x} i_x \bullet j_x \tag{3.2}$$

where i,j are the element indices of the WHT matrix, and M is the matrix order. Additionally, the symbol (•) denotes a binary AND operation between the bits of the binary representation (i_x and j_x) of the element indices i and j respectively, and x is the length of the binary digits of i_x and j_x. For example, a WHT matrix of order 2 can be written as [56]

$$WHT_2 = \begin{bmatrix} WH_{1,1} & WH_{1,2} \\ WH_{2,1} & WH_{2,2} \end{bmatrix} = \frac{1}{\sqrt{2}} \begin{bmatrix} 1 & 1 \\ 1 & -1 \end{bmatrix} \tag{3.3}$$

Alternatively, the matrix can be constructed recursively by defining Hadamard identity $WH_1=1$ and WH_M as:

$$WHT_M = \frac{1}{\sqrt{2}} \begin{bmatrix} WH_{M/2} & WH_{M/2} \\ WH_{M/2} & -WH_{M/2} \end{bmatrix} \tag{3.4}$$

Since the WHT matrix is real, symmetric, and orthogonal, these are valid relations:

$$WHT_M = WHT_M^* = WHT_M^T \tag{3.5}$$

$$WHT_M \, WHT_M = I_M \tag{3.6}$$

[2] Based on the subtraction operation is essentially implemented with an adder and two's compliments.

where * stands for complex conjugate, T for transpose operation, and I_M is an identity matrix of order M.

Furthermore, since WHT matrix is symmetric, both the forward and inverse transformations are identical. A Walsh-Hadamard transform for a sequence $x(m)$ can be defined as:

$$X(k) = \sum_{m=0}^{M-1} WH_{k,m} x_m \qquad k = 0,1,\dots,M-1 \tag{3.7}$$

where $WH_{k,m}$ is an element of the WHT matrix. Figure 3.1 shows the signal flow graph of this transform. This transform distributes the input symbol energy over all subcarriers uniformly because all the elements in the WHT matrix have equal magnitude.

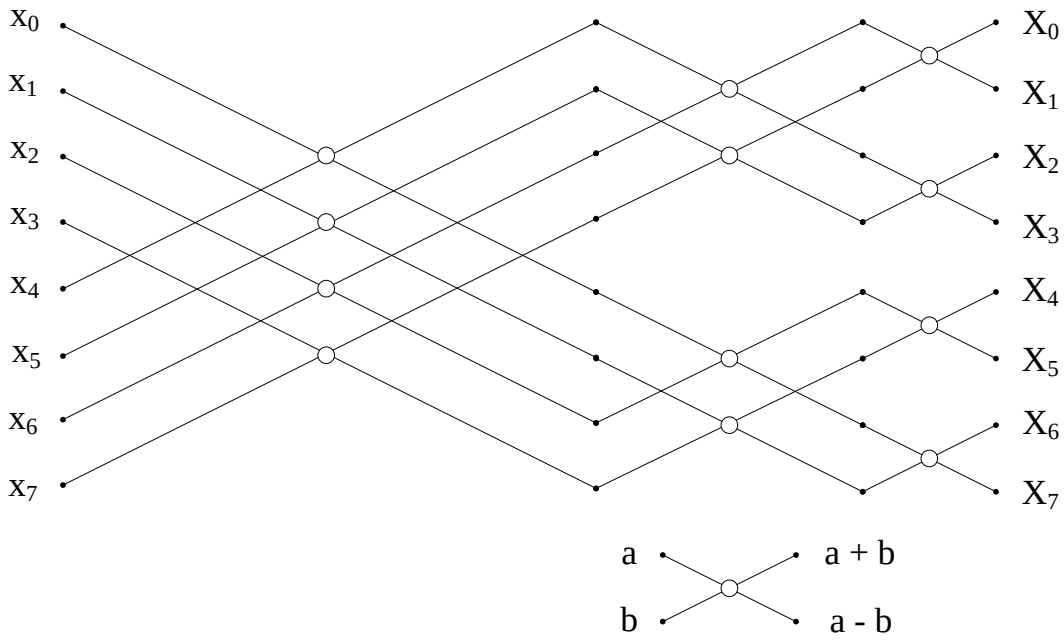

Figure 3.1 Signal flow graph for the Walsh-Hadamard transform of order 8.

3.4. WHT/OFDM/OQAM System

One of the main constrains for the OFDM/OQAM system to be feasible and to maintain orthogonality that the input data must be real symbols so that a well localized in time and frequency filter exists and belongs to the Gabor family as Balian-Low theorem states [7, 57]. Therefore, the integration of the WHT in the system requires maintaining a real input to the modulator block. Consequently, the WHT may be added to the system

before the C2R block as in Figure 3.2, which requires $M \log_2 M$ complex additions or in other word $2M \log_2 M$ real additions.

Since the WHT is real transform, so a real input produces a real output. In order to reduce the computational complexity to increase the efficiency of implementation, the WHT can be placed after the C2R block. As a result, this shift in the location of WHT block reduces the hardware requirement for the WHT by 50% as compared with the previous proposal. Since the entire computations take place with real inputs instead of complex inputs, so it only requires $M \log_2 M$ real additions. It will be shown later in this chapter that this shift in the location of the WHT is useful for further reduction in the complexity of the system by utilizing more efficient fast transform.

Figure 3.2 depicts the proposed WHT/OFDM/OQAM block diagram. The WHT distributes uniformly the input symbol $c_{i,n}$ over all subcarriers without expansion or reduction in system bandwidth. This uniform distribution improves the frequency diversity of the transmitted symbol as every subcarrier is constructed of combination of the entire transmitted symbol data. Therefore, the system can overcome strong fading on some subcarriers, which leads to better performance over frequency selective fading channels [44, 46, 58].

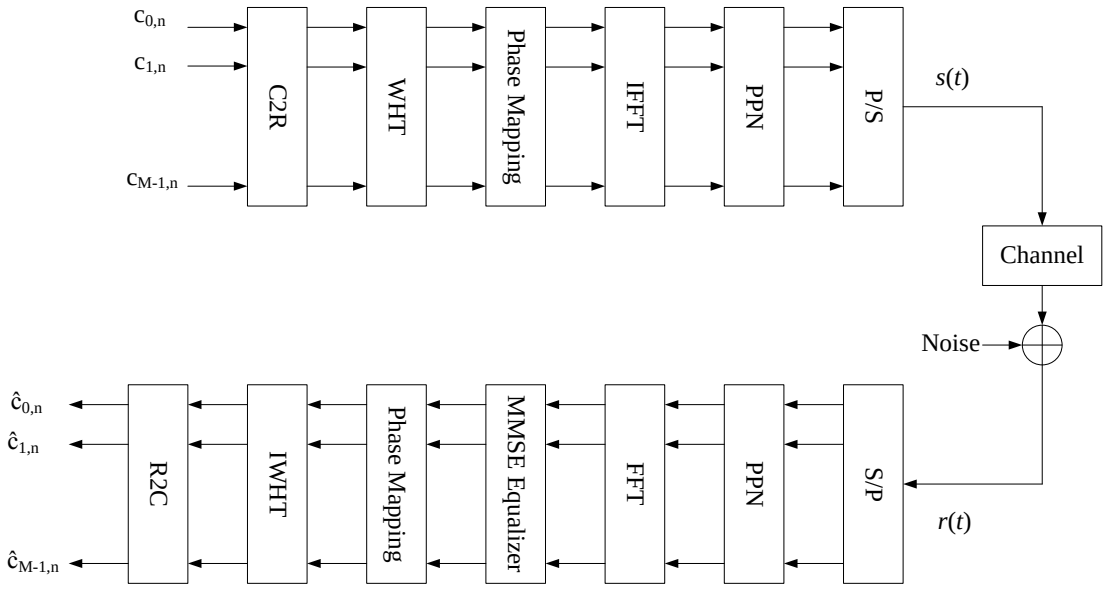

Figure 3.2 The proposed WHT/OFDM/OQAM system.

3.5. Analysis of the WHT/OFDM/OQAM Transmission

To gain better understanding of the performance of the WHT/OFDM/OQAM system, the theoretical transmission model is derived over frequency selective multipath slow fading channels. This model helps to derive the theoretical bit error rate of the system. In addition, the effect of using different prototype filters with different time and frequency localisations can be analysed.

3.5.1. Transmission model

The core of the WHT/OFDM/OQAM system is the OFDM/OQAM system itself. However, the transmitted symbols need to be distributed by the Walsh Hadamard transform after the QAM modulator, as mentioned earlier.

The complex coefficients $c_{i,n}$ that originated from the QAM modulator is converted to real numbers $x_{i,n}$ using the C2R block which introduces a delay of τ_o between the real and the imaginary parts of the complex numbers, as explained previously. Therefore, the output of the C2R can be written as [18, 54, 59-60]

$$x_{i,2n} = Re(c_{i,n}) \tag{3.8}$$

$$x_{i,2n+1} = \mathrm{Im}(c_{i,n}) \tag{3.9}$$

The WHT operation for distributing all the input symbol coefficients over all subcarriers is carried out for *m=0, 1 … M-1*:

$$a_{m,n} = \sum_{i=0}^{M-1} WH_{m,i}\, x_{i,n} \tag{3.10}$$

Now, the continuous-time version of the transmitted signal can be expressed same as the one for the OFDM/OQAM as

$$\begin{aligned} s(t) &= \sum_{m=0}^{M-1} \sum_{n=-\infty}^{\infty} \sum_{i=0}^{M-1} WH_{m,i}\, x_{i,n}\, \theta_{m,n} g(t - n\tau_o) e^{j2\pi mt/M} \\ &= \sum_{m=0}^{M-1} \sum_{n=-\infty}^{\infty} a_{m,n} \underbrace{\theta_{m,n} g(t - n\tau_o) e^{j2\pi mt/M}}_{g_{m,n}(t)} \end{aligned} \tag{3.11}$$

where

$$\theta_{m,n} = e^{j(\pi/2)(m+n)} = j^{m+n} \tag{3.12}$$

The frequency selective time invariant multipath fading channel can be represented by FIR filter with complex coefficients. The impulse response can be expressed as

$$h(t,\tau) = \sum_{d=0}^{D-1} h_d\, \delta(t - \tau_d) \tag{3.13}$$

where h_d is complex path gain of d^{th} path, τ_d is the delay of d^{th} path, D is the total number of channel paths, and δ (·) is Kronecker delta function. Without loss of generality, it can be assumed that h_d is a set of independent path gains that are normalised such that $\sum_{d=0}^{D-1} E\{|h_d|^2\} = 1$. In order to maintain the causality of the system, τ_0 is assumed equal to zero i.e. (τ_0 = 0) [61].

The corresponding frequency domain of the channel model can be written as

$$H_m = \sum_{d=0}^{D-1} h_d\, e^{-j2\pi m\tau_d/M} \qquad m = 0, 1, \ldots, M-1 \tag{3.14}$$

For the derivation simplicity, the noise term is ignored at this point. Therefore, the received signal $r(t)$ is equal to:

$$\begin{aligned} r(t) &= s(t) \otimes h(t) \\ &= \sum_{d=0}^{D-1} h(t,\tau_d) s(t-\tau_d) \\ &= \sum_{d=0}^{D-1} h_d \sum_{n=-\infty}^{\infty} \sum_{m=0}^{M-1} a_{m,n} g(t-\tau_d - n\tau_o)\theta_{m,n} e^{j2\pi m(t-\tau_d)/M} \end{aligned} \tag{3.15}$$

where $\otimes$ denotes convolution operation.

Assuming the number of subcarriers M is large enough, so the channel is a flat fading at each subcarrier, therefore, each subcarrier bandwidth is less than the channel coherence bandwidth. As a result, it is valid to assume that the variations in the prototype filter relatively small in time over the interval ($\tau_0 - \tau_{D-1}$), which can be written as

$$g(t - \tau_d - n\tau_o) \approx g(t - n\tau_o) \tag{3.16}$$

At the receiver, the received signal is demodulated by passing through the matched filterbank of the receiver as the following:

$$
\begin{aligned}
y_{m_o\,,\,n_o} &= \int_{-\infty}^{\infty} r(t) g^*_{m_o\,,\,n_o}(t)\, dt \\
&= \sum_{n=-\infty}^{\infty} \sum_{m=0}^{M-1} a_{m,n}\, \Delta\theta \sum_{d=0}^{D-1} h_d e^{-\frac{j2\pi\, m\, \tau_d}{M}} \\
&\times \int_{-\infty}^{\infty} g(t - n\tau_o) g(t - n_o\tau_o)\; e^{j\frac{2\pi}{M}(m-m_o)t} dt
\end{aligned}
\tag{3.17}
$$

where $\Delta\theta = j^{(m+n)-(m_o+n_o)}$.

This equation can be written in a compact way using ambiguity function based expression. The expression for the ambiguity function that mentioned before can be recalled back:

$$
Ag(\tau, v) = \int_{-\infty}^{\infty} g\left(t + \frac{\tau}{2}\right) g^*\left(t - \frac{\tau}{2}\right) e^{j2\pi v t} dt \tag{3.18}
$$

By changing the variables of equation (3.17) as $\xi + \frac{\tau'}{2} = t - n\tau_o$ and $\xi - \frac{\tau'}{2} = t - n_o\tau_o$, and $g(t)$ is known as a real function, then $g(t) = g^*(t)$, that results in:

$$
\begin{aligned}
y_{m_o\,,\,n_o} &= \sum_{n=-\infty}^{\infty} \sum_{m=0}^{M-1} a_{m,n}\, \Delta\theta \sum_{d=0}^{D-1} h_d e^{-\frac{j2\pi\, m\, \tau_d}{M}} \\
&\times \int_{-\infty}^{\infty} g(\xi + \frac{\tau'}{2}) g(\xi - \frac{\tau'}{2})\; e^{j\frac{2\pi}{M}(m-m_o)(\xi + \frac{(n+n_o)\tau_o}{2})} d\xi
\end{aligned}
\tag{3.19}
$$

which leads to:

$$
\begin{aligned}
y_{m_o\,,\,n_o} &= \sum_{n=-\infty}^{\infty} \sum_{m=0}^{M-1} a_{m,n}\, \Delta\theta e^{j\frac{\pi}{2}(m-m_o)(n+n_o)} \underbrace{\sum_{d=0}^{D-1} h_d e^{-\frac{j2\pi\, m\, \tau_d}{M}}}_{H_m} \\
&\times Ag\left[(n_o - n)\tau_o\,, (m - m_o)\frac{1}{M}\right]
\end{aligned}
\tag{3.20}
$$

The above equation can be arranged by splitting the summations over *m* and *n* in two parts, one for $m,n = m_o,n_o$ and one for $m,n \neq m_o,n_o$, so:

$$
\begin{aligned}
y_{m_o\,,\,n_o} &= H_{m_o} a_{m_o\,,\,n_o} \\
&+ \sum_{m,n \neq m_o\,,\,n_o} a_{m,n}\, \Delta\theta e^{j\frac{\pi}{2}(m-m_o)(n+n_o)} H_m
\end{aligned}
\tag{3.21}
$$

$$\times\ Ag\left[(n_o - n)\tau_o\ , (m - m_o)\frac{1}{M}\right]$$

Now the equalization stage is considered and set to be zero-forcing type for simplicity. In addition, the AWGN noise term η is included with (3.21), therefore this equation can be written as

$$\begin{aligned}\hat{a}_{m_o\ ,\ n_o} &= a_{m_o\ ,\ n_o} \\ &+ \underbrace{\sum_{m,n\ \neq\ m_o\ ,\ n_o} a_{m,n}\,\Theta_{m,n}\frac{H_m}{H_{m_o}}Ag\left[(n_o - n)\tau_o\ , (m - m_o)\frac{1}{M}\right]}_{I_{m_o\ ,\ n_o}:\ ISI+ICI} + \frac{\eta_{m_o,\ n_o}}{H_{m_o}} \\ &= a_{m_o\ ,\ n_o} + I_{m_o\ ,\ n_o} + \psi_{m_o\ ,\ n_o} \\ &= a_{m_o\ ,\ n_o} + \underbrace{I_{m_o\ ,\ n_o}\big|_{(m=m_o, n\neq n_o)}}_{ISI} + \underbrace{I_{m_o\ ,\ n_o}\big|_{(m\neq m_o,)}}_{ICI} + \psi_{m_o\ ,\ n_o}\end{aligned} \tag{3.22}$$

where $\Theta_{m,n} = \Delta\theta e^{j\frac{\pi}{2}(m-m_o)(n+n_o)}$, $I_{m_o\ ,\ n_o}$ represents the interference caused by the surrounding subcarriers to the designated subcarrier at m_o,n_o and $\psi_{m_o\ ,\ n_o}$ stands for the equalized noise term.

To reconstruct the transmitted symbol, the inverse Walsh-Hadamard transform needs to be applied to the demodulated symbol $\hat{a}_{m\ ,n}$

$$\begin{aligned}\hat{x}_{q\ ,n_o} &= \sum_{m=0}^{M-1} WH_{q,m}\,(a_{m\ ,\ n_o} + I_{m\ ,\ n_o} + \psi_{m\ ,\ n_o}) \\ &= \sum_{i=0}^{M-1} x_{i,n} \sum_{m=0}^{M-1} WH_{q,m}\,WH_{m,i} + \sum_{m=0}^{M-1} WH_{q,m}\,I_{m,\ n_o} + \sum_{m=0}^{M-1} WH_{q,m}\,\psi_{m,n_o}\end{aligned} \tag{3.23}$$

The WHT matrix being orthogonal, that is,

$$\sum_{m=0}^{M-1} WH_{q,m}\,WH_{m,i} = \begin{cases}1 & if\ \ q = i \\ 0 & if\ q \neq i\end{cases} \tag{3.24}$$

Finally, the recovered symbol before taking the real part is obtained:

$$\hat{x}_{q\ ,n_o} = x_{q,\ n_o} + \underbrace{\sum_{m=0}^{M-1} WH_{q,m}\,I_{m\ ,\ n_o}}_{CI_{q\ ,n_o}} + \underbrace{\sum_{m=0}^{M-1} WH_{q,m}\,\psi_{m\ ,\ n_o}}_{\Psi_{q\ ,n_o}} \tag{3.25}$$

Therefore, the demodulated symbol consists of the original transmitted symbol plus two not welcomed terms; the first one $CI_{q\ ,n_o}$ belongs to the residual interference from the

surrounding subcarriers, and the second one Ψ_{q,n_o} belongs to the additive white Gaussian noise. The analysis of the interference term takes place in the next section.

The noise term in (3.25) needs in-depth study; the WHT spreads the noise effect uniformly on all the subcarriers, which might be beneficial at the first thought. However, if the channel has weak or zero value at certain frequency (or frequencies), this results in an infant value for ψ_{m,n_o} that spreads over all the other subcarriers. Consequently, the whole symbol coefficients are corrupted and degradation in the performance of the system resulted. In order to overcome this problem, a minimum mean square error equalizer is exploited instead of the ZF equalizer to mitigate the amplification of the noise term.

3.5.2. Analysis of the inherited interference

In WHT/OQAM and OQAM modulators, the minimum length of the filter is equal to *M* while the expansion factor is only *M/2*, which at all times is less than the length of the prototype filter. Therefore, there is permanent overlap between successive symbols and this overlap depends on the length of the prototype filter being used. In other words, there is always an interference exist in the demodulator side even for the transmission over an ideal channel [18, 59-60, 62].

From the previous equations (3.25) and (3.22), the interference term CI_{q,n_o} which originated from I_{m_o,n_o} for each subcarrier refers to the inter-symbol interference (ISI) when $m = m_o$ and $n \neq n_o$ and the inter-carrier interference (ICI) when $m \neq m_o$ and $n = n_o$. This complex interference is generated from the neighbouring subcarriers to the designated one. This interference can be best interpreted in the time-frequency lattice illustrated in Figure 3.3.

The chosen subcarrier at m_o,n_o is affected by the majority of the interference from the 1st-tap neighbours indicated by the green colour. As the zone is extended to include the 2nd-tap neighbours indicated by the blue colour, the interference power decreases. However, this interference power distribution depends on the time-frequency localisation of the selected prototype filter. Therefore, the localisation in time and frequency can limit this interference to smaller zones.

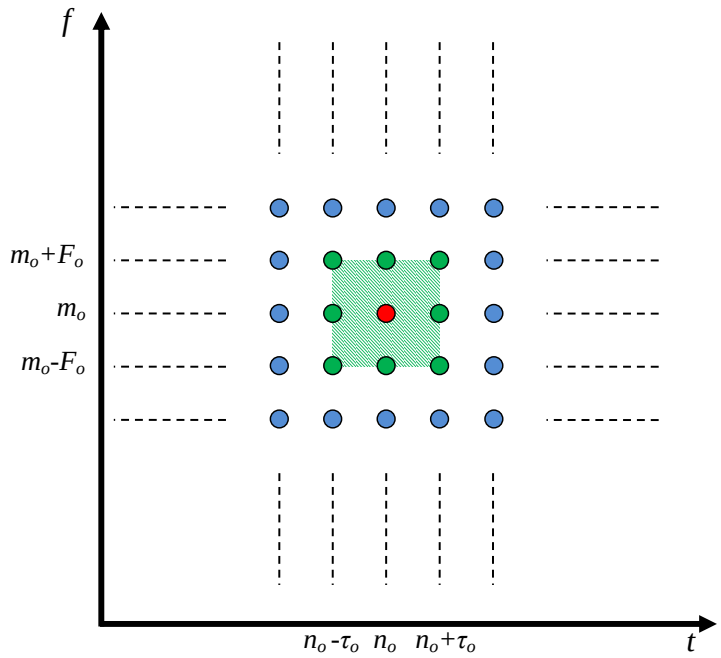

Figure 3.3 Time-Frequency lattice

To gain more insight view, Figure 3.4 gives better understanding of the energy distribution on the time-frequency plane for the IOTA prototype filter of length $4M$ or for short refereed to IOTA4. The energy of the pulse, from its name, is isotropically distributed in both time and frequency directions. However, the bulk of the energy can be limited to the 2^{nd}-tap zone. This limits the interference of any subcarrier filter with this prototype filter to no more than 3^{rd}-tap zone. Therefore, this confirms the importance of selecting an appropriate prototype filter in the design process.

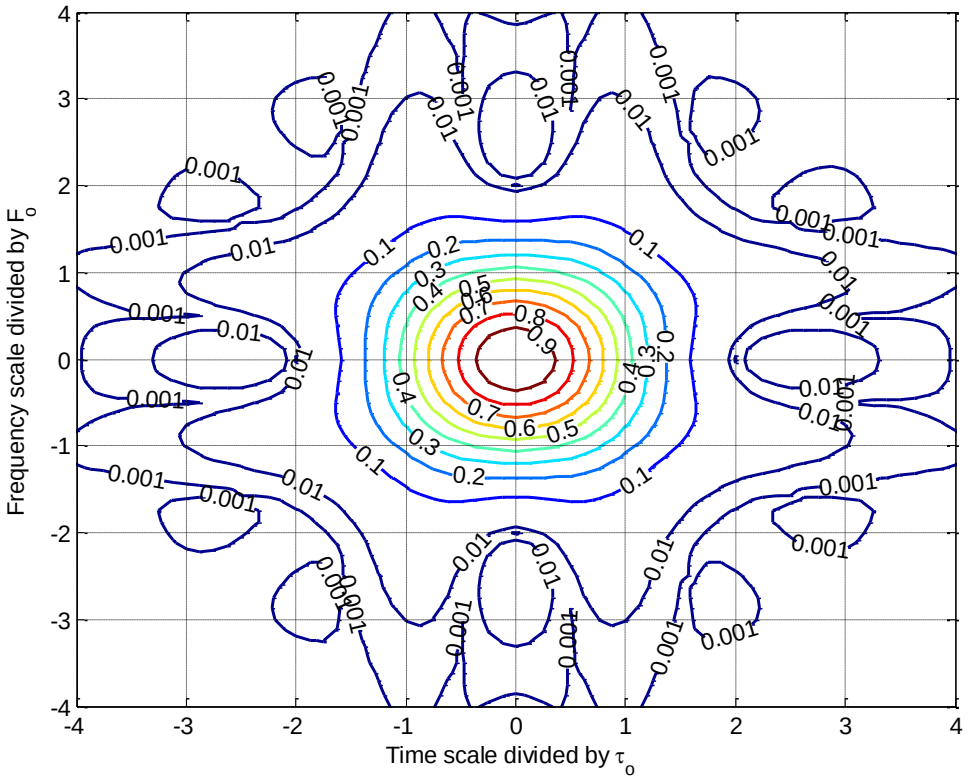

Figure 3.4 IOTA4 prototype filter time-frequency localisation

Although it is mentioned the interference is already existed in the system even over an ideal channel, it is important to differentiate between the ideal case and the fading channel. For an ideal channel that has neither distortion nor noise, despite the interference existence, the system can still reconstruct the transmitted symbol in the real field utilizing the orthogonality condition of the OQAM. This is possible because the allowed interference only present as a pure imaginary term, which is taken away at the demodulator side. In term of mathematics, by recalling equation (3.22) for the distortion free and noiseless channel, it can be written as

$$\begin{aligned}\hat{a}_{m_o\,,\,n_o} &= a_{m_o\,,\,n_o} + \sum_{m,n \neq m_o\,,\,n_o} a_{m,n}\,\Theta_{m,n} Ag\left[(n_o - n)\tau_o\,,(m - m_o)\frac{1}{M}\right] \\ &= a_{m_o\,,\,n_o} + I_{m_o\,,\,n_o}\end{aligned} \tag{3.26}$$

Due to the orthogonality condition the term $\Theta_{m,n} Ag\left[(n_o - n)\tau_o\,,(m - m_o)\frac{1}{M}\right]$ is a pure imaginary value, as a result $I_{m_o\,,\,n_o}$ is removed at the R2C block.

Alternatively, for the fading channel situation, the effect of the channel needs to be included by adding the channel term $\frac{H_m}{H_{m_o}}$ to the previous equation. This makes the value of $I_{m_o\,,\,n_o}$ not anymore a pure imaginary and takes a complex value as shown below

$$I_{m_o\,,\,n_o} = \sum_{m,n \neq m_o\,,\,n_o} a_{m,n}\Theta_{m,n}\frac{H_m}{H_{m_o}} Ag\left[(n_o - n)\tau_o\,,(m - m_o)\frac{1}{M}\right] \tag{3.27}$$

However, if the channel coefficients are assumed to slightly varying or be the same as H_{m_o} for the neighbouring subcarriers and the prototype filter is well localised in time and frequency then the real value of $I_{m_o\,,\,n_o}$ can be regarded equal to zero or below the noise level and can be ignored [60].

Although this assumption is correct, the effect of this interference remain depends on the type of the channel, and the constellation order of the modulation scheme being exploited. In the high constellation orders, higher signal to noise ratio is required to meet certain level of bit error rate, this increases the energy carried over $a_{m,n}$ and raises the interference level. However, for order of constellation equals to 16 the effect can be neglected.

3.5.3. Theoretical bit error rate (BER) analysis

To evaluate the performance of this system compared with other systems, the bit error rate is utilised as a metric. Therefore, the aim of this section is to derive a mathematical form to calculate the BER over different kind of environments. The best way to do that is by utilising the matrix representation as Figure 3.5, which explains the analysed system with matrix notations. The received symbol, which contains the residual interference and the additive white Gaussian noise, can be expressed as [46, 63]

$$\widehat{\boldsymbol{X}} = \boldsymbol{WHT^{-1}\,\Theta^{-1}Q\,F\,P^{-1}(P\,F^{-1}\,\Theta\,WHT\,X \otimes h) + WHT^{-1}\,\Theta^{-1}QFP^{-1}v} \tag{3.28}$$

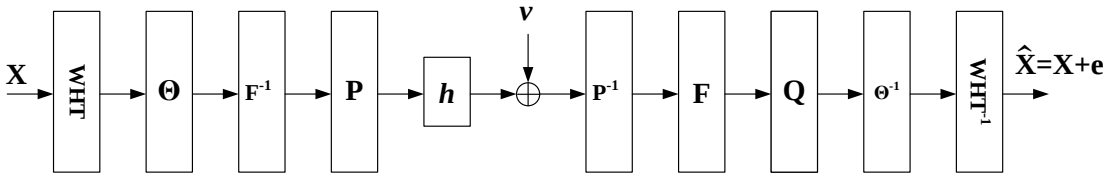

Figure 3.5 The analysed WHT/OFDM/OQAM system

where $\boldsymbol{X} = [x_0, x_1, \ldots, x_{M-1}]^T$ is the transmitted real symbol, $\boldsymbol{WHT} = \boldsymbol{WHT^{-1}}$ is the Walsh-Hadamard matrix of size *M* x *M*, $\boldsymbol{\Theta}$ is a diagonal matrix with diagonal elements equal to j^m with *m= 0, 1, ..., M-1*, while $\boldsymbol{\Theta^{-1}}$ is the complex conjugate of the $\boldsymbol{\Theta}$. In addition, $\boldsymbol{F}$ and $\boldsymbol{F^{-1}}$ are the DFT and IDFT matrices respectively. Moreover, $\boldsymbol{P}$ and $\boldsymbol{P^{-1}}$ are diagonal matrices with the filter polyphase elements on the diagonal. The channel is indicated by $\boldsymbol{h}$ to represent the impulse response of the channel, while the AWGN is symbolised by the addition of $\boldsymbol{v}$. The equalization stage indicated by $\boldsymbol{Q}$ corresponds to the MMSE equalizer matrix with diagonal elements equal to $\frac{\gamma H_m^*}{1+\gamma|H_m|^2}$ with γ refers to the signal to noise ratio E_s/N_o and H_m to the channel frequency response with index *m*.

To reorganize equation (3.28) by utilizing the outcome from equation (3.21) and (3.22) which separate the useful coefficients from the interference ones, it can be written as

$$\widehat{\boldsymbol{X}} = \underbrace{\boldsymbol{WHT^{-1}}\,\boldsymbol{Q}\,\boldsymbol{H}\,\boldsymbol{A}}_{\boldsymbol{\Gamma}} + \boldsymbol{WHT^{-1}}\,\boldsymbol{Q}\,\boldsymbol{B} + \boldsymbol{WHT^{-1}}\,\boldsymbol{Q\Lambda} \tag{3.29}$$

with $\boldsymbol{A}$ is a vector with elements can be calculated using (3.10), $\boldsymbol{B}$ is the residual interference vector with each element is computed the same way of (3.27) taking the ZF term out yielding to $\sum_{m,n \neq m_o\,,\,n_o} a_{m,n}\Theta_{m,n}\,H_m Ag\left[(n_o - n)\tau_o\,,(m - m_o)\frac{1}{M}\right]$, and $\boldsymbol{\Lambda}$ is the filtered AWGN vector or the frequency domain noise vector.

Since the noise elements in $\boldsymbol{v}$ are complex uncorrelated Gaussian random variables with variance N_o with equal variance to the real and imaginary parts, the elements of $\boldsymbol{\Lambda}$ maintain the same properties with the same variance because of the unitary property of the receiver filterbank matrix. Subsequently, the real part only is taken at the output that contains half of the noise power. It is worth noting that the reconstruction process of the complex symbol via R2C block from two successive received symbols $\widehat{X}$ that has a variance σ_x^2 means a restoration to the noise level, thus no gain is expected from that.

The first case to be considered is the transmission over AWGN channel. So the received symbol can be simply evaluated by setting $H_m = 1$ in (3.29) and taking the real part of the received symbol as

$$\Re\,(\,\widehat{\boldsymbol{X}} = \boldsymbol{WHT^{-1}}\,\boldsymbol{WHT}\,\boldsymbol{X} + \boldsymbol{WHT^{-1}}\,\boldsymbol{B}|\boldsymbol{H} = 1 + \boldsymbol{WHT^{-1}}\,\boldsymbol{\Lambda})$$

$$\widehat{\boldsymbol{X}} = \boldsymbol{X} + \Re(\boldsymbol{WHT^{-1}}\,\boldsymbol{B}|\boldsymbol{H} = 1) + \Re(\boldsymbol{WHT^{-1}}\,\boldsymbol{\Lambda}) \tag{3.30}$$

By the definition of OFDM/OQAM the term $(\boldsymbol{WHT^{-1}}\boldsymbol{B}|\boldsymbol{H} = 1)$ is a pure imaginary so it equals to zero. Nevertheless, if the prototype filter is not very well localized in time

and frequency or for the case of NPR this term holds a small complex value that might affect the output.

The general form for the signal to noise ratio at any subcarrier can be expressed as [46]

$$SNR_m = \frac{E\{|\Gamma_m|^2\}}{E\{|\hat{x}_m|^2\} - E\{|x_m|^2\}} \tag{3.31}$$

Therefore the expected value $E\{|\Gamma_m|^2\}$ can be evaluated as

$$E\{|\Gamma_m|^2\} = \sigma_x^2 \tag{3.32}$$

while the error variance can be computed as

$$\begin{aligned} E\{|\hat{x}_m|^2\} - E\{|x_m|^2\} &= \sigma_x^2 + (\sigma_x^2 \alpha | H_m = 1) \ + \frac{N_o}{2} - \sigma_x^2 \\ &= (\sigma_x^2 \alpha | H_m = 1) \ + \frac{N_o}{2} \end{aligned} \tag{3.33}$$

with

$$\alpha = \sum_{m,n \neq m_o\,,\, n_o} \left| \Re \left\{ \Theta_{m,n} H_m A g \left[(n_o - n)\tau_o\,, (m - m_o)\frac{1}{M} \right] \right\} \right|^2 \tag{3.34}$$

It worth to mention that WHT matrix is a unitary matrix so that $\sum_m |WH|^2 = 1$ which is not affecting the power of the signal, thus it can be omitted from the calculations. For that reason, it is easily to notice that the addition of the WHT on the system does not affect the performance of the system over AWGN channel. In addition, since the fact that the interference is composed of the sum of random variables, thus the interference can be assumed to have Gaussian distribution. Moreover, the complex symbol at the transmitter input has a variance of E_s with equal variance for both parts, real and imaginary. Therefore, when the staggering process takes place the resulting real symbols have variance of $\sigma_x^2 = E_s/2$.

So the SNR at subcarrier *m* on a flat fading channel can be written as

$$\begin{aligned} SNR_m^{AWGN} &= \frac{\sigma_x^2}{(\sigma_x^2 \alpha | H_m = 1) + \frac{N_o}{2}} \\ &= \frac{E_s}{(E_s \alpha | H_m = 1) + N_o} \\ &= \frac{\gamma}{(\gamma \alpha | H_m = 1) + 1} \end{aligned} \tag{3.35}$$

Therefore, the theoretical bit error rate (BER) for B-QAM modulation and a constellation (Gray-coded) of order 2^b ($b = \log_2 B$) can be calculated using this closed-form expression:

$$\mathcal{P}^{AWGN} = \frac{1}{M}\sum_{m=0}^{M-1}\frac{4}{b}\left(1-\frac{1}{\sqrt{B}}\right) erfc\left(\sqrt{\frac{3\,SNR_m^{AWGN}}{(B-1)}}\right) \tag{3.36}$$

where *erfc*(*x*) or the Q-function can be defined as $erfc(x) = \frac{1}{\sqrt{2\pi}}\int_x^{\infty} e^{\frac{t^2}{2}}dt.$

In order to ensure the previous analysis is valid and accurate, a simulation program is used to show a comparison between the theoretical and simulation results. A comparison between theoretical BER and simulation results is demonstrated in Figure 3.6 for three different constellation orders; 16, 64 and 256. The number of subcarrier used is 128 and the filer is IOTA4. These results confirm the correctness and the accuracy of the previously derived equations.

For the frequency selective channel situation, the equalization stage is inevitable to compensate for the channel destruction on the transmitted signal. The equalizer stage is set to be minimum mean square error (MMSE) type for the reason given previously. By referring back to (3.29) and (3.31) the received symbol can be written as

$$\Re(\widehat{\boldsymbol{X}} = \boldsymbol{WHT^{-1}\,Q\,H\,A + WHT^{-1}\,Q\,B + WHT^{-1}\,Q\Lambda}) \tag{3.37}$$

Now the error signal is the difference between the received symbol and the transmitted one as the following equation:

$$\begin{aligned}\boldsymbol{e} &= \widehat{\boldsymbol{X}} - \boldsymbol{X}\\ &= \Re(\boldsymbol{WHT^{-1}\,Q\,H\,A + WHT^{-1}\,Q\,B + WHT^{-1}\,Q\Lambda - WHT^{-1}I\,WHTX})\\ &= \Re(\boldsymbol{WHT^{-1}\,(Q\,H - I\,)WHTX + WHT^{-1}\,Q\,B + WHT^{-1}\,Q\Lambda})\end{aligned} \tag{3.38}$$

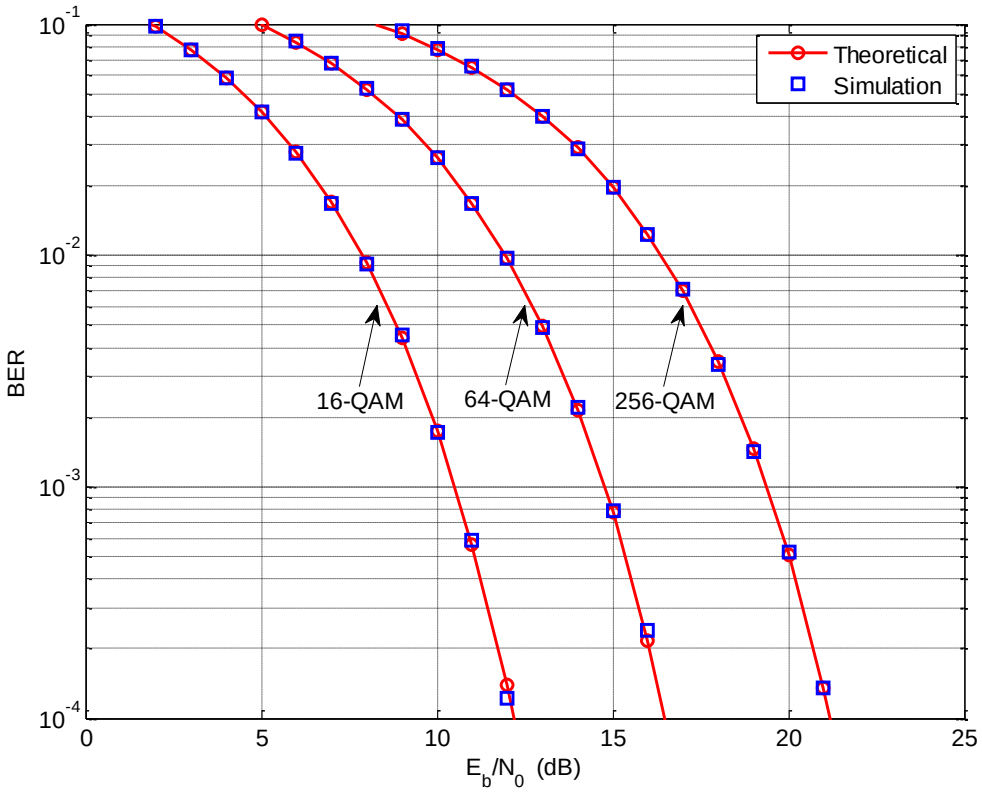

Figure 3.6 Theoretical and simulation comparison for the BER over AWGN channel with M=128 and IOTA4 filter.

where ***I*** represents an identity matrix. The input symbols are assumed to be uncorrelated with variance $\sigma_x^2 = E_s/2$ as indicated previously. Therefore, the expected value of the error signal has this equation:

$$E\{|e_m|^2\} = \sum_{q=0}^{M-1} |WH_{i,q}|^2 \frac{\sigma_x^2}{(1+\gamma|H_m|^2)^2} + \sum_{q=0}^{M-1} |WH_{i,q}|^2 \frac{\sigma_x^2\, \alpha\, \gamma^2 |H_m|^2}{(1+\gamma|H_m|^2)^2}$$
$$+ \sum_{q=0}^{M-1} |WH_{i,q}|^2 \frac{N_o\, \gamma^2 |H_m|^2}{2(1+\gamma|H_m|^2)^2}$$
$$= \sum_{q=0}^{M-1} |WH_{i,q}|^2 \frac{E_s(1+\alpha\, \gamma^2|H_m|^2 + \gamma\, |H_m|^2)}{2(1+\gamma|H_m|^2)^2} \quad (3.39)$$

While the expected value of the received m^{th} subcarrier can be expressed by utilizing (3.37) as

$$E\{|\hat{x}_m|^2\} = \sum_{q=0}^{M-1} |WH_{i,q}|^2 \frac{\sigma_x^2\, \gamma^2 |H_m|^4}{(1+\gamma|H_m|^2)^2} + \sum_{q=0}^{M-1} |WH_{i,q}|^2 \frac{\sigma_x^2\, \alpha\, \gamma^2 |H_m|^2}{(1+\gamma|H_m|^2)^2} \quad (3.40)$$

$$+\sum_{q=0}^{M-1}\left|WH_{i,q}\right|^2\frac{N_o\,\gamma^2|H_m|^2}{2(1+\gamma|H_m|^2)^2}$$

$$=\sum_{q=0}^{M-1}\left|WH_{i,q}\right|^2\frac{E_s(\,\gamma^2|H_m|^4+\alpha\,\gamma^2|H_m|^2+\gamma\,|H_m|^2)}{2(1+\gamma|H_m|^2)^2}$$

Therefore, the signal to noise ratio for subcarrier of index m is the result of the division process as

$$SNR_m^{f-select}=\frac{E\{|\hat{x}_m|^2\}}{E\{|e_m|^2\}}$$

$$=\frac{\sum_{q=0}^{M-1}\left|WH_{i,q}\right|^2\frac{(\,\gamma^2|H_m|^4+\alpha\,\gamma^2|H_m|^2+\gamma\,|H_m|^2)}{(1+\gamma|H_m|^2)^2}}{\sum_{q=0}^{M-1}\left|WH_{i,q}\right|^2\frac{(1+\alpha\,\gamma^2|H_m|^2+\gamma\,|H_m|^2)}{(1+\gamma|H_m|^2)^2}} \tag{3.41}$$

Consequently, the theoretical BER for the B-QAM (Gray-coded) over frequency selective multipath channel can be calculated using the following closed form expression:

$$\mathcal{P}^{f-select}=\frac{1}{M}\sum_{m=0}^{M-1}\frac{4}{b}\left(1-\frac{1}{\sqrt{B}}\right)erfc\left(\sqrt{\frac{3\,SNR_m^{f-select}}{(B-1)}}\right) \tag{3.42}$$

To compare between the theoretical BER evaluated by the derived equations and the simulation results, two different scenarios are used over different channels. The first system is utilizing 128 subcarriers with IOTA4 prototype filter to transmit 20000 symbols over the modified Stanford University Interim 4 (SUI-4) channel model [64-65]. Figure 3.7 shows system performance with three QAM modulation orders: 16, 64, and 256. The theoretical BER curves in all the three modulation orders match approximately the simulation ones.

On the other hand, system two utilises 1024 subcarrier and the prototype is IOTA4. The channel is set to be the ITU-Pedestrian type B channel. The results are illustrated in Figure 3.8 for three different modulation orders: 16, 64, and 256. The theoretical BER results show very close match to the simulation results in all the provided cases. The small differences between the theoretical and simulation results are all encountered by the approximation and the assumptions undertaken to simplify the mathematical derivation. In conclusion, this proves the correctness of the analysis and the derived equations.

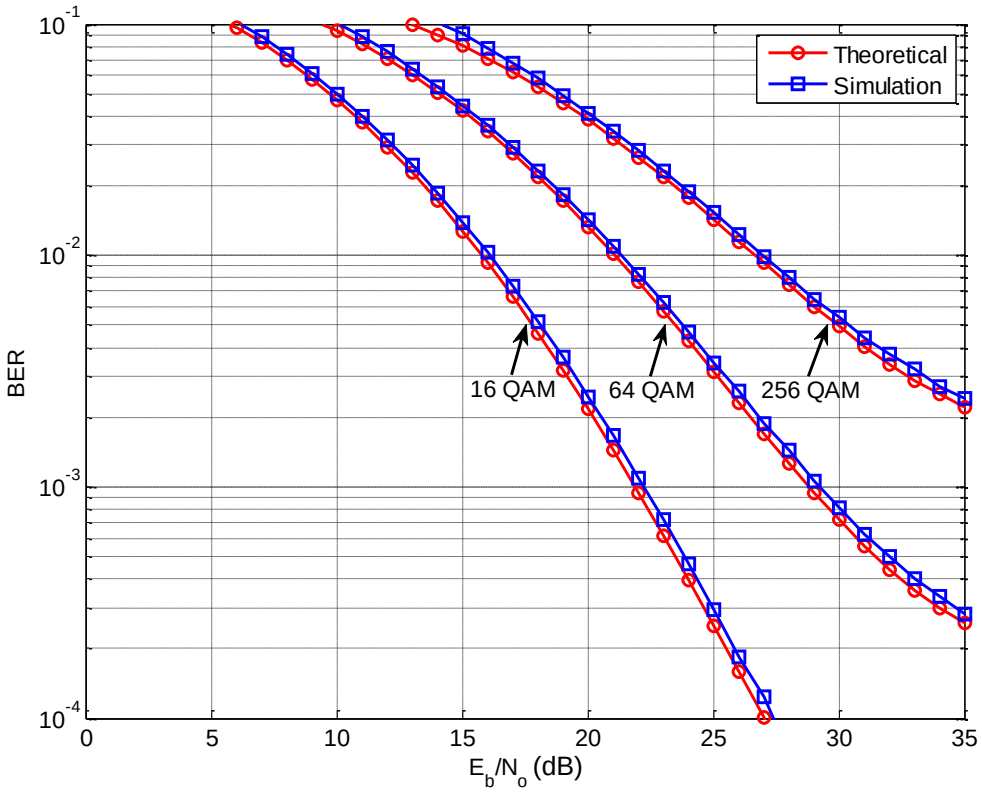

Figure 3.7 Theoretical and Simulation BER over SUI-4 channel with M=128

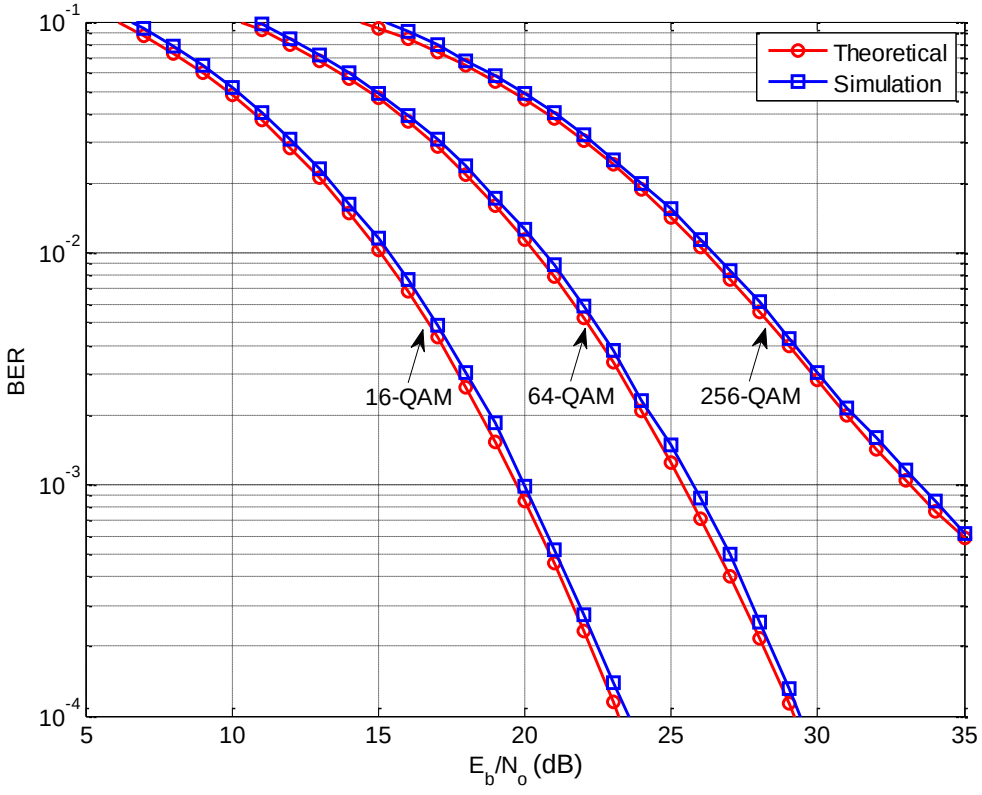

Figure 3.8 Theoretical and simulation BER over ITU-Ped. B channel with M=1024.

3.5.4. System performance

To investigate the performance of the proposed system, the WHT/OQAM is simulated alongside with normal OQAM and CP-OFDM. All systems are simulated over the same multipath fading channels. Moreover, the frame work of the WiMAX system is chosen to evaluate the efficiency of the new method. To compensate for the channel effects, WHT/OQAM employed a minimum mean square error equalizer while the other two systems utilized sufficient zero-forcing equalizers. In addition, maximum likelihood detectors are implemented in the receivers. Furthermore, the simulation is carried out using the Monte Carlo method. It is worth noting that the demodulation process is performed based on the assumption of perfect channel estimation, and perfect carrier frequency synchronization.

The main simulation parameters are set as the following:

16-QAM modulation (Gray-coded).
Number of subcarriers $M = 1024$.
Cyclic prefix length CP = $M / 4 = 256$.
IOTA pulse shaping prototype filter is utilized.
Overlapping factor $K = 4$.
Transmission bandwidth = 10 MHz.
No coding is applied.

Three channel models are used to test the system: the ITU-Pedestrian B, ITU-Vehicular A and ITU-Vehicular B [66], which comply with mobile WiMAX standard IEEE 802.16e. The power delay profiles for the three channels are given in Table 3.1. In all three cases, the OQAM system outperformed CP-OFDM by 10 $\log_{10}$ (M+CP)/M = 0.9691 dB due to the absence of power loss associated with the CP [59].

In the ITU- Pedestrian type B channel, the speed is set to 3 km/h. Alongside the simulation results, the calculated theoretical BER is also illustrated on Figure 3.9. The addition of the WHT to the system improved the bit error rate at 10^{-3} by 7dB for the OQAM case and around 8dB for the CP-OFDM. This improvement increases with the increase of signal power E_b/N_o. This improvement confirms the superiority of the proposed system over the conventional systems as a result of the frequency diversity achieved by the WHT to mitigate the deep fade on some subcarriers, while keeping all the desired properties of the OQAM such as the full usable transmission bandwidth and the lower out of band energy dissipation.

Tap	ITU-Pedestrian B		ITU-Vehicular A		ITU-Vehicular B	
	Relative delay (ns)	Average power (dB)	Relative delay (ns)	Average power (dB)	Relative delay (ns)	Average power (dB)
1	0	0	0	0.0	0	–2.5
2	200	–0.9	310	–1.0	300	0
3	800	–4.9	710	–9.0	8900	–12.8
4	1200	–8.0	1090	–10.0	12900	–10.0
5	2300	–7.8	1730	–15.0	17100	–25.2
6	3700	–23.9	2510	–20.0	20000	–16.0

Table 3.1 power delay profile of different ITU channel models.

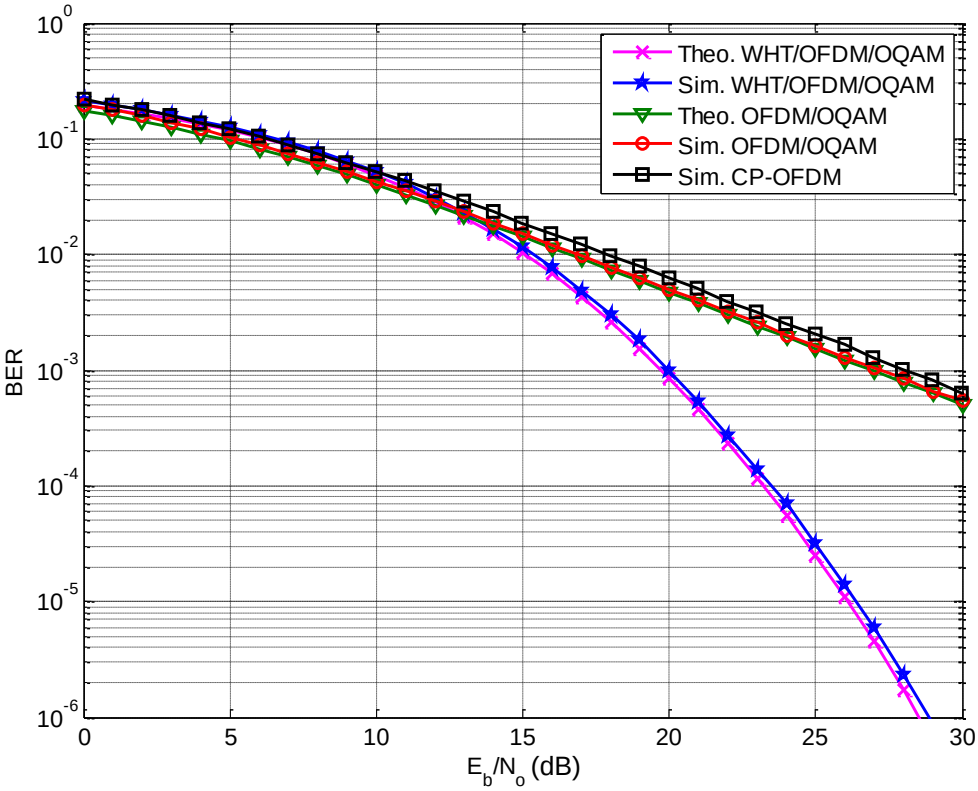

Figure 3.9 A comparison between WHT/OQAM, OQAM, and CP-OFDM over ITU-Pedestrian type B channel

In the second case, the ITU- Vehicular type A channel is selected to test the performance of the three systems. This channel model is considered while setting the speed to 60 km/h. The theoretical BER is also given in addition to the simulation results. The proposed system achieved a robust gain in BER at 10^{-3} of 5 dB compared to the OQAM and around 6dB in contrast to the CP-OFDM as depicted in Figure 3.10.

Again, the WHT/OQAM showed resilience to the fading channel and maintain better performance in term of the BER without any loss in the transmission capacity to employ channel coding.

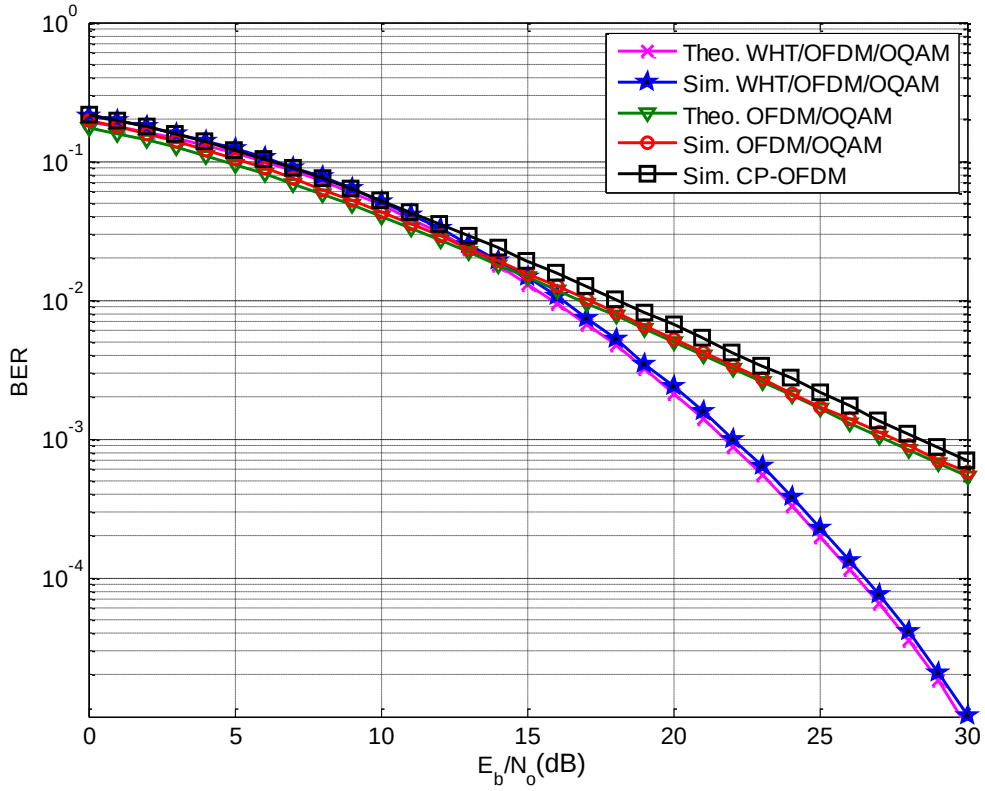

Figure 3.10 WHT/OQAM compared to OQAM and CP-OFDM over ITU-Vehicular type A channel

Likewise, since OQAM system and consequently WHT/OQAM are both sensitive to the delay spread of the channel, therefore, a higher delay spread channel profile is used to evaluate the new technique. The WHT/OQAM performed well over the ITU- Vehicular type B channel even with a higher delay spread that caused the OQAM performance to floor compared to the CP-OFDM as illustrated in Figure 3.11. The gain obtained in this situation is approximately 6 dB at $2x10^{-3}$ BER for the OQAM and 5dB in the CP-OFDM circumstances. This analysis is carried out with a speed of 120km/h.

From the previous results, the WHT/OQAM system demonstrated consistent performance over different varieties of channels. As a result, the new system features a resilience performance over multipath channels, a full utilization for the transmission bandwidth, and lower out of band energy dispersion. The integration of the transform in the system might increase the system complexity at the first glance, but the next section

will demonstrate how it is possible to reduce the complexity of the system to make it more efficient for implementation.

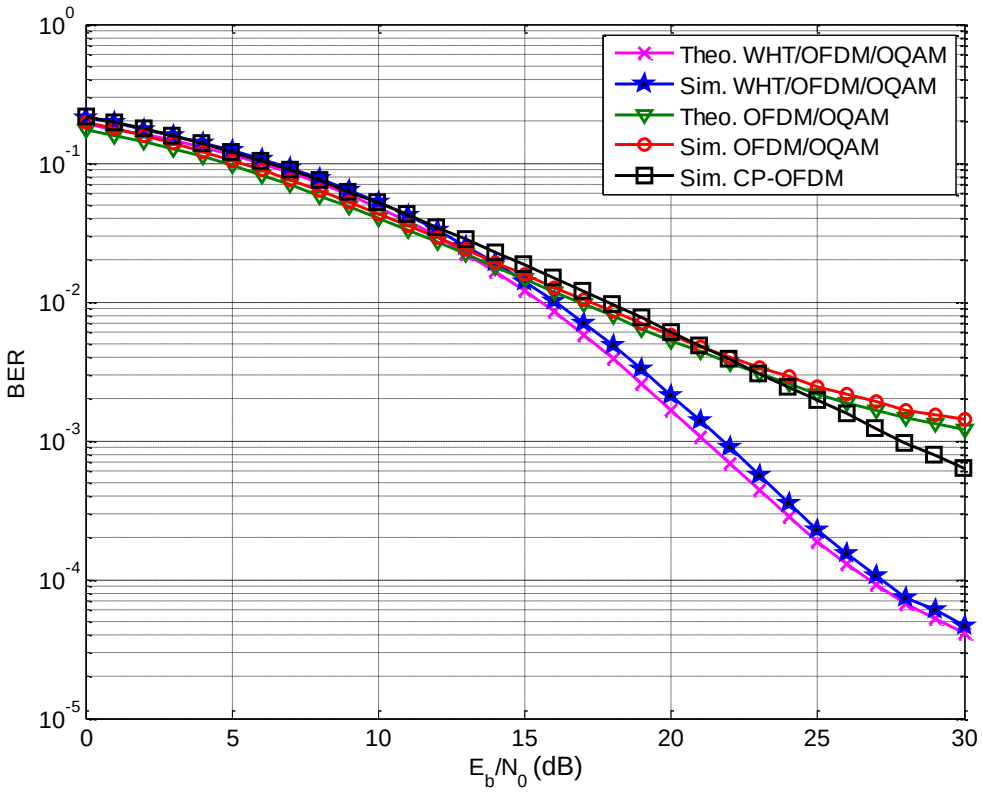

Figure 3.11 BER characteristics over the ITU- Vehicular type B channel for the three systems

3.6. WHT/OFDM/OQAM Based on Fast Algorithm

The OQAM system with all the superiorities over the conventional OFDM still suffers from the increased implementation complexity due to the addition of the filters at the transmitter and the receiver sides. However, by employing DFT filter banks with polyphase concept as stated by [18], it is possible to decrease the computational complexity. On the other hand, adding WHT to the system increases the complexity, so the motivation is to find an alternative way to implement the system and keep the complexity as low as possible.

3.6.1. Development of the V- Transform

Fast algorithms for the combination of the WHT and the FFT are already existed [46, 67-68], nevertheless, in the circumstance of WHT/OQAM, those fast algorithms do not

fit properly. By referring back to Figure 3.2, the phase mapping block demands to be considered before any fast algorithm can be developed.

The phase mapping matrix is a diagonal matrix with elements depend not only on the subcarrier index, but also on the time index as stated in equation (2.1). Therefore, this mapping matrix can be split into two parts, as illustrated in Figure 3.12: frequency or subcarrier dependant and time dependant. As a result, the diagonal elements of subcarrier dependant matrix $\boldsymbol{J}$ are replaced by j^{m^2} where m is the diagonal element index and $j = \sqrt{-1}$. For instance, $\boldsymbol{J_4}$ can be written as

$$\boldsymbol{J}_4 = \begin{bmatrix} 1 & 0 & 0 & 0 \\ 0 & j & 0 & 0 \\ 0 & 0 & 1 & 0 \\ 0 & 0 & 0 & j \end{bmatrix} \tag{3.43}$$

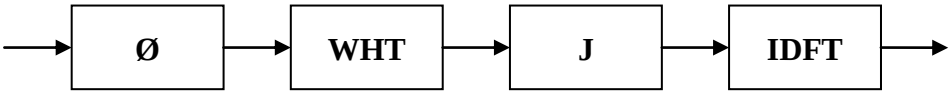

Figure 3.12 The resulting configuration for the phase mapping matrices

This phase mapping matrix is placed after the WHT matrix. Whereas, the time dependant matrix $\boldsymbol{Ø}$ needs to be shifted prior to the WHT matrix with all diagonal elements set to be:

$$\boldsymbol{Ø} = \begin{cases} \boldsymbol{I} & n\ even \\ -j\boldsymbol{I} & n\ odd \end{cases} \tag{3.44}$$

Taking the time associated matrix out, the three matrices can be expressed as

$$\boldsymbol{Y}_M = \frac{1}{M}\boldsymbol{DFT}_M^{-1}\boldsymbol{J}_M\,\boldsymbol{WHT}_M \tag{3.45}$$

where $\boldsymbol{DFT}_M^{-1}$ is the IDFT matrix of order M with twiddle factor $w^n = e^{j\frac{2\pi mn}{M}}$. The IDFT matrix can be re-written in row reverse order with lower order matrices as

$$\boldsymbol{IDFTR}_M = \begin{bmatrix} \boldsymbol{A}_{\frac{M}{2}} & \boldsymbol{A}_{\frac{M}{2}} \\ \boldsymbol{B}_{\frac{M}{2}} & -\boldsymbol{B}_{\frac{M}{2}} \end{bmatrix} \tag{3.46}$$

In addition, the WHT matrix and the $\boldsymbol{J}$ matrix also can be expressed in lower order matrices as

$$\boldsymbol{WHT}_M = \begin{bmatrix} \boldsymbol{WHT}_{\frac{M}{2}} & \boldsymbol{WHT}_{\frac{M}{2}} \\ \boldsymbol{WHT}_{\frac{M}{2}} & -\boldsymbol{WHT}_{\frac{M}{2}} \end{bmatrix} \tag{3.47}$$

$$\boldsymbol{J}_M = \begin{bmatrix} \boldsymbol{J}_{\frac{M}{2}} & 0 \\ 0 & \boldsymbol{J}_{\frac{M}{2}} \end{bmatrix} \tag{3.48}$$

By evaluating (3.46),(3.47), and (3.48) into (3.45) yields:

$$\begin{aligned} \boldsymbol{V}_M &= \frac{1}{M} \begin{bmatrix} \boldsymbol{A}_{\frac{M}{2}} & \boldsymbol{A}_{\frac{M}{2}} \\ \boldsymbol{B}_{\frac{M}{2}} & -\boldsymbol{B}_{\frac{M}{2}} \end{bmatrix} \begin{bmatrix} \boldsymbol{J}_{\frac{M}{2}} & 0 \\ 0 & \boldsymbol{J}_{\frac{M}{2}} \end{bmatrix} \begin{bmatrix} \boldsymbol{WHT}_{\frac{M}{2}} & \boldsymbol{WHT}_{\frac{M}{2}} \\ \boldsymbol{WHT}_{\frac{M}{2}} & -\boldsymbol{WHT}_{\frac{M}{2}} \end{bmatrix} \\ &= \frac{1}{M} \begin{bmatrix} 2\boldsymbol{A}_{\frac{M}{2}} \boldsymbol{J}_{\frac{M}{2}} \boldsymbol{WHT}_{\frac{M}{2}} & 0 \\ 0 & 2\boldsymbol{B}_{\frac{M}{2}} \boldsymbol{J}_{\frac{M}{2}} \boldsymbol{WHT}_{\frac{M}{2}} \end{bmatrix} \end{aligned} \tag{3.49}$$

This factorization procedure can be done $\log_2 M$ times to generate a general form matrix as the following:

$$\boldsymbol{V}_M = \frac{1}{M} \times \begin{bmatrix} \frac{M}{2}\boldsymbol{A}_2\boldsymbol{J}_2\boldsymbol{WHT}_2 & 0 & \cdots & 0 & 0 \\ 0 & \frac{M}{2}\boldsymbol{B}_2\boldsymbol{J}_2\boldsymbol{WHT}_2 & & 0 & 0 \\ \vdots & & \ddots & & \vdots \\ 0 & 0 & & 4\boldsymbol{B}_{\frac{M}{4}}\boldsymbol{J}_{\frac{M}{4}}\boldsymbol{WHT}_{\frac{M}{4}} & 0 \\ 0 & 0 & \cdots & 0 & 2\boldsymbol{B}_{\frac{M}{2}}\boldsymbol{J}_{\frac{M}{2}}\boldsymbol{WHT}_{\frac{M}{2}} \end{bmatrix} \tag{3.50}$$

Although it is possible to factorize **V** matrix of any order, for simplicity, the case of M=8 is taken as an example. Equation (3.49) with order 8 can be described as

$$\boldsymbol{V}_8 = \frac{1}{8} \begin{bmatrix} 2\boldsymbol{A}_4 \boldsymbol{J}_4 \boldsymbol{WHT}_4 & 0 \\ 0 & 2\boldsymbol{B}_4 \boldsymbol{J}_4 \boldsymbol{WHT}_4 \end{bmatrix} \tag{3.51}$$

with

$$\boldsymbol{A}_4 = \begin{bmatrix} 1 & 1 & 1 & 1 \\ 1 & -1 & 1 & -1 \\ 1 & -w^2 & -1 & w^2 \\ 1 & w^2 & -1 & -w^2 \end{bmatrix} \tag{3.52}$$

$$\boldsymbol{B}_4 = \begin{bmatrix} 1 & -w^3 & -w^2 & -w \\ 1 & w^3 & -w^2 & w \\ 1 & w & w^2 & -w^3 \\ 1 & w & w^2 & w^3 \end{bmatrix} \tag{3.53}$$

Hence:

$$2\boldsymbol{A}_4\boldsymbol{J}_4\boldsymbol{WHT}_4 = 2\begin{bmatrix}1 & 1 & 1 & 1\\ 1 & -1 & 1 & -1\\ 1 & -w^2 & -1 & w^2\\ 1 & w^2 & -1 & -w^2\end{bmatrix}\begin{bmatrix}1 & 0 & 0 & 0\\ 0 & j & 0 & 0\\ 0 & 0 & 1 & 0\\ 0 & 0 & 0 & j\end{bmatrix}\begin{bmatrix}1 & 1 & 1 & 1\\ 1 & -1 & 1 & -1\\ 1 & 1 & -1 & -1\\ 1 & -1 & -1 & 1\end{bmatrix}$$

$$= \begin{bmatrix} 2-2w^2 & 2+2w^2 & 0 & 0\\ 2+2w^2 & 2-2w^2 & 0 & 0\\ 0 & 0 & 0 & 4\\ 0 & 0 & 4 & 0\end{bmatrix} \tag{3.54}$$

$$\boldsymbol{B}_4\boldsymbol{J}_4\boldsymbol{WHT}_4 = \begin{bmatrix}1 & -w^3 & -w^2 & -w\\ 1 & w^3 & -w^2 & w\\ 1 & w & w^2 & -w^3\\ 1 & w & w^2 & w^3\end{bmatrix}\begin{bmatrix}1 & 0 & 0 & 0\\ 0 & j & 0 & 0\\ 0 & 0 & 1 & 0\\ 0 & 0 & 0 & j\end{bmatrix}\begin{bmatrix}1 & 1 & 1 & 1\\ 1 & -1 & 1 & -1\\ 1 & 1 & -1 & -1\\ 1 & -1 & -1 & 1\end{bmatrix}$$

$$= \begin{bmatrix}1-jw-w^2-jw^3 & 1+jw-w^2+jw^3 & 1+jw+w^2-jw^3 & 1-jw+w^2+jw^3\\ 1+jw-w^2+jw^3 & 1-jw-w^2-jw^3 & 1-jw+w^2+jw^3 & 1+jw+w^2-jw^3\\ 1-jw+w^2-jw^3 & 1+jw+w^2+jw^3 & 1-jw-w^2+jw^3 & 1+jw-w^2-jw^3\\ 1+jw+w^2+jw^3 & 1-jw+w^2-jw^3 & 1+jw-w^2-jw^3 & 1-jw-w^2+jw^3\end{bmatrix} \tag{3.55}$$

However, equation (3.55) can be simplified more by factorizing it into sparse matrices, which reduces the computational cost of multiplication by **V** matrix, which leads to a faster algorithm for the evaluation of the **V** transform. After simple mathematical evaluations, the resulting matrix equals to

$$\boldsymbol{V}_8 = \begin{bmatrix} & & & & 0 & 0 & 0 & 0\\ & & \boldsymbol{D} & & 0 & 0 & 0 & 0\\ & & & & 0 & 0 & 0 & 0\\ & & & & 0 & 0 & 0 & 0\\ 0 & 0 & 0 & 0 & & & & \\ 0 & 0 & 0 & 0 & & \boldsymbol{E} & & \\ 0 & 0 & 0 & 0 & & & & \\ 0 & 0 & 0 & 0 & & & & \end{bmatrix} \tag{3.56}$$

with **D** and **E** equal to

$$\boldsymbol{D} = \begin{bmatrix}0.5-0.5w^2 & 0.5+0.5w^2 & 0 & 0\\ 0.5+0.5w^2 & 0.5-0.5w^2 & 0 & 0\\ 0 & 0 & 0 & 1\\ 0 & 0 & 1 & 0\end{bmatrix} \tag{3.57}$$

$$\boldsymbol{E} = \frac{1}{4}\begin{bmatrix}0 & 0 & 1-w & 1+w\\ 0 & 0 & 1+w & 1-w\\ 1+w^3 & 1-w^3 & 0 & 0\\ 1-w^3 & 1+w^3 & 0 & 0\end{bmatrix} \times \begin{bmatrix}1+w^2 & 0 & 1-w^2 & 0\\ 0 & 1+w^2 & 0 & 1-w^2\\ 1-w^2 & 0 & 1+w^2 & 0\\ 0 & 1-w^2 & 0 & 1+w^2\end{bmatrix} \tag{3.58}$$

The signal flow graph of the V transform is demonstrated in Figure 3.13.

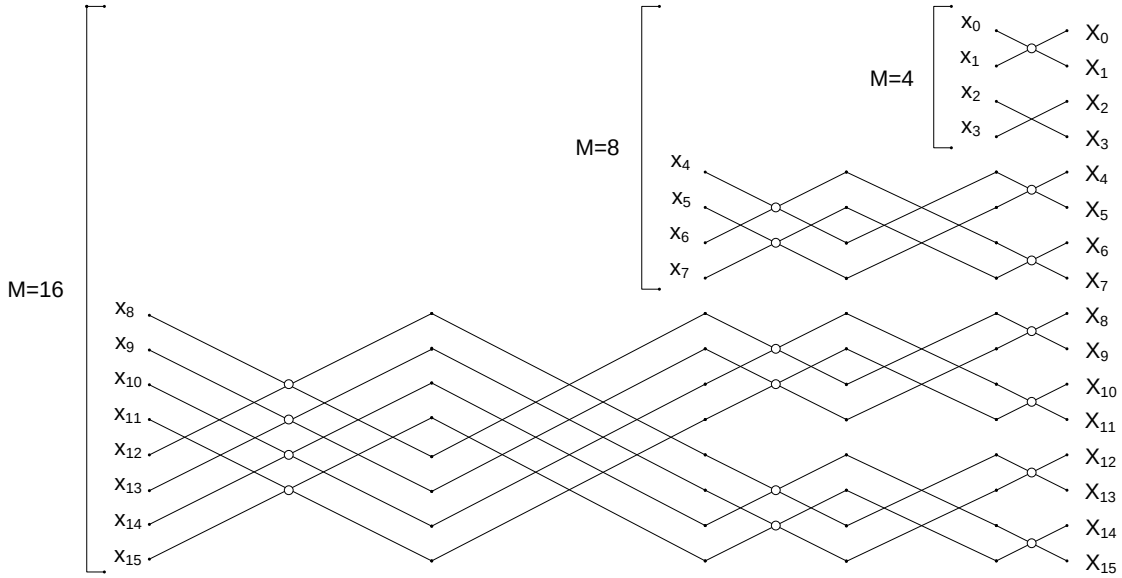

Figure 3.13 Signal flow graph for the **V** transform of order 16

3.6.2. Complexity evaluation

The computation of the resulting **V** matrix can be calculated using relatively simple radix-2 butterflies as illustrated in Figure 3.14. Each butterfly consists of three complex additions and one complex multiplication, which can be expressed for two inputs *a* and *b* as

$$out_1 = a - (a - b)\, w_1^o \tag{3.59}$$

$$out_2 = b + (a - b)\, w_1^o \tag{3.60}$$

with a twiddle factor equals to $w_1^o = (1 - w^o)/2$ and o is an integer value between 0 and *M*/2-1 according to the used butterfly.

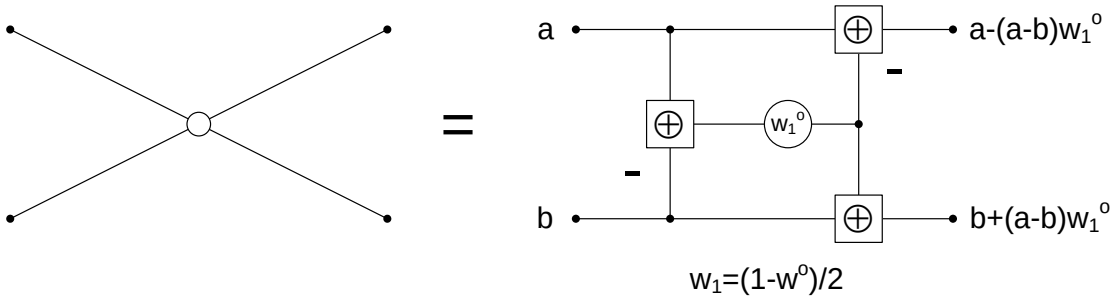

Figure 3.14 An efficient butterfly for the **V** transform

By referring back to equations (3.56), (3.57), and (3.58), clearly, the number of zero elements represents around two thirds of the matrix elements, which indicates a reduction in the number of arithmetic operations required for the calculation of the output. In addition, the distribution of these zero elements gives the **V** matrix a block diagonal structure, which has positive implications on the peak to average power ratio of the system, as it will be described in the next chapter. Furthermore, this relatively simple structure makes the extension of the transform for higher orders by just extending the lower part as demonstrated in Figure 3.13.

In the cascaded implementation by utilizing separated WHT and IFFT blocks, the WHT requires $M \log_2 M$ complex additions. Although the IDFT matrix[3] is considered in the derivation of the **V** matrix, the IFFT is the logical way to go in the implementation process for its simple structure. Therefore, the IFFT block needs $M/2 \log_2 M$ complex multiplications and $M \log_2 M$ complex additions. So the total number of complex additions required is $2M \log_2 M$ [46, 67].

On the other hand, for the V transform case, each butterfly illustrated in Figure 3.14 utilizes one multiplier and three adders, as stated earlier. In addition, the transform requires $\log_2 M$ -1 stages, which leads to a total number of used butterflies of $M/2 \log_2 M - (M\text{-}1)$. Hence, the total number (including trivial multiplications) of complex multiplications C_{Multi} and the complex additions C_{Add} can be expressed as

$$C_{Multi} = \frac{M}{2}\log_2 M - (M-1) \tag{3.61}$$

$$C_{Add} = \frac{3M}{2}\log_2 M - 3(M-1) \tag{3.62}$$

To compare the complexity of implementing the V transform over the cascaded implementation of the separated matrices. It is more relevant to compute the number of real operations (additions and multiplications) necessary for their implementations. In general, a complex addition is equivalent to two real additions, while a complex multiplication requires four real multiplications and two real additions. Consequently, the previous equations can be re-written to consider real operations only as:

$$R_{Multi} = 2M \log_2 M - 4(M-1) \tag{3.63}$$

$$R_{Add} = 4M \log_2 M - 8(M-1) \tag{3.64}$$

[3] The IDFT matrix requires M^2 complex multiplications and $M(M\text{-}1)$ complex addition for direct implementation which is not practical with large values of M.

Moreover, in the case of the WHT/OQAM system, the input is known to be only real; therefore, the output consists of *M*/2-1complex conjugate elements. As a result, the computational complexity can be halved leading to:

$$RTx_{Multi} = M \log_2 M - 2(M-1) \tag{3.65}$$

$$RTx_{Add} = 2M \log_2 M - 4(M-1) \tag{3.66}$$

At the same time, the cascaded implementation via WHT and IFFT considering real operations and the modification explained in section 3.4 which already reduce the WHT requirement to $M \log_2 M$ real additions can be expressed as

$$DTx_{Multi} = 2M \log_2 M \tag{3.67}$$

$$DTx_{Add} = 4M \log_2 M \tag{3.68}$$

From those equations, Table 3.2 can be calculated to illustrate the reduction in the complexity. Furthermore, Figure 3.15 and Figure 3.16 demonstrate the gain in the hardware with the increase of the input size M.

M	V-Transform		Cascaded WHT-IFFT	
	RTx_{Multi}	RTx_{Add}	DTx_{Multi}	DTx_{Add}
64	258	516	768	1536
128	642	1284	1792	3584
256	1538	3076	4096	8192
512	3586	7172	9216	18432
1024	8194	16388	20480	40960

Table 3.2 Comparison between the cascaded WHT-IFFT and V-transform implementation requirements in term of real operations

Clearly, the development of the V-transform leads to a significant fall in the system hardware complexity to achieve 60 percent reduction in both the number of real multipliers and adders for M = 1024. This remarkable reduction in the complexity adds another advantage to the WHT/OQAM modulation system over the conventional OFDM system.

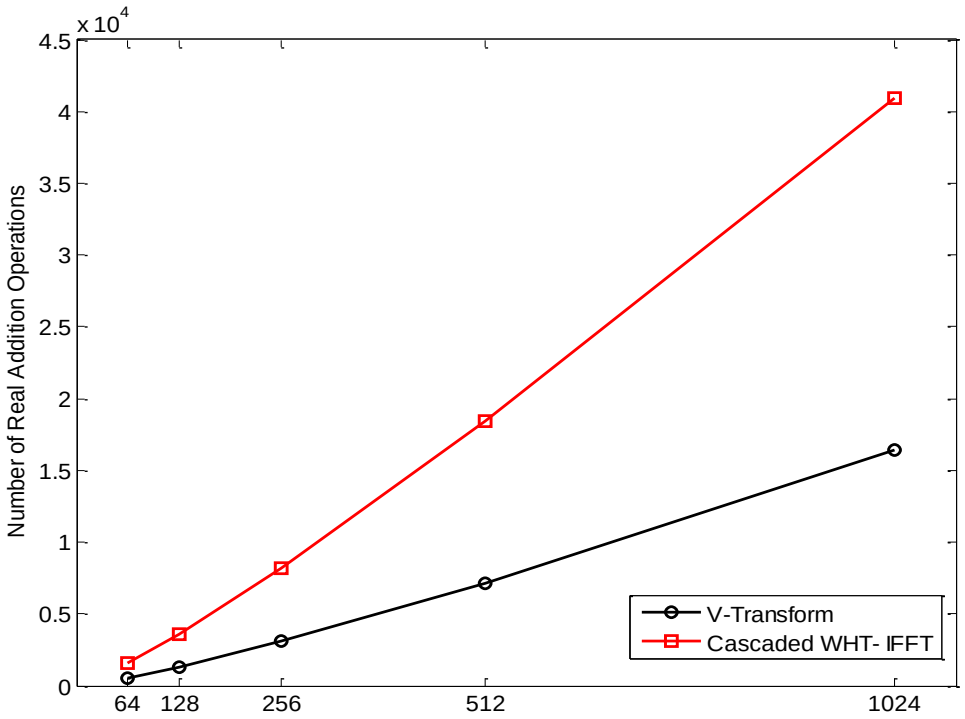

Figure 3.15 Comparison between V-transform and cascaded WHT-IFFT in the number of real additions

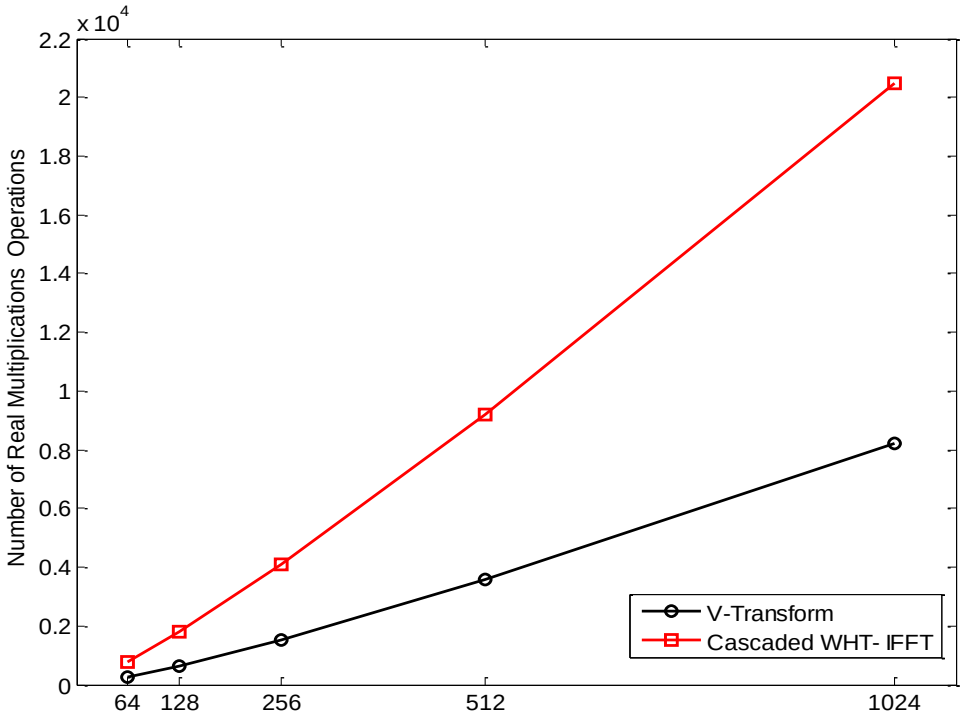

Figure 3.16 Comparison between V-transform and cascaded WHT-IFFT in the number of real multiplications

3.7. Conclusion and Summary

In this chapter, a new modulation system is introduced. This system combines Walsh-Hadamard transform with OFDM/OQAM. Walsh-Hadamard transform spread the data uniformly over all the OFDM/OQAM subcarriers, which results in an improvement in the frequency diversity of the transmitted symbol. The transmission model of the system is fully analysed over AWGN channels and multipath fading channels. In addition, the inherited interference of the system is fully discussed. Moreover, the theoretical bit error rate is derived and verified. Furthermore, the performance of the proposed system is tested using computer simulations over different channels to confirm the superiority over the conventional systems by around 6 dB of gain at 10^{-3}.

The integration of the Walsh-Hadamard transform is also investigated in two directions: cascaded and fast algorithm. In the situation of cascaded implementation with WHT matrix and IFFT blocks, the location of the WHT matrix is selected to give 50 percent reduction in the hardware requirement for the integration. On the other hand, a fast algorithm is developed to combine the WHT, the phase mapping, and the IFFT blocks into one structure. The resulting structure can be implemented using relatively simple butterflies. The new transform leads to more reduction in the complexity with 60 percent over the cascaded implementation direction.

Chapter 4. Spectrum Efficiency and PAPR Reduction for the WHT/OQAM

4.1. Introduction

The benefit from exploiting pulse shape filtering in the OFDM/OQAM is not only to eliminate the requirement of the guard bands, but also to reduce the out of band energy transmission, which improves the spectral isolation from the neighbouring systems. Although this depends on the prototype filter being utilised, the resulting stop band attenuation is still higher than OFDM with square pulses.

In addition, one of the main downsides in OFDM system is the high peak to average power ratio (PAPR), which is caused by the large variations in the signal envelop. Hence, the signal can be described to have a wide dynamic range especially with large number of subcarriers. The problem lies with the high power amplifiers, as they lack that wide linear dynamic range on their amplification characteristics. Therefore, a nonlinear distortion might occur which causes an interference that leads to deterioration in the bit error rate of the system and increase in the out of band energy, which is affecting the other system that utilize nearby frequencies.

Subsequently, many techniques have evolved aiming to decrease the severity of this distortion by reducing the variations in the signal envelope. Some of these methods are capable of high reduction in the PAPR but cause more damage in term of the BER and the out of band radiation and others maintain lower PAPR on the cost of increased computational complexity.

The high PAPR phenomenon is a common issue in the majority of the multicarrier modulation systems; thus, OFDM/OQAM is no exception in this case, but would it be any difference in the case of WHT/OQAM.

Therefore, the aim of this chapter is to examine the effect of integrating WHT on the power spectral density for the WHT/OQAM. In addition, this chapter aims to investigate the problem of PAPR in the WHT/OQAM and the possibilities to reduce PAPR. Furthermore, the consequences of adding high power amplifier to the system requires further study.

This chapter is structured as the following: Section 4.2 provides an overview of the related work in the literatures. Section 4.3 demonstrates the power spectral density, while Section 4.3.1 the mathematical analysis of the power spectral density is presented. In Section 4.3.2, different prototype filters power spectral densities are illustrated and compared. In addition, the PAPR is discussed in Section 4.4, whilst the improved PAPR of WHT/OQAM is explained in Section 4.4.2. Moreover, a review of the existence PAPR reduction methods is presented in Section 4.5. The proposed Walsh overlapped selective mapping (WOSLM) is demonstrated in Section 4.5.1. Next, the novel simplified selective mapping (SSLM) is discussed in Section 4.5.2. In Section 4.5.3 the third new method know as Walsh partial transmit sequence (WPTS) is explained. Furthermore, the effect of the high power amplifier on the performance of the WHT/OQAM is illustrated in Section 4.6. Conclusion and summary are presented in Section 4.7

4.2. Related Work

The spectrum of the OFDM/OQAM was investigated in [69-70]. The pulse shapes of the OQAM have a major advantage over the OFDM in which they achieve higher stop band attenuation. However, the attenuation level depends on the prototype filter being selected for the modulator. The effect of the nonlinearity in the characteristics of the power amplifiers was also considered and the OQAM proved to keep maintaining better stop band attenuation over the OFDM.

While the analysis and the reduction of the PAPR in the OFDM system is attracting considerable attention and research [71-72], there is a few number of researches has been conducted for the PAPR in the OQAM case [73-75]. The analysis of the PAPR of the OQAM system was demonstrated in [73]. The effect on the PAPR for the chosen prototype filter was also considered, and concludes that the orthogonal and even for the nearly orthogonal filters their effect is negligible.

Only one technique to reduce PAPR for the OQAM existed [74-75]. The proposed method adapts one of the OFDM methods known as the selective mapping (SLM) to work with the OQAM. The proposed algorithm examines the overlapping between the successive OQAM symbols and takes it into the consideration when the calculation of the PAPR takes place. Although, this technique leads to a reasonable PAPR reduction, the involved implementation complexity is high.

4.3. Power Spectral Density of WHT/OQAM

The power spectral density (PSD) gives better understanding to the power distribution in the frequency domain. Since the spectrum efficiency is one of the important factors in the design of the wireless communication system due to the overcrowded spectrum, then it is fundamental to study the PSD of the WHT/OQAM. In addition, the OFDM system is considered as the metric system, so a comparison with its PSD is required especially if the new system offer any kind of improvement over the standard one.

4.3.1. Analysis of the PSD

The power spectral density represents the Fourier transform of the autocorrelation (Ac) of the signal (s) [4, 69]:

$$PSD_s(f) = \mathcal{F}\{Ac_s(\tau)\} = \int_{-\infty}^{\infty} Ac_s(\tau)\, e^{-j2\pi f\tau} d\tau \tag{4.1}$$

By recalling the WHT/OQAM signal from the previous chapter:

$$\begin{aligned} s(t) &= \sum_{m=0}^{M-1} \sum_{n=-\infty}^{\infty} \sum_{i=0}^{M-1} WH_{m,i}\, x_{i,n}\, \theta_{m,n} g(t - n\tau_o) e^{j2\pi mt/M} \\ &= \sum_{m=0}^{M-1} \sum_{n=-\infty}^{\infty} a_{m,n} \underbrace{\theta_{m,n} g(t - n\tau_o) e^{j2\pi mt/M}}_{g_{m,n}(t)} \end{aligned} \tag{4.2}$$

The input coefficients are assumed to be uncorrelated with zero mean and variance $\sigma_x^2 = E_s/2$ as indicated previously, then the autocorrelation of the s(t) can be calculated from the expected value of s(t) [4, 69]:

$$\begin{aligned} Ac_s(t,\tau) &= E\{s(t)\, s^*(t-\tau)\} \\ &= \sigma_x^2 \sum_{m=0}^{M-1} \sum_{n=-\infty}^{\infty} g(t - n\tau_o) g^*(t - \tau - n\tau_o)\, e^{j2\pi mF_o\tau} \end{aligned} \tag{4.3}$$

Since the signal of the WHT/OQAM is periodic with a period τ_o, then it is valid to write:

$$\begin{aligned} Ac_s(t + \tau_o, \tau) &= Ac_s(t, \tau) \\ E\{s(t)\} &= E\{s(t + \tau_o)\} = 0 \end{aligned} \tag{4.4}$$

Therefore, the autocorrelation and the mean are periodical, which means the signal is a cyclostationary function. Hence, it is more relevant to introduce the average autocorrelation that can be defined as

$$\overline{Ac_s}(\tau) = \frac{1}{\tau_o}\int_0^{\tau_o} Ac_s(t,\tau)\, dt \tag{4.5}$$

whose Fourier transform is the average power spectral density. By substituting (4.3) into (4.5) results in:

$$\begin{aligned}
\overline{Ac_s}(\tau) &= \frac{\sigma_x^2}{\tau_o}\sum_{m=0}^{M-1} e^{j2\pi mF_o\tau} \sum_{n=-\infty}^{\infty}\int_0^{\tau_o} g(t-n\tau_o)g^*(t-\tau-n\tau_o)\ dt \\
&= \frac{\sigma_x^2}{\tau_o}\sum_{m=0}^{M-1} e^{j2\pi mF_o\tau} \sum_{n=-\infty}^{\infty}\int_{-n\tau_o}^{\tau_o-n\tau_o} g(t)g^*(t-\tau)\ dt \\
&= \frac{\sigma_x^2}{\tau_o}\sum_{m=0}^{M-1} e^{j2\pi mF_o\tau} \int_{-\infty}^{\infty} g(t)g^*(t-\tau)\ dt \\
&= \frac{\sigma_x^2}{\tau_o}\left(g(\tau)\otimes g^*(-\tau)\right)\sum_{m=0}^{M-1} e^{j2\pi mF_o\tau}
\end{aligned} \tag{4.6}$$

The result of equation (4.6) needs to be evaluated in (4.1) to calculate the PSD as the following:

$$\begin{aligned}
PSD_s(f) = \mathcal{F}\{\overline{Ac_s}(\tau)\} &= \frac{\sigma_x^2}{\tau_o}\,\mathcal{F}\left\{\left(g(\tau)\otimes g^*(-\tau)\right)\right\} \otimes \mathcal{F}\left\{\sum_{m=0}^{M-1} e^{j2\pi mF_o\tau}\right\} \\
&= \frac{\sigma_x^2}{\tau_o}\left(\mathcal{F}\{g(\tau)\}\times\mathcal{F}\{g^*(-\tau)\}\right) \otimes \left(\sum_{m=0}^{M-1}\delta(f-mF_o)\right)
\end{aligned} \tag{4.7}$$

with δ represents Kronecker delta function. Taking the Fourier transform for the first part: $\mathcal{F}\{g(\tau)\} = G(f)$ and $\mathcal{F}\{g^*(-\tau)\} = G^*(f)$, yields:

$$\begin{aligned}
PSD_s(f) &= \frac{\sigma_x^2}{\tau_o}(G(f)\times G^*(f)) \otimes \left(\sum_{m=0}^{M-1}\delta(f-mF_o)\right) \\
&= \frac{\sigma_x^2}{\tau_o}|G(f)|^2 \otimes \left(\sum_{m=0}^{M-1}\delta(f-mF_o)\right) \\
&= \frac{\sigma_x^2}{\tau_o}\sum_{m=0}^{M-1}|G(f-mF_o)|^2
\end{aligned} \tag{4.8}$$

The final result of equation (4.8) indicates that the spectrum depends on pulse shape being exploited, hence, the WHT/OQAM and the OQAM can both have better spectrum than the conventional OFDM with the appropriate prototype filter. In addition, the

addition of the WHT to the OQAM does not affect the spectrum of the system and maintain this valuable feature.

4.3.2. Simulation results

The derived term in (4.8) can be applied for the OFDM technique knowing that the filters being used are simply square. As a result, the frequency response of these pulses can be expressed as

$$\mathcal{F}\{\sqcap_{T_o}(t)\} = sinc(\pi T_o f) \tag{4.9}$$

with $T = T_o$ and $F = 1/T_o$. The variance of the complex input coefficients equal to $Es = \sigma_c^2$. As a result, the PSD of the OFDM can be evaluated using (4.8) and (4.9) such as

$$PSD_{OFDM}(f) = \frac{\sigma_c^2}{T_o} \sum_{m=0}^{M-1} |sinc(\pi T_o(f - mF_o))|^2 \tag{4.10}$$

The PSD of the OFDM system are depicted in Figure 4.1 and Figure 4.2. On the linear scale, the shape of the spectrum takes the rectangular shape [31]. It is easy to notice at the edges of the spectrum the trails of the *sinc* function that construct the rectangle. However, the logarithmic scale is able to demonstrate adequate understanding for the attenuation levels at the out of band areas as illustrated in Figure 4.2. The first side lobe level is -10.15 dB with 128 subcarriers, which indicates high loss in the power outside the desired transmitted signal.

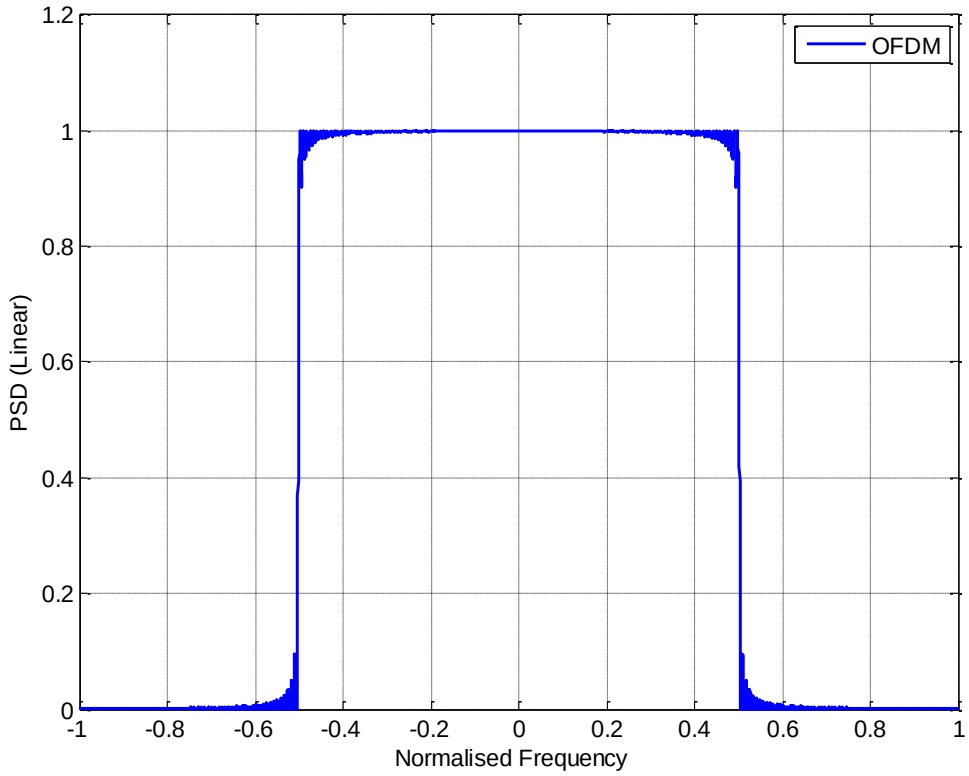

Figure 4.1 PSD of the OFDM system with *M=128* on linear scale

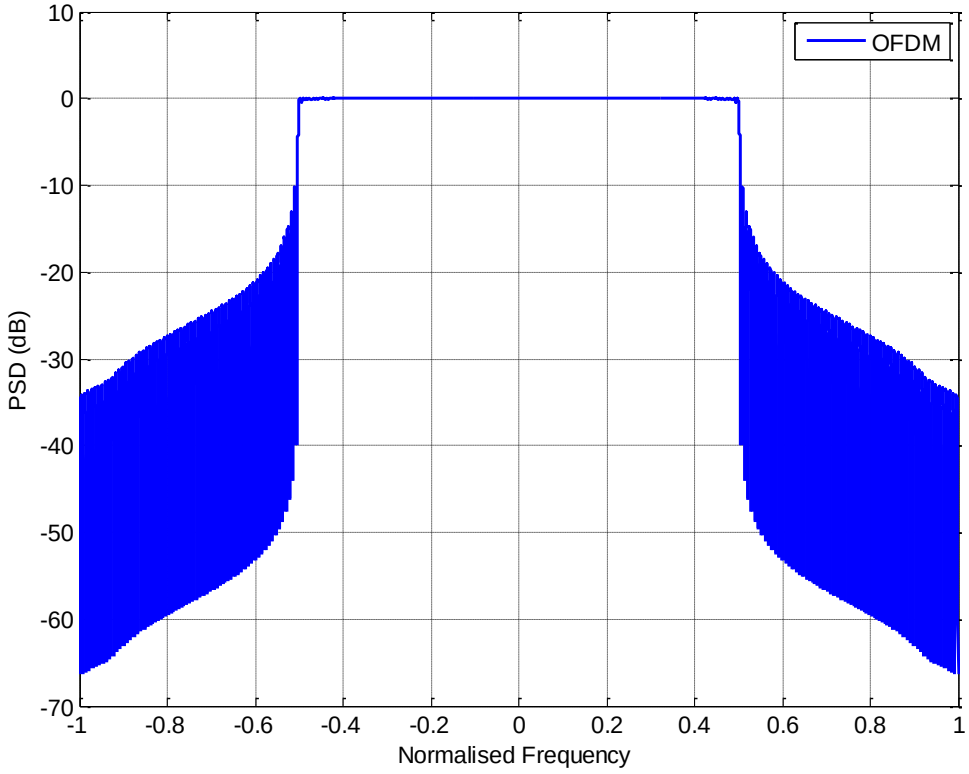

Figure 4.2 PSD of the OFDM system with *M=128* on logarithmic scale

On the other hand, the implementation of the pulse shaping in the modulator for the WHT/OQAM gives better control on the level of the attenuation achievable in the stop band. Consequently, the prototype filter characteristics play the major role in controlling the resulting spectrum.

To assess the effect of the filter type and order on the PSD of the system, three different filters are considered: SRRC, IOTA, and the MIA. These filters are chosen with three different lengths: *L=M*, *L=4M*, and *L=8M*. The resultant PSDs for each filter are demonstrated in Figure 4.3, Figure 4.4, and Figure 4.5.

For the WHT/OQAM with square root raised cosine (SRRC) filter illustrated in Figure 4.3, the increase of the filter length to *L=4M* improved the first side lobe from -11.7dB to -29.3dB, and this attenuation improves to -39.46dB by increasing the length of the filter to *L=8M*.

While, the WHT/OQAM with the IOTA filter shown in Figure 4.4 express around the same level of attenuation for *L=M* of 11.92dB. However, by increasing the length to *L=4M* and *L=8M*, the resultant attenuation is 34.6dB and 35.3dB respectively.

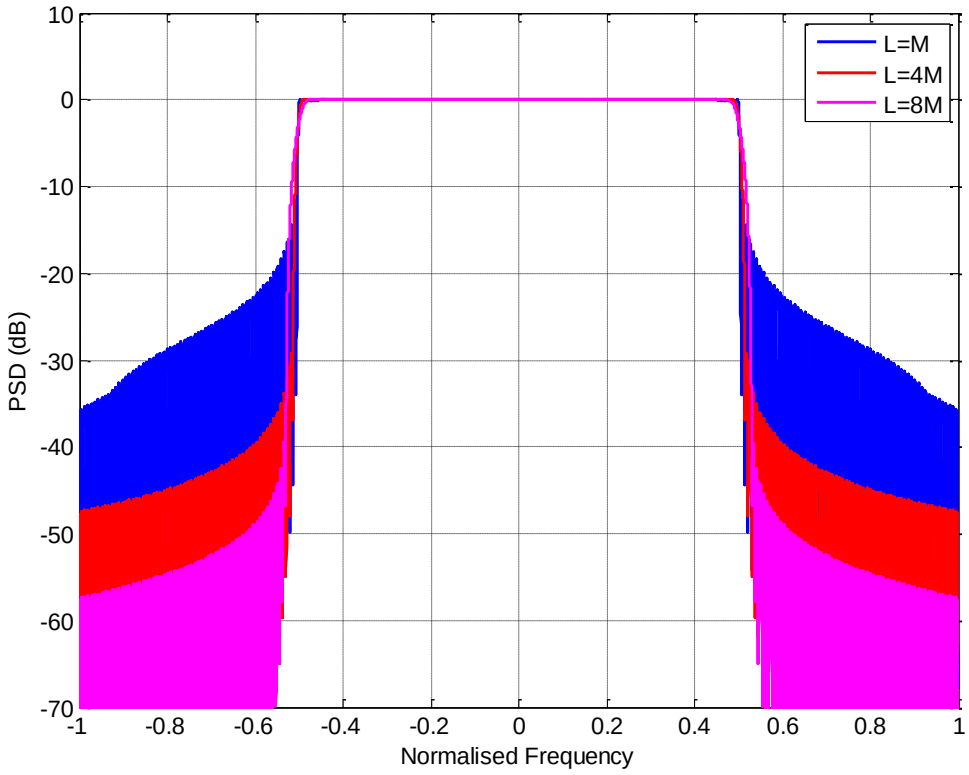

Figure 4.3 PSD of the WHT/OQAM system with *M=128* and SRRC filter

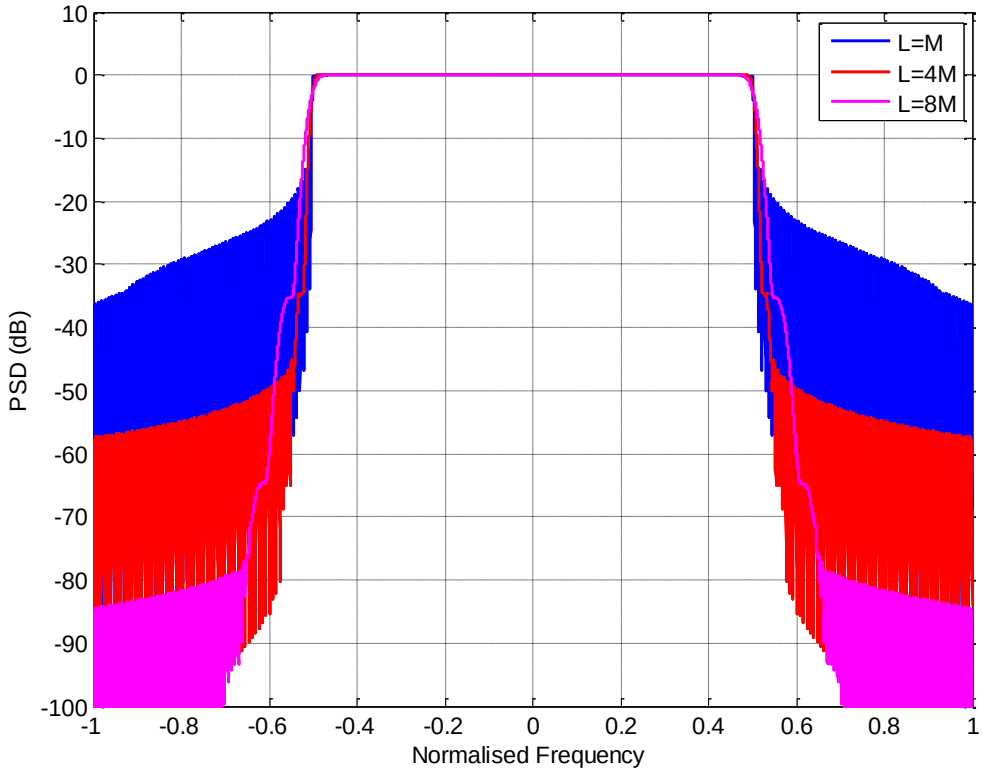

Figure 4.4 PSD of the WHT/OQAM system with *M=128* and IOTA filter

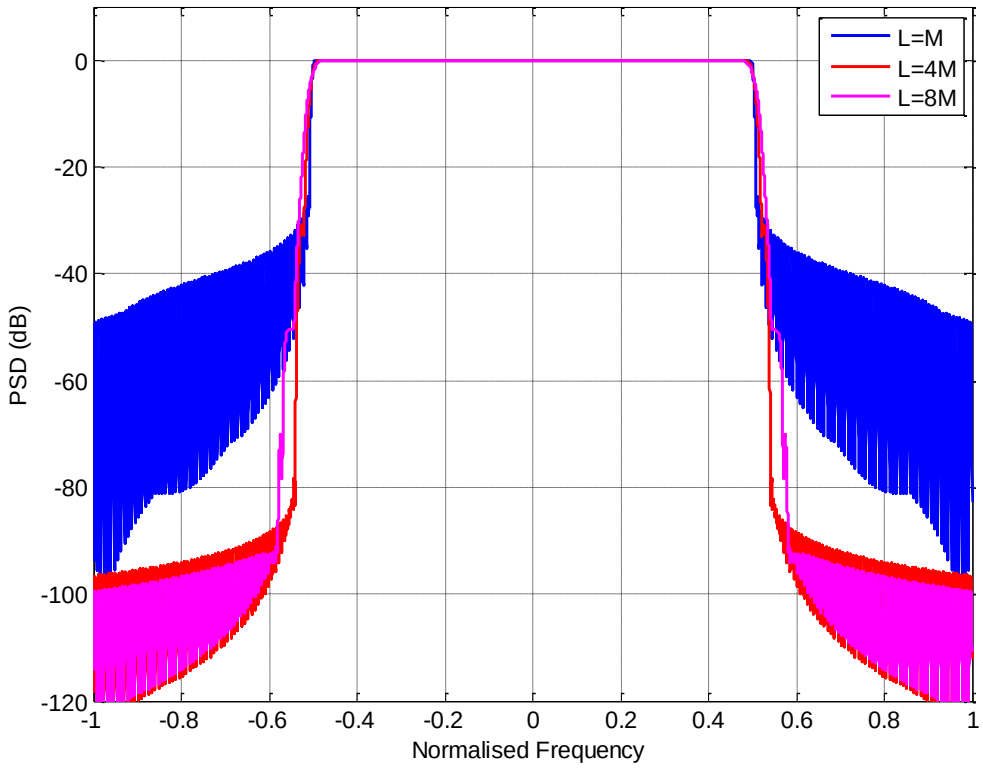

Figure 4.5 PSD of the WHT/OQAM system with *M=128* and MIA filter

The optimized MIA filter depicted in Figure 4.5, can be utilized for higher level of attenuations compared with previous examples. Therefore, the first side lobe level of -26.22dB can be achieved with filter length of *L=M*. By increasing the length to *L=4M*, this level improves to -30.9dB. Furthermore, the side lobe level for the case of *L=8M* is equal to -50.42dB. However, other factors such as the localization need to be considered during the choice of the prototype filter.

To compare between the OFDM and the WHT/OQAM PSD, the previous filters are selected and the number of subcarrier is set to *M=1024*. To show the differences in the spectral response, a zoomed section of the spectrum is illustrated in Figure 4.6. It is clear from the figure the improved attenuation for the out of band power as a result of utilizing more effective filters than the square pulse. While the OFDM first side lobe level of -10dB, the SRRC with *L=4M* managed to achieve -29.4dB. In addition, the first side lobe of the IOTA with the same length of *4M* is -35dB. Moreover, the optimized MIA filter with length of only *M* is capable of attenuating the signals to -36.3dB. These figures increase with the increase of the frequency, which makes the WHT/OQAM a better option in term of the spectrum contamination as a compared with the OFDM system.

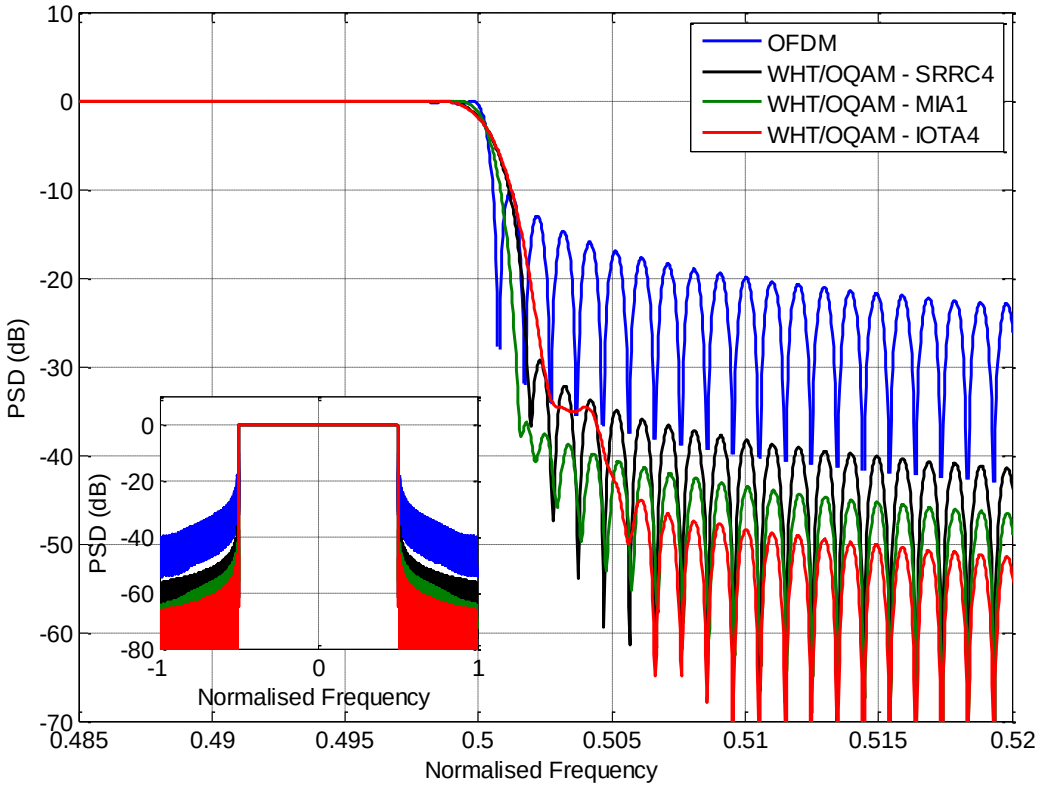

Figure 4.6 A comparison between OFDM and WHT/OQAM PSDs with *M=1024*

4.4. PAPR of the WHT/OQAM System

The aims of this section are to analyse the peak to average power ratio in the WHT/OQAM system and discover the significant implication of adding WHT to the OQAM system.

4.4.1. PAPR of the WHT/OQAM

The peak to average ratio is a parameter used to give an indication of the variation in the signal envelop calculated from the division of the peak of the signal by its average. The lowest value for this ratio is one; therefore, an increase in the ratio value reflects an increase in the dynamic range of the signal.

In multicarrier modulation systems such as OFDM and WHT/OQAM, the transmitted signal is composite of *M* statistically independent subcarriers stacked together by means of summation. This combination produces nonconstant or uneven envelop signal. The peak to average power ratio (PAPR) of the transmitted signal in the continuous time domain can be calculated as follows [71-72, 76]:

$$PAPR_c = \frac{max_{[0,T]}|s(t)|^2}{\frac{1}{T}\int_0^T |s(t)|^2\, dt} \tag{4.11}$$

However, WHT/OQAM symbol length depends on the length of the prototype filter being used that could be multiple of *M* depending on the overlap factor value *K*. The shortest possible length is equal to *M*, even with that short length there is still an overlapping between successive symbols as explained earlier. Additionally, the transmission rate of the WHT/OQAM is the same as the OFDM, which sends one complex symbol during *M* samples. Therefore, the symbol duration over which the PAPR is calculated for the WHT/OQAM is considered a window of *M* samples [73]. The PAPR for the discrete signal of the WHT/OQAM can be expressed as

$$PAPR_d = \frac{max_{k\in\{0,\dots,M-1\}}|s[k]|^2}{E\{|s[k]|^2\}} \tag{4.12}$$

Nevertheless, because of the random nature of the PAPR, it is more effective to study its complementary cumulative distribution function (CCDF), which can be defined as the probability of PAPR variable being over a certain reference value ζ [71, 73].

4.4.2. CCDF of the WHT/OQAM

The unitary property of the WHT maintains the input power level at the output vector. Nevertheless, the peak power value of the signal is reduced. This leads to a reduction in the PAPR of the system [46, 48, 77].

The reduction in the peak value is related to the construction of the transmitter matrix being utilized. For instance, the IDFT matrix contains *M* none zero elements in each row (or column), for example *M=8*:

$$IDFT_8 = \frac{1}{4} \times \begin{bmatrix} 1.4142 & 1.4142 & 1.4142 & 1.4142 & 1.4142 & 1.4142 & 1.4142 & 1.4142 \\ 1.4142 & 1+j1 & j1.4142 & -1+j1 & -1.4142 & -1-j1 & -j1.4142 & 1-j1 \\ 1.4142 & j1.4142 & -1.4142 & -j1.4142 & 1.4142 & j1.4142 & -1.4142 & -j1.4142 \\ 1.4142 & -1+j1 & -j1.4142 & 1+j1 & -1.4142 & 1-j1 & j1.4142 & -1-j1 \\ 1.4142 & -1.4142 & 1.4142 & -1.4142 & 1.4142 & -1.4142 & 1.4142 & -1.4142 \\ 1.4142 & -1-j1 & j1.4142 & 1-j1 & -1.4142 & 1+j1 & -j1.4142 & -1+j1 \\ 1.4142 & -j1.4142 & -1.4142 & j1.4142 & 1.4142 & -j1.4142 & -1.4142 & 1.4142 \\ 1.4142 & 1-j1 & -j1.4142 & -1-j1 & -1.4142 & -1+j1 & j1.4142 & 1+j1 \end{bmatrix} \quad (4.13)$$

While the derived matrix in the previous chapter, the V matrix, includes a minimum of *M/2* none zero elements in each row or column, for example *M=8*:

$$V_8 = \frac{1}{4} \times \begin{bmatrix} 2+j2 & 2-j2 & 0 & 0 & 0 & 0 & 0 & 0 \\ 2-j2 & 2+j2 & 0 & 0 & 0 & 0 & 0 & 0 \\ 0 & 0 & 0 & 4 & 0 & 0 & 0 & 0 \\ 0 & 0 & 4 & 0 & 0 & 0 & 0 & 0 \\ 0 & 0 & 0 & 0 & -0.4142+j1 & 2.4142+j1 & 1+j0.4142 & 1-j2.4142 \\ 0 & 0 & 0 & 0 & 2.4142+j1 & -0.4142+j1 & 1-j2.4142 & 1+j0.4142 \\ 0 & 0 & 0 & 0 & -0.4142-j1 & 2.4142-j1 & 1-j0.4142 & 1+j2.4142 \\ 0 & 0 & 0 & 0 & 2.4142-j1 & -0.4142-j1 & 1+j2.4142 & 1-j0.4142 \end{bmatrix} \quad (4.14)$$

Consequently , this matrix has a block diagonal structure that reduces the upper bound of the peak power by half because each of the M output subcarriers involves less than or equal to the sum of *M/2* samples, compared with the former matrix that require *M* samples for each *M* subcarriers [78]. This decrease in the upper bound indicates a decrease in the PAPR value of the system.

To verify PAPR reduction of the WHT/OQAM compared to the OQAM or the standard OFDM, computer simulation program is produced with a system modulated with 4-QAM and filtered with IOTA4. The number of subcarriers is selected to be a multiple of two with values of *M*=64, 128, 256, and 1024. The same number of subcarriers is chosen for the OFDM and the OQAM systems. The OQAM system utilises the same prototype filter. The resulting CCDF curves are illustrated in Figure 4.7.

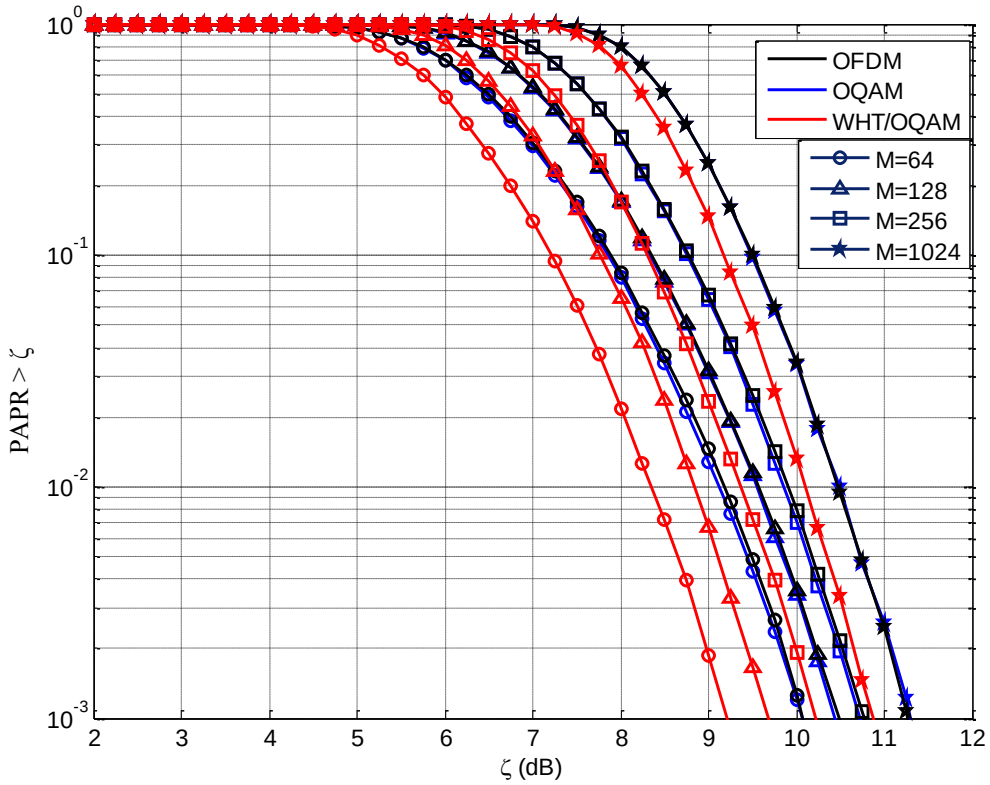

Figure 4.7 Comparison between the PAPR of the WHT/OQAM, OQAM and OFDM

The simulation results for more than 30000 transmitted symbols in each case, clearly demonstrates less values for the PAPR in the transmitted signal of WHT/OQAM compared with the other systems. The improvement ranges between 0.4dB to 0.9dB at 10^{-3} of the CCDF. It is worth to mention that this improvement requires no side information to be sent as some of the PAPR reductions methods.

4.5. PAPR Reduction Methods

As stated earlier, there are few publications concerning PAPR reduction of the OQAM system [74-75]. However, the research is mainly focused on the standard OFDM system. Various techniques have been proposed to tackle this problem and generally can be classified into three main categories: block-coding technique, clip effect transformation, and probabilistic approach. For example: amplitude clipping, clipping and filtering, coding scheme, phase optimisation, partial transmit sequence, and selective mapping. This thesis focus on two methods only: the partial transmit sequence (PTS), and the selective mapping (SLM). These methods are efficient and improve the bit error rate of the system compared to the other schemes. Nevertheless, these techniques involve some side information to be sent to the receiver to allow the

decoding process, which affect the usable bandwidth. For the interested readers, they can refer for these references for extra reading [79-83].

4.5.1. The Walsh overlapped selective mapping algorithm (WOSLM)

The only technique for the PAPR reduction for the OQAM system was proposed in [75]. Thus, this technique is re-adapted for the case of the WHT/OQAM. The method is originally based on the classic selective mapping for the OFDM introduced in [84].

In the standard selective mapping (SLM) scheme, different versions of the same transmitted OFDM symbol are generated by multiplying the input coefficients with U different codes of length equal to the length of the input coefficients vector of M. These U codes maintain the initial constellation, in another word, if the input vector with M elements (x_m) is modulated initially with 16-QAM, then the resultant vector elements $x_m^{(u)}$ ($u=1, \ldots, U$) are still hold points of the 16-QAM constellation. These different versions are then sent to U-OFDM modulators as demonstrated in Figure 4.8. At the output of these modulators, a comparison stage selects the lowest PAPR signal and records the index of the selected code. These indices are then sent with the transmitted signal so that the receiver can decode the signal back. The number of bits required to be transmitted as side information is $log_2 U$, which depends on the number of codes being used.

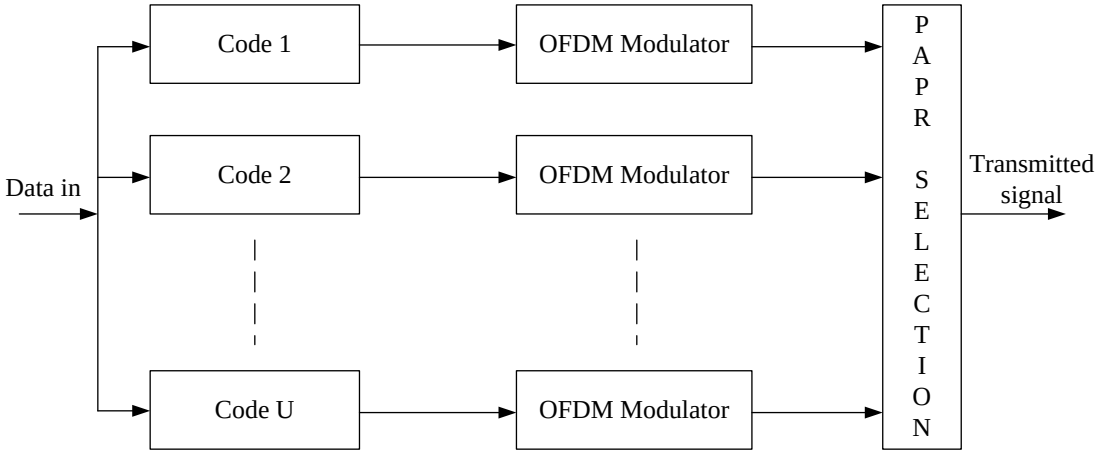

Figure 4.8 Standard selective mapping technique in OFDM

However, this simple method cannot be applied directly to the OQAM or the WHT/OQAM systems. This is because of the overlap that occurs between the successive coefficients s in these systems resulting from utilizing pulse shapes [75]. For example, if a WHT/OQAM modulator is utilized instead of the OFDM modulator as explained previously, then the QAM modulated coefficients x is multiplied by the code

vector $d^{(u)}$ (u=1, …, U) with a matching length (M) to generate U different versions of the vector x. The output signals of the modulators denoted by $s(t)^{(u)}$ is then compared to choose the one with the lowest PAPR at the period $\mathcal{T}_k = \{k\,\tau_o, (k+1)\,\tau_o\}$ resulted with the code u_k. Hence, the transmitted signal can be written as

$$s(t) = \sum_{k=0}^{\infty} s^{(u_k)}(t)_{|\mathbb{T}_k} \tag{4.15}$$

with $s^{u_k}(t)_{|\mathbb{T}_k}$represents the signal $s^{u_k}(t)$ limited within the period $\mathcal{T}_k$. This can be reflected on the modulator signal such that for all k:

$$s^{i_k}(t)_{|\mathbb{T}_k} = \sum_{m=0}^{M-1} \sum_{n=-\infty}^{\infty} \sum_{i=0}^{M-1} WH_{m,i} x_{i,n}^{(u_k)} g_{m,n}(t)_{|\mathbb{T}_k} \tag{4.16}$$

Since, the prototype filter length is normally longer than the period τ_o, then, the one with a limited period $g_{m,n}(t)_{|\mathbb{T}_k} \neq g_{m,n}(t)$, which leads to loss of the orthogonality property between the system filters as:

$$\langle g_{m,n}(t)_{|\mathbb{T}_k}, g_{m',n'}(t) \rangle \neq \delta_{m,m'}\delta_{n,n'} \tag{4.17}$$

Therefore, the demodulation process of the transmitted coefficients s fails to estimate the correct value of the transmitted coefficients. Consequently, the direct implementation of the SLM method cannot work with both: the OQAM and the WHT/OQAM.

There are two solutions presented in this thesis to overcome this problem, the first one is to re-adapt and enhance the existed technique in [74-75] that called overlapped selective mapping (OSLM) for the case of the WHT/OQAM. The second solution is to apply a newly proposed scheme in this thesis called simplified selective mapping algorithm (SSLM) that will be explained in the next section.

The OSLM method takes into the consideration the overlap between the successive coefficients s. This implies the data to be processed in a matrix form not as individual vectors like in the ordinary SLM. This method is re-adapted and improved for the WHT/OQAM system purpose. This enhanced algorithm over the OSLM is better identified with the inclusion of the Walsh in the name to become Walsh overlapped selective mapping algorithm (WOSLM).

The WOLSM process can be explained by the aid of Figure 4.9, which illustrates a simple case scenario of an overlapping between the symbols with a short filter of length L=1M i.e. the overlapping factor is equal to one.

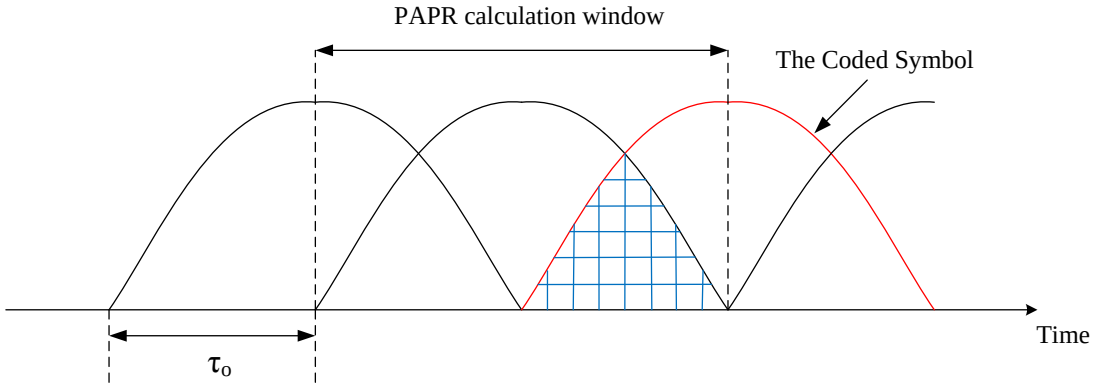

Figure 4.9 Overlapped coefficients s and the WOSLM principle

In this example, the first followed by the second set of coefficients are modulated with the WHT/OQAM modulator, the third set of coefficients is coded by one of the *U* codes then modulated by the WHT/OQAM system (identified with red). The PAPR measurement is carried out over a window of the pulse shape length for all the *U* codes and the code that produces the minimum PAPR is selected and stored. This process is repeated for the next symbol, but in this case, the second symbol is the chosen one from the previous selection process.

To generalise this algorithm, it can be described in a step-by-step manner as the following:

1- The code generation: the code vectors $d^{(u)}$ (u=1, …, U) need to be generated with length equals to the number of subcarriers M. these codes need to be shared between the transmitter and the receiver sides.

2- Creation of the first 2K coefficients vectors: the first 2K data vectors can be exempted of the multiplication with any code, though they are stored in a matrix of size M x $2K$:

$$X_{2K} = (x_{i,n}^{(1)})_{0 \le i \le M-1, 1 \le n \le 2K} \tag{4.18}$$

3- Addition of the coding vector: U versions of the coefficients' vector are generated. These U versions are used to create U extended matrices that contain the original matrix X_{2K} and the U editions of the data vector:

$$X_{2K+1}^{(u)} = \begin{bmatrix} X_{2K} & x_{i,2K+1}^{(u)} \end{bmatrix} \quad (4.19)$$

4- PAPR selection: All the *U* extended matrices are modulated with WHT/OQAM, and then the PAPR is calculated for each output over a window of length equal to the pulse shape length L. This window is located over the symbol of interest, which is the one before the coded vector symbol to contain all the alteration caused by the coded vector symbol addition to the output. The branch with a code index u_{2K+1} that produce the lowest PAPR is selected and stored. Then the matrix X_{2K} is replaced by $X_{2K+1} = X_{2K+1}^{(u_{2K+1})}$ and maintains a size of *M* x *2K*.

5- Repeating step 3 and 4 for the following data: In this step, the coded vector from step 3 is assigned to be the symbol of interest and a new vector is going to be the coded one. So the matrix of consideration in the interval $k > 2K$ is:

$$X_{k+1}^{(u)} = \begin{bmatrix} X_k & x_{i,k+1}^{(u)} \end{bmatrix} \quad (4.20)$$

6- Transmitting the resulting matrix: the resulting data matrix that has the lowest PAPR is then transmitted with the WHT/OQAM modulator.

The WOSLM block diagram is depicted in Figure 4.10. Since this technique stores the data that produces the lowest PAPR and then transmits it via WHT/OQAM modulator, the orthogonality of the filterbank is maintained and the demodulation process will only require the index of the codes to decode the signal.

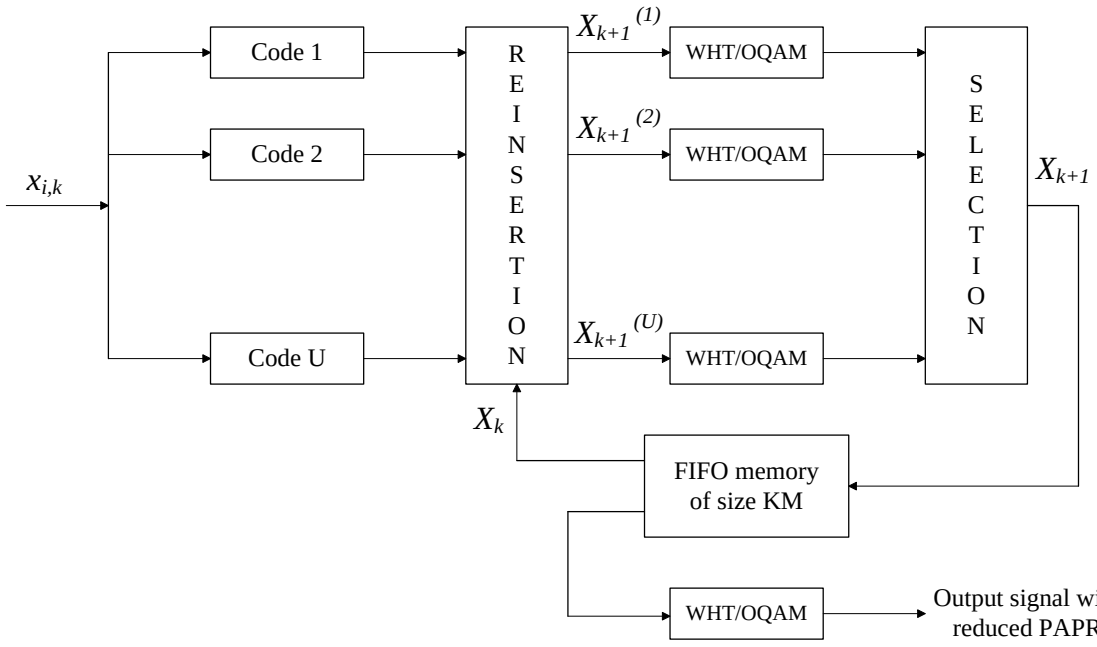

Figure 4.10 Walsh Overlapped Selective Mapping technique

The difference between WOSLM method and the OSLM method is the location of the PAPR measurement window. In the OSLM, the window is placed over the coded symbol, while in the WOSLM, the window is located over the previous symbol or the one called the symbol of interest. Furthermore, the inclusion of the WHT in the system that helps to improve the PAPR as explained previously.

To investigate the efficiency of this technique, WHT/OQAM system with 64 subcarriers is selected to be simulated on computer program. The data is randomly generated and modulated with 4-QAM first then staggered to prepare the transmitted data. The IOTA pulse shape is chosen with overlapping factor of K=4. It is also interesting to compare this algorithm performance versus the OSLM and the SLM. As a result, an OQAM system with identical specifications to the WHT/OQAM system is utilized with OSLM technique. Furthermore, the SLM method is verified with OFDM system with 64 subcarriers and 4-QAM modulator.

The resulting CCDF curves for the WOSLM and the OSLM are demonstrated in Figure 4.11, while the comparison with the SLM is illustrated in Figure 4.12. The WOLSM algorithm results reveal a considerable improvement in the PAPR reduction over the OSLM method. The WOSLM algorithm achieved a remarkable reduction ranged 1.9 - 2.9 dB at a threshold of 10^{-3} with U varies between 2 to 8. However, the OSLM technique attained less reduction to the PAPR ranged between 1 - 2 dB at 10^{-3} with the increase of the number of the coded branches from 2 to 8.

Comparing the WOSLM with the standard SLM, the WOSLM is performing well considering the complexity of the signal of the WHT/OQAM in term of the overlapping compared to the classical OFDM signal. Although SLM achieves a decrease in the PAPR at threshold of 10^{-3} varies between 1.7 – 3.4 dB with U=2 – 8, the resulting WHT/OQAM signal has lower PAPR compared to the OFDM signal in all cases with the matching number of coded branches as demonstrated in Figure 4.12.

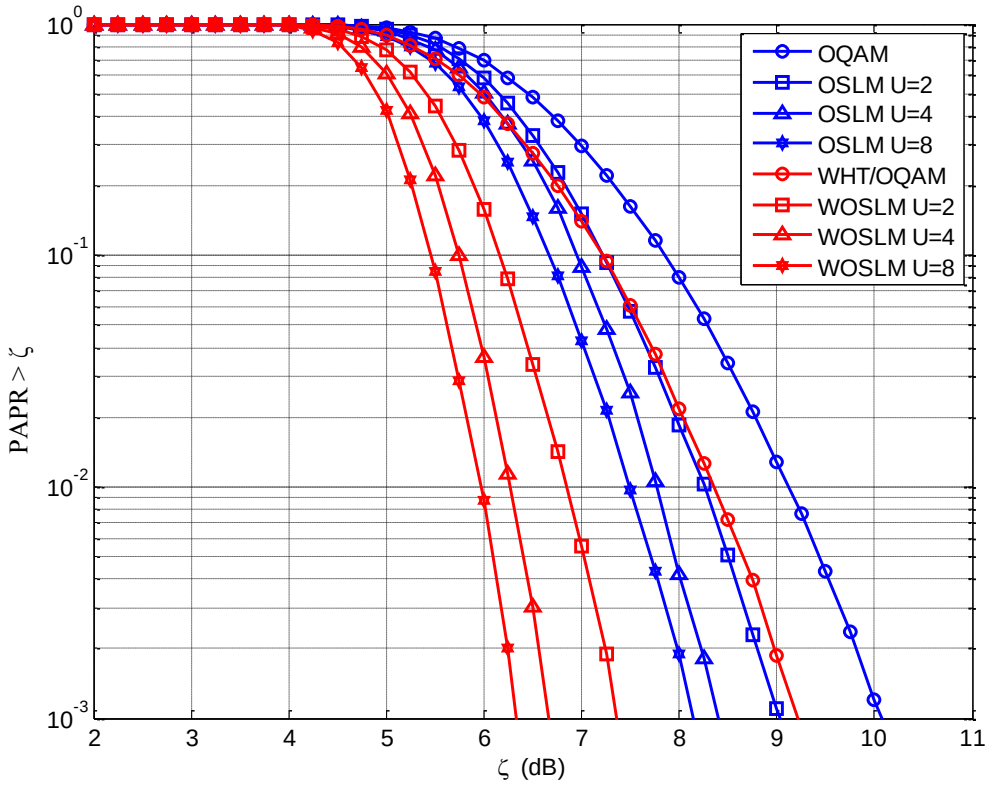

Figure 4.11 The WOSLM algorithm compared to the OSLM

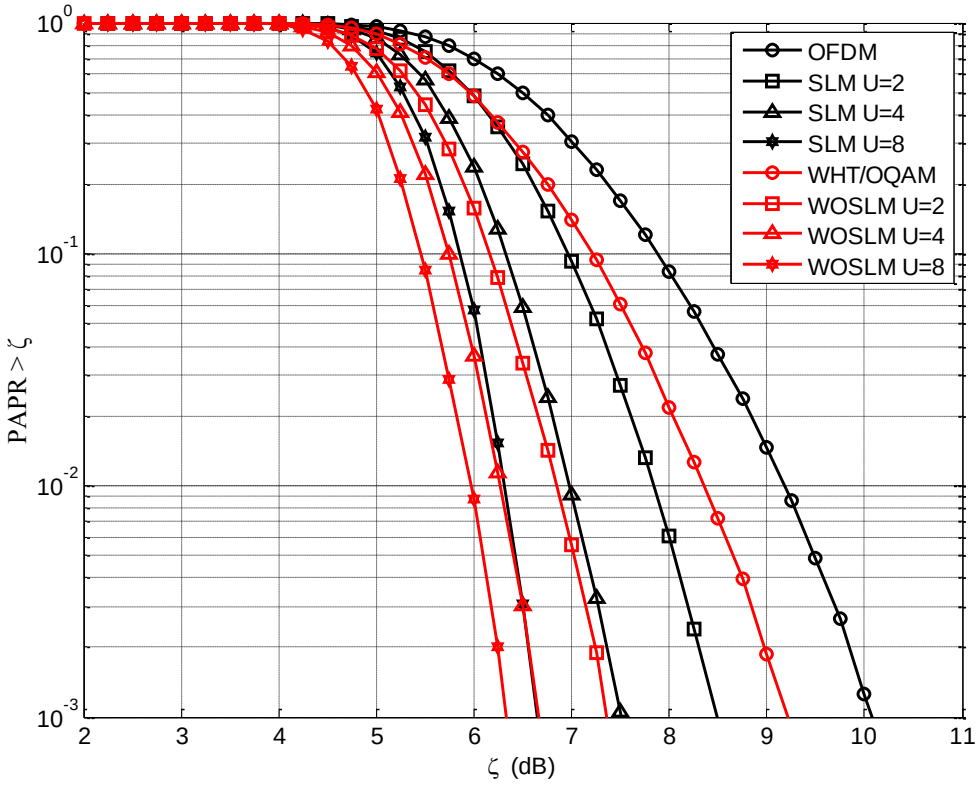

Figure 4.12 The WOSLM algorithm compared to the SLM

Throughout the description of the WOLSM algorithm, the overlapping factor *K* that associated with the length of prototype filter was the main consideration to maintain the orthogonality between the subcarriers. Consequently, to assess the influence of the overlapping factor on the WOSLM algorithm, a computer simulation is utilized. The selected WHT/OQAM system to be analysed has a number of subcarriers set to 64 and the 4-QAM as the modulator for the data. The number of coded branches is equal to four and the prototype filter is IOTA. Then, three different values are considered for *K*=1, 4, and 8. The resulting CCDF curves are presented in Figure 4.13. The shortest filter (IOTA1) with *K*=1indicates an improvement over the other longer filters with higher values for *K*=4, and 8 by at least 0.1 dB at 10^{-3}. However, the increase in the overlapping factor from 4 to 8 has little impact on the results and the difference is only 0.06 dB at threshold of 10^{-3}. In general, the impact of decreasing the length of the filter on the performance of the WOSLM is small value, nevertheless it can be useful in term of the computational complexity.

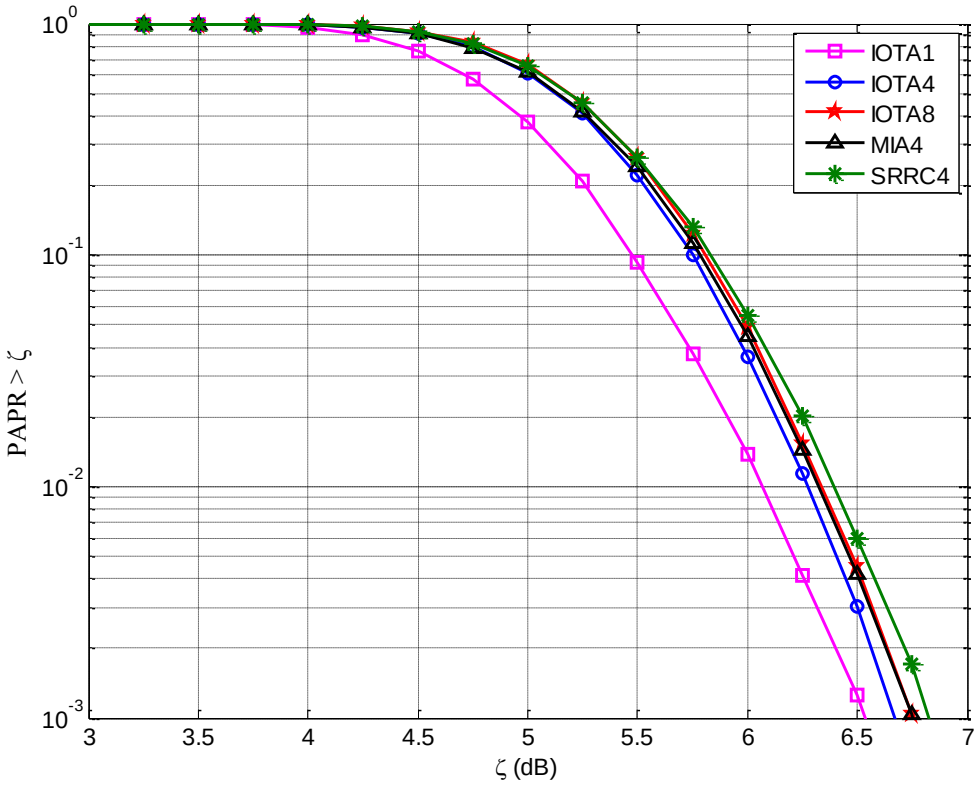

Figure 4.13 Effects of changing the prototype filter on the WOSLM performance

In addition, the choice of the prototype filter is also examined. By utilising the previous system simulation setup, the performance of the WQOLSM with SRRC and the MIA filters are compared to the result with the IOTA pulse shape. The overlapping factor is

considered equal to 4 for both filters, and the results are illustrated in Figure 4.13. The difference in the response is within 0.1dB at threshold of 10^{-3}, which indicates the insignificant consequences of the filter choice on the resulting PAPR value.

4.5.2. Simplified selective mapping algorithm (SSLM)

Although the WOSLM algorithm produces impressive results, the calculation complexity is high as well. As a result, a simplified method to reduce the PAPR of the WHT/OQAM is proposed and called simplified selective mapping algorithm (SSLM). This method maintains the orthogonality between the subcarriers and reduces the latency of the processing compared to the WOSLM.

This algorithm can be described best with the assistance of Figure 4.14. In the previous section, the overlapping characteristic in the signal of the WHT/OQAM and the OQAM systems caused the identified issue of the loss of the orthogonality with the direct implementation of the SLM technique. As a result, the WOSLM and OSLM algorithms considered that overlapping in their criteria.

To overcome this problem, a new proposal is investigated. The new proposal suggests decomposing the WHT/OQAM modulator into two parts: the V transform and the polyphase network (PPN) blocks. Then the decision block that measures the PAPR and selects the lowest one required to be shifted prior to the polyphase block. This shift of the decision block location helps to process the output vectors from the V transform prior to the filtering stage i.e. these vectors are still of length equal to the number of subcarriers *M* and the overlapping is not existed yet.

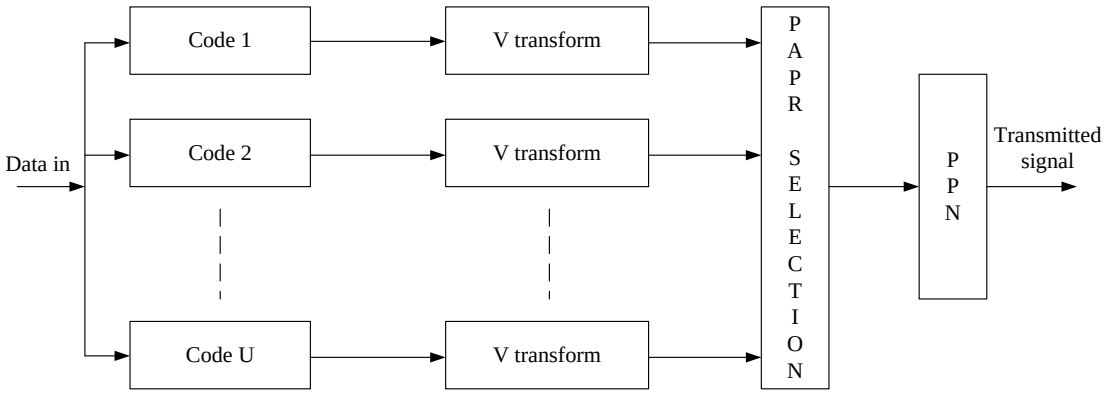

Figure 4.14 The simplified selective mapping (SSLM) algorithm block diagram

The algorithm process the input data as the following:

1- *U* codes generation: These coding vectors of length equal to the number of subcarriers need to be shared between the both sides of the communication system.
2- Generation of *U* versions data vectors: the input data vector is multiplied with each coding vector to produce *U* variations of the input signal.
3- V transform: each of the coded vectors is processed with the V transform that represents the first part of the WHT/OQAM modulator.
4- PAPR calculation and selection: the PAPR of each output vector of the V transform is calculated. The vector that has the lowest PAPR is selected and the code index is stored.
5- Filtering with the PPN: The chosen vector is then filtered with the polyphase network block and prepared to be transmitted.

These simple procedures produce an output with lower PAPR and maintain the orthogonality between the successive output vectors as the filtering process is taking part afterwards. In addition, the complexity of the calculation is marginally reduced compared to WOSLM algorithm. Moreover, the latency of the SSLM is by far less than the WOSLM technique, as the selected symbol is directly transmitted, while in the WOLSM the data required to be stored then re-modulated which encounter double the latency of the modulator. This is crucial point for the high speed communication systems.

Computer simulation program is used to assess the performance of the SSLM algorithm and compare it with WOSLM method. The number of subcarriers is 64 and the 4-QAM is used to modulated the data prior to the staggering stage. The IOTA4 is the prototype filter in the WHT/OQAM transmitter. The number of coding vectors is set to be 2, 4, and 8. The resulting simulated CCDF curves are presented in Figure 4.15.

The SSLM algorithm produce relatively lower PAPR reduction compared to the OWSLM due to the lack of consideration to the overlapping phenomena between the consecutive symbols. This reduction is varied between 0.5 – 1 dB at threshold of 10^{-3} and for a number of branches of 2 up to 8. Meanwhile, these results are in the same league if they are compared to the outcome of the OSLM technique depicted in Figure 4.11.

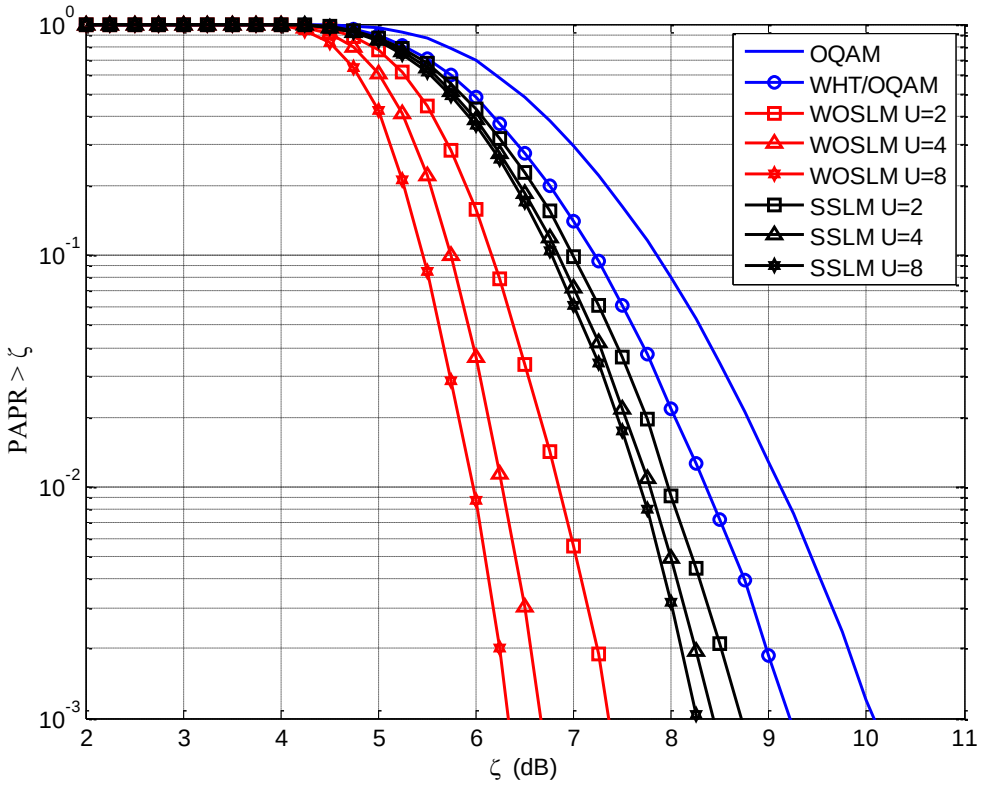

Figure 4.15 The SSLM algorithm compared to the WOSLM

The main attraction of this algorithm beside the low latency is the lower computational complexity compared to the WOLSM. This can be concluded by simply comparing the block diagram of each technique, Figure 4.10 and Figure 4.14. Nevertheless, the mathematical representation of the calculation complexity is worth investigation [85].

For the SSLM, each of the U input vectors requires M real multiplications at the coding stage, however, by assuming, the first vector holds the original version, then this stage requires M (U-1) real multiplications. Each V transform involves $M \log_2 M - 2$ (M-1) real multiplications and $2M \log_2 M - 4$ (M-1) real addition as explained at the previous chapter. To calculate the PAPR, the power of each element in the output vectors requires $2UM$ real multiplications and UM real additions.

On the other hand, the WOSLM method processes matrices of size M x $2K$+1 in each branch. Though, the coding process still require M (U-1) real multiplications as assumed previously. Each WHT/OQAM modulator is constructed from two stages: the V transform and the filtering stage. The V transform processes the extended matrix in each branch. Subsequently, the output matrix is filtered by the polyphase block that involves $4KM$ ($2K$+1) real multiplications and $2KM$ ($2K$+1) real additions. The output

of the filtering stage required to be multiplexed which conducts a 2*KM* (2*K*-1) real additions. The PAPR calculation window is extended in the case of the WOSLM to cover the length of the pulse shape; therefore, the computation of the power for *KM* elements involves 2*UKM* real multiplications and *UKM* real additions.

In the same manner, the computational complexity of the standard SLM can be calculated. The resulting computational complexity of the three methods is summarised in Table 4.1. In addition, a numerical representation of the arithmetic operations included in each of the three techniques is produced in Table 4.2 for the case of U=8 and *K*=4. Moreover, Figure 4.16 and Figure 4.17 present comparison between real addition and multiplication operations involved in SSLM and the WOSLM for different number of subcarriers and overlapping factor *K*=4.

The results indicate a massive reduction in the computational complexity in the SSLM algorithm compared to the WOSLM technique. This reduction in the real addition operations is 93.8% for *U*=8 and *M*=1024, while the decrease in the number of real multiplications is 95.16% for the same number of branches and subcarriers. These substantial figures in the computational complexity reduction of the SSLM compared to the WOLSM makes the SSLM an attractive choice for mobile systems that depends on limited power supply.

Furthermore, the SSLM achieves a considerable reduction in the complexity compared to the standard SLM, though this is not shown graphically. As the SSLM cuts the complexity by 48% for the real additions and 57.34% for the real multiplication operations for a system utilises 1024 subcarrier and 8 branches for the PAPR reduction. The involvement of the V transform in the implementation of the WHT/OQAM provides the ability to attain lower computational complexity.

SSLM real additions	$UM(2\log_2 M - 3) + 4U$
SSLM real multiplications	$UM(\log_2 M + 1) + 2U - M$
WOSLM real additions	$2U(2K+1)\big(M\log_2 M - 2(M-1)\big) + UKM(8K+1)$
WOSLM real multiplications	$UM\big((2K+1)\log_2 M + 2K(4K+3)\big) - U(M-1)(4K+1)$
SLM real additions	$UM(3\log_2 M + 1) + 2M(U-1)$
SLM real multiplications	$2UM(\log_2 M + 1) + 4M(U-1)$

Table 4.1 Computational complexity of SSLM, WOSLM, and SLM algorithms

M	SSLM real additions	SSLM real multiplications	WOSLM real addition	WOSLM real multiplications	SLM real addition	SLM real multiplications
64	4640	3536	104736	96904	10624	8960
128	11296	8080	227616	202888	24320	19968
256	26656	18192	491808	424072	54784	44032
512	61472	40464	1057056	884872	121856	96256
1024	139296	89104	2261280	1843336	268288	208896

Table 4.2 Numerical results for the real arithmetic operations involved for U=8 and K=4 in the SSLM, WOSLM, and SLM techniques.

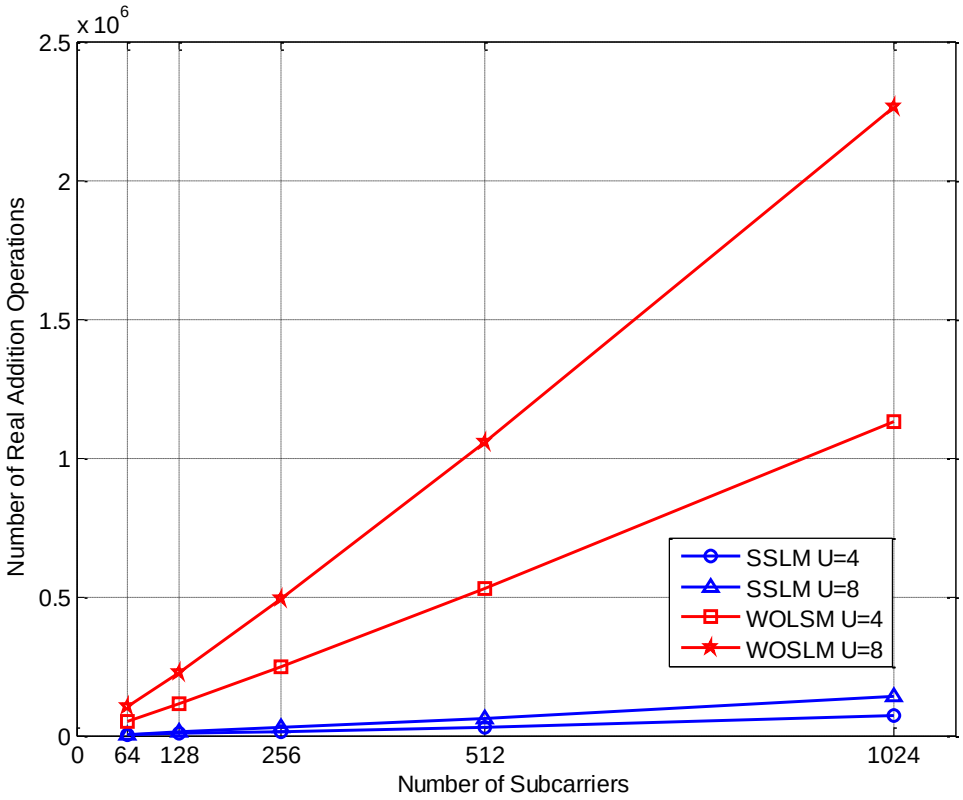

Figure 4.16 Comparison between the SSLM and the WOSLM algorithms in the number of real additions

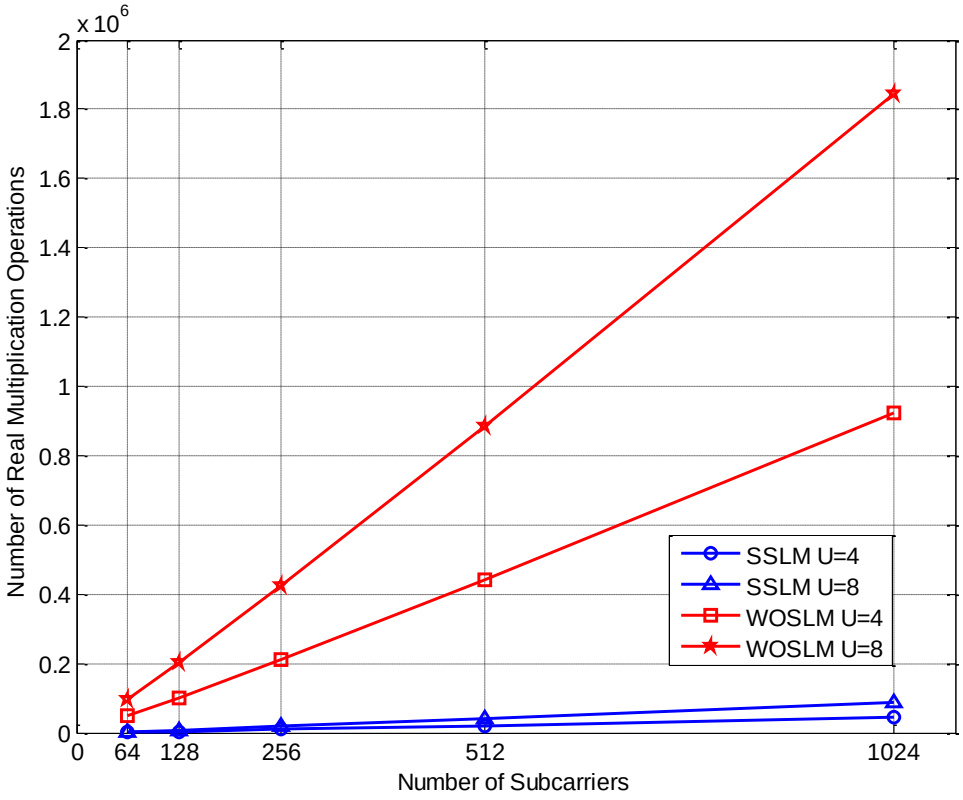

Figure 4.17 Comparison between the SSLM and the WOSLM algorithms in the number of real multiplications

4.5.3. Walsh partial transmit sequence algorithm (WPTS)

The introduction of the SSLM algorithm opens up the possibility to investigate the performance of another PAPR reduction method known as partial transmit sequence (PTS). This technique was introduced first in [82] for the conventional OFDM system. However, the direct implementation of this method to the WHT/OQAM or the OQAM systems is causing a loss of orthogonality as explained earlier. The principle explained in the SSLM algorithm is extended to adapt PTS method for the WHT/OQAM system.

In this technique, the input data block of length M is partitioned to U disjoints sets $x^{(u)}$ (u=0,1, …., U-1). Each partition elements maintain their locations in the original data block and set to zero the other elements. Mathematically, this can be expressed as

$$x^{(u)} = \left[0_{0:\frac{uM}{U}-1} \quad x^{(u)}_{\left(\frac{uM}{U}\right):\frac{(u+1)M}{U}-1} \; 0_{\frac{(u+1)M}{U}:M}\right]^T \tag{4.21}$$

Each of these vectors is transformed via the V transform that can be represented as the following:

$$X_k^{(u)} = \sum_{m=0}^{M-1} \sum_{k=-\infty}^{\infty} \sum_{i=0}^{M-1} WH_{m,i} x_{i,k}^{(u)} e^{j2\pi mk/M} \tag{4.22}$$

Subsequently, these transformed vectors are multiplied by the complex rotation factor $b^{(u)} = \{\mp 1, \mp j\}$ to generate different versions. Next, they are summed to produce the output vector as

$$X_k = \sum_{u=0}^{U-1} b^{(u)} X_k^{(u)} \tag{4.23}$$

The principle of the PTS is finding the optimal selection of the rotation factors that produce the lowest PAPR in the output. Therefore, the outcome of (4.23) is exploited to calculate the PAPR and select the one with the lowest value. Finally, the selected vector is filtered with the PPN block and transmitted. It is worth to mention that the index of the selected combination of the rotation factors is required to be transmitted as side information to the receiver. The block diagram of the WPTS algorithm is illustrated in Figure 4.18.

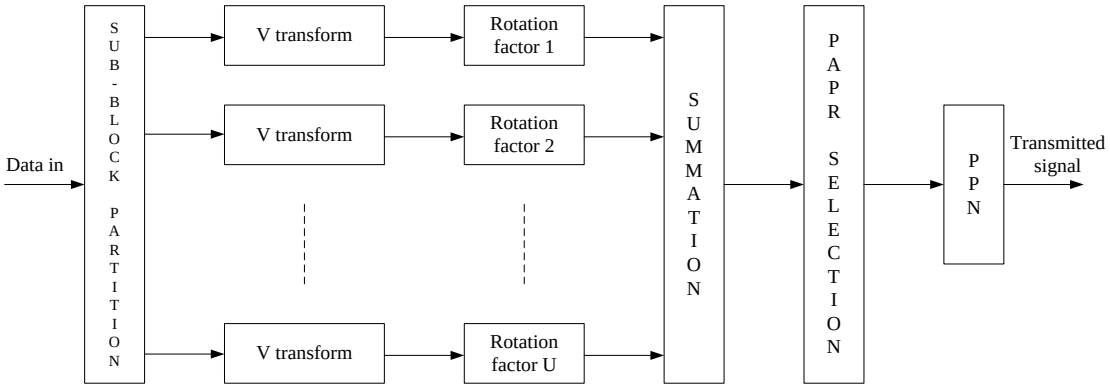

Figure 4.18 Walsh partial transmit sequence (WPTS) algorithm block diagram

To assess the performance of this algorithm, the technique is applied by means of computer simulation on WHT/OQAM system with 64 subcarriers. The data is mapped by 4-QAM. The prototype filter selected to be IOTA4. The resulting performances for different values of *U* are depicted in Figure 4.19.

The gain of this technique ranged between 0.4 – 1 dB for *U*=4 – 16. These results are compared to the results produced by the SSLM from the previous section. Although, there is a small difference in the reduction of the PAPR of each method, the WPTS required double the number of branches of the SSLM to produce matching outcome. As a result, the calculation complexity is twice as that one used in SSLM. Even with this

higher complexity, it is still well below the complexity required by the WOSLM or the OSLM.

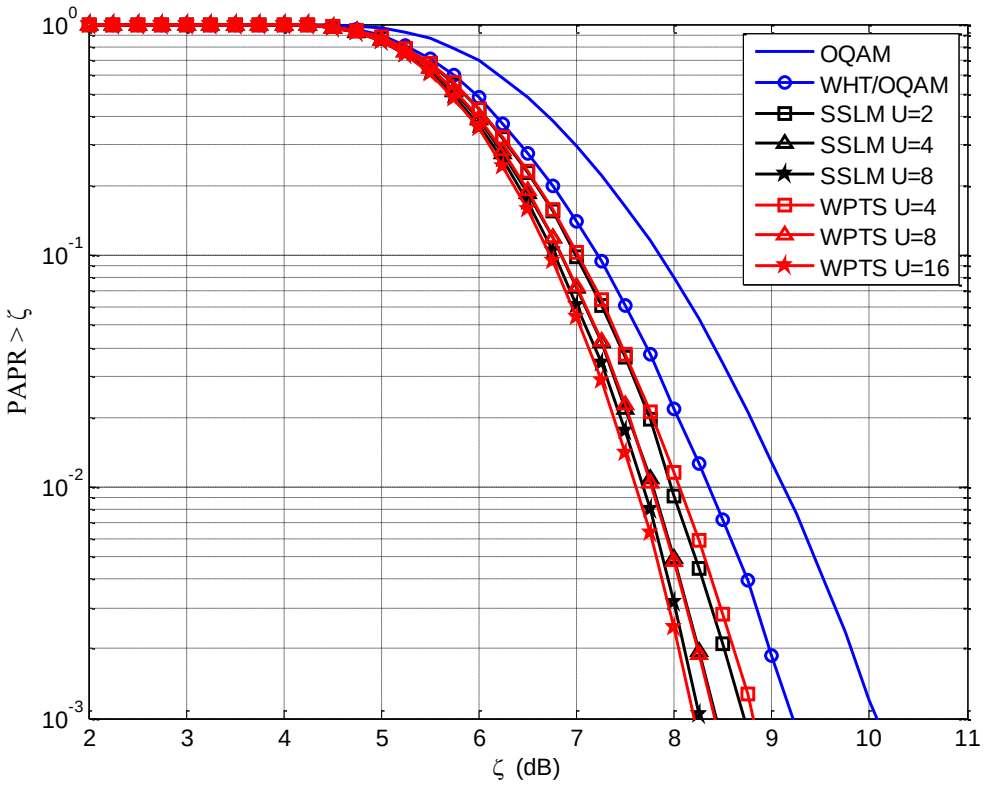

Figure 4.19 The WPTS algorithm compared to the SSLM algorithm

4.6. High Power Amplifier Effects

In this section, the implication of the distortion caused by high power amplifiers (HPA) is discussed. Power amplifiers are essential part of any transmitter to provide the essential power for the modulated signal to be delivered to the receiver. These devices vary in types and characteristics depend on the applications they are designed for.

The main problem with high power amplifiers is the nonlinearity in the amplification characteristics, which causes a nonlinear distortion in the amplified signal as illustrated in Figure 4.20. This distortion can be classified into two types: the in band intermodulation distortion and the out band intermodulation distortion [31, 86-87]. The in band is responsible for BER degradation, while the out band is causing spectral re-growth that results in an interference with the neighbouring systems.

The effect of the nonlinear distortion increases with more of the input signal works at the nonlinear part of the amplification curve. One approach for mitigation is to back-off

the power amplifier from working at the saturation region so the signal is amplified at the linear zone. However, as explained earlier, the large fluctuations in the signal envelope of multicarrier modulation forces for a high back-off, which causes a lower output power and loss in the efficiency of the amplifier. As a result, PAPR reduction methods introduced previously are the other way to go to improve the efficiency of the amplification and reduce the level of the distortion.

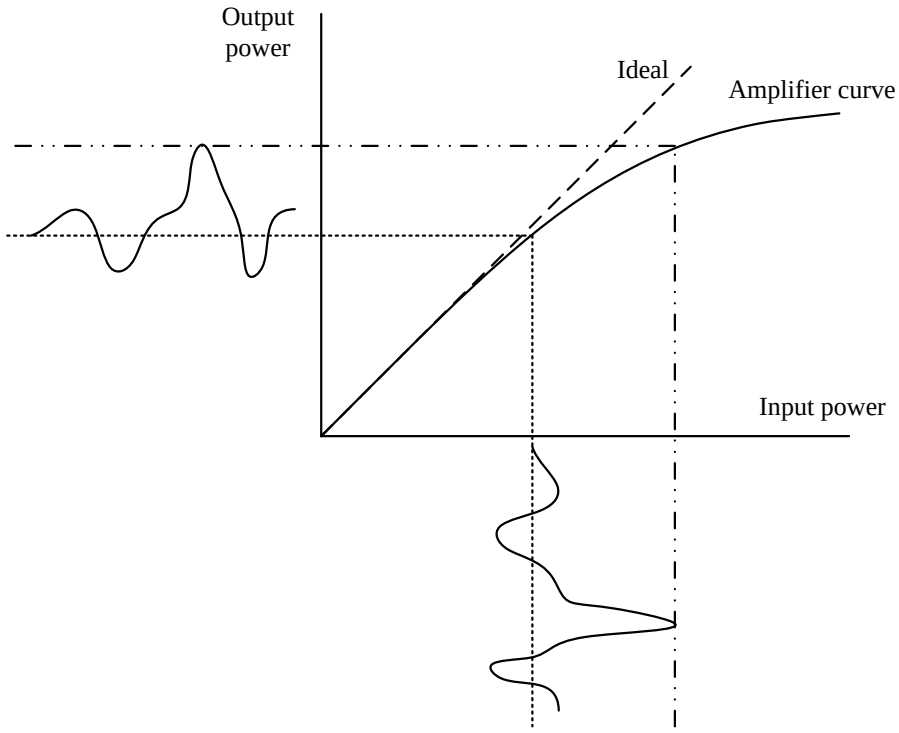

Figure 4.20 Illustration of the relation between input and output of the power amplifier

In general, there are two main types of high power amplifiers: the travelling wave tube (TWT) and the solid-state power amplifiers (SSPA). For each type, there are two parameters to represent their transfer function: the amplitude/amplitude conversion (AM/AM) and the amplitude/phase conversion (AM/PM) [4, 32, 69]. Along the transfer function, the other parameter associated with HPA is the operation point, which identified by the back-off. The input back-off (IBO) can be expressed as

$$IBO = 20\ \log_{10}\left(\frac{S}{\sqrt{P_s}}\right)\ dB \tag{4.24}$$

here S stands for the amplitude of the input signal which drives the amplifier to saturation. This value is considered equals to S=1 in this analysis. While, P_s corresponds to the statistical power of the input signal $s(t)$.

Travelling wave tube HPA is used in satellite communications, which is beyond the scope of this thesis. However, the solid state power amplifier is the common type in mobile communications that is considered in this work.

The SSPA is characterised by linear AM/AM conversion for the small signals and negligible AM/PM conversion. The transfer function of the amplitude can be expressed as the following:

$$G(A) = \frac{A}{(1 + A^{2p})^{(1/2p)}} \tag{4.25}$$

with A represents the input signal envelop and p is the smoothing factor. The characteristic of the SSPA is depicted in Figure 4.21 for different values of p and an IBO = 0 dB.

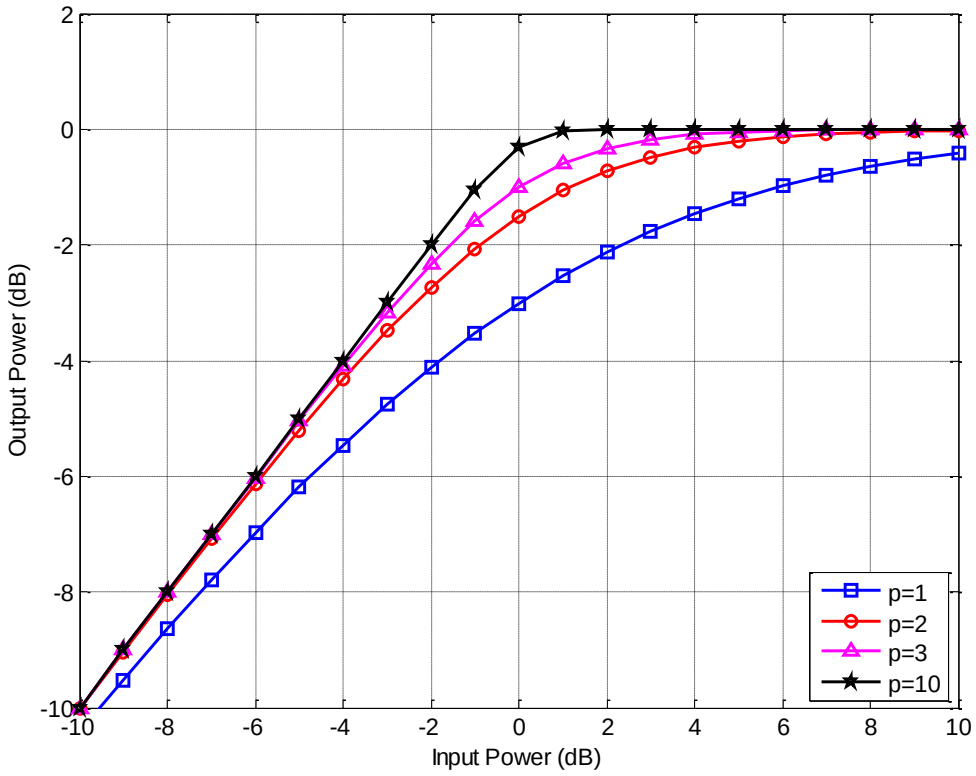

Figure 4.21 AM/AM conversion for the SSPA amplifier

To evaluate the effect of HPA on WHT/OQAM system, a computer simulation is utilised with the flowing set of parameters:

- Number of subcarriers M=128.
- 4-QAM and 16-QAM mapping.

- MIA with overlapping factor K=4.
- SSPA with p=3.
- ITU-Pedestrian type B.
- IBO = 0, 3, 5, 7 dB.
- No channel coding.

The performances of the systems are illustrated in Figure 4.22. Furthermore, the OQAM system is tested with the same initial conditions and the results are included in Figure 4.22. For the low constellation order i.e. 4-QAM, both systems performed very well and the effect of the HPA on WHT/OQAM is more apparent than on OQAM system when comparing both cases of *IBO* = 0dB and *IBO* = 3dB. In addition, the WHT/OQAM maintains its superiority over OQAM system by quite margin of 14- 16dB at BER of 10^{-4}.

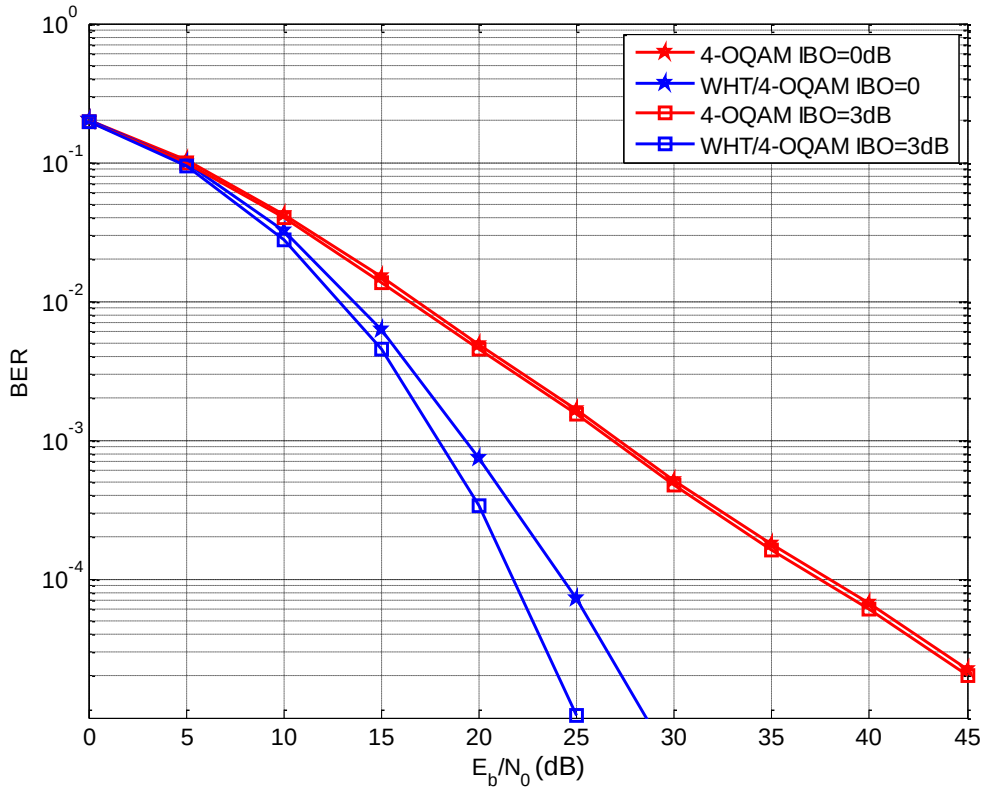

Figure 4.22 WHT/4-OQAM and 4-OQAM performances over ITU-Pedestrian type B with SSPA

Nevertheless, by increasing the mapping order to 16-QAM, both systems performances deteriorate severely with *IBO* = 0dB as illustrated in Figure 4.23. By increasing the *IBO* to 3dB, both systems start to improve though WHT/OQAM curve started to flattened

after E_b/N_o of 30 dB while the OQAM maintains its linear response. By increasing the *IBO* further to 5dB or even 7dB, the WHT/OQAM attains better performance and takes back the advantage over the OQAM by around 10-12 dB of gain at 10^{-4} BER.

This degradation in the performance of WHT/OQAM is related to the spreading property of the WHT. As the WHT spreads the local effect of the intermodulation distortion over all the subcarriers, this would increase the interference level and the BER. The same merit that enhances the performance over the frequency selective channel acts in the opposite direction with HPA.

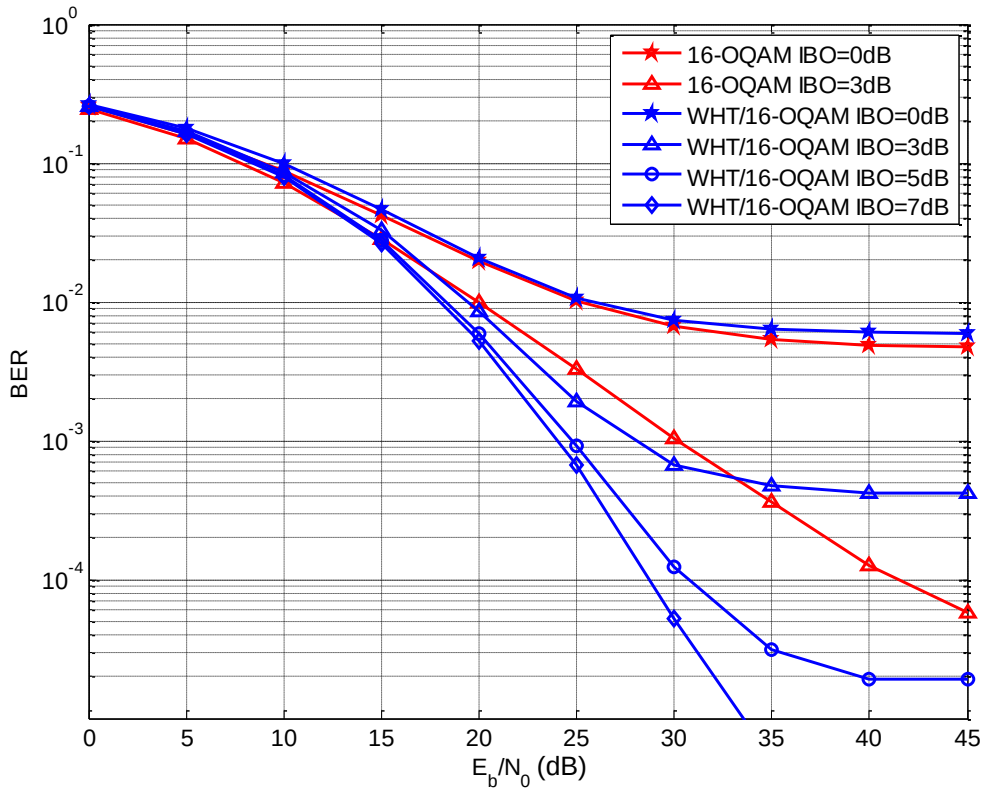

Figure 4.23 WHT/16-OQAM and 16-OQAM performances over ITU-Pedestrian type B with SSPA

Apparently, the reduction in the PAPR induced by the addition of the WHT is not quite effective in the high order constellation and the low IBO values because of the distortion distribution caused by the WHT. However, the introduced algorithms to produce lower PAPR in the signal might answer the query and restore back the superiority of the WHT/OQAM. Consequently, the system is re-examined with the inclusion of the WOSLM and the SSLM algorithms and *IBO* set to 3 dB. The resulting performances are demonstrated in Figure 4.24.

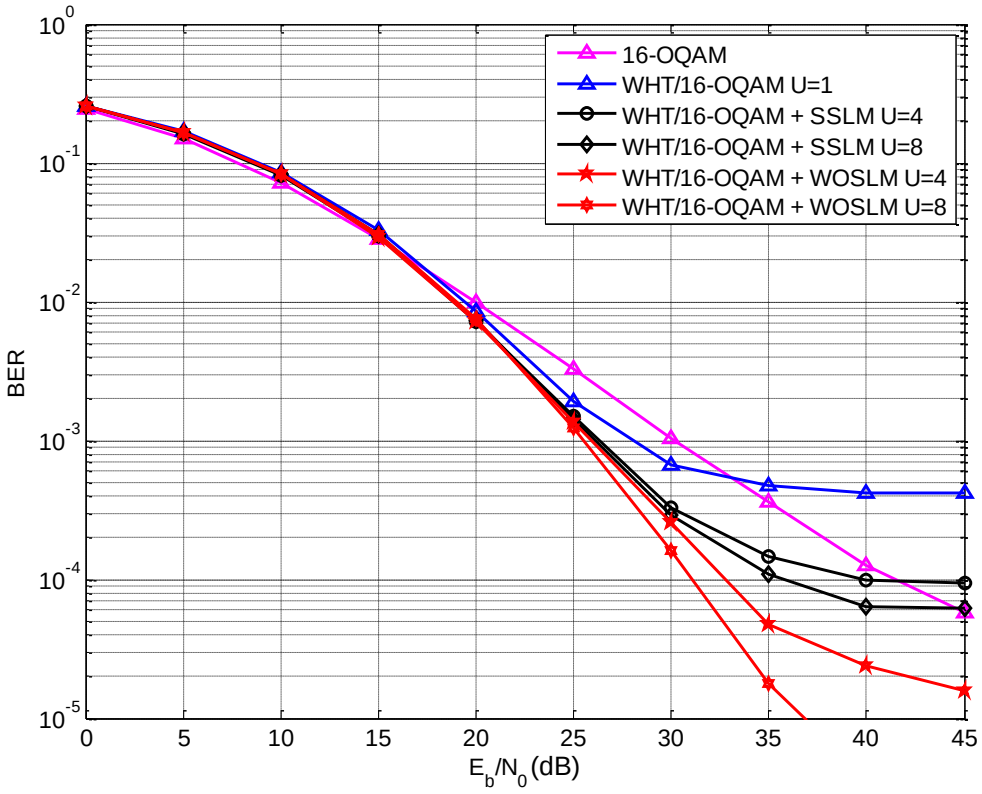

Figure 4.24 WHT/OQAM performances over ITU-Pedestrian type B with SSPA, *IBO*=3dB, and PAPR reduction algorithms

As expected from the CCDF curves of the SSLM, the improvement resulting from the SSLM algorithm is less than the other one from the WOSLM. The system restores its peak performance with WOLSM algorithm when the number of branches U=8 to achieve a gain of 11 dB at BER of 10^{-4} and 9 dB with U=4. The SSLM algorithm is also reasonably performing well, since nearly 2 dB of gain at 10^{-4} BER is produced with U=4 and almost 6 dB with U=8. Although the SSLM could not reduce all the impact of the nonlinearity of the HPA, certainly, it can bring down the BER to the functional level.

4.7. Conclusion and Summary

In this chapter, the power spectral density of the WHT/OQAM system was investigated. The new system, WHT/OQAM, maintains the capability of the OQAM system to produce a higher level of attenuation for the out of band signals compared to the conventional OFDM. The theoretical analysis of the power spectral density was developed. In addition, different prototype filters were exploited to compare their resulting power spectral densities.

The problem with the majority of the multicarrier modulation techniques is the high ratio of the peak to average power that affect the performance with the presence of the high power amplifiers. This problem was addressed for the WHT/OQAM and the attained lower ratio was discussed.

Furthermore, three new algorithms were introduced to reduce PAPR. The first method named Walsh overlapped selective mapping (WOSLM) takes the effect of overlapping between consecutive symbols into consideration to achieve remarkable reduction in the PAPR. The other two novel methods named simplified selective mapping (SSLM) and Walsh partial transmit sequence (WPTS) exclude the overlapping effect in the calculation to lower the calculation complexity cost. Both methods produce decent reduction in the PAPR values.

Finally, the consequences of the nonlinearity in the high power amplifier characteristics were demonstrated. The PAPR reduction methods were combined with high power amplifier to investigate their efficiency and the capability of the system to maintain its dominance over the conventional systems.

Chapter 5. Channel and Carrier Frequency Offset Estimations for WHT/OQAM

5.1. Introduction

In the previous chapters, the system operation was considered with perfect knowledge of the transmission channel coefficients and full time-frequency synchronisation. In practical environments, the channel is unknown to the receiver and requires a stage to determine these coefficients to employ them at the equalization stage. In addition, the receiver must be fully synchronised with the transmitter in order to demodulate the transmitted signal successfully.

In the case of WHT/OQAM (the same is applied for the OQAM), the orthogonality only exists in the real field. Thus, the imaginary part contains an interference resulted from the surrounding coefficients, as explained previously. Because of this lack of orthogonality between the real and imaginary parts, the existing methods to estimate channel coefficients for OFDM system cannot be applied directly to WHT/OQAM or OQAM.

Multicarrier modulations are sensitive to the carrier frequency offset (CFO) that results from the difference between the local oscillators frequencies at both side of the system. As a result, degradation in the subcarriers amplitudes and increase in the ICI level in the received signal, which leads to a deterioration in the system performance. Consequently, the CFO has to be rectified prior to the data reception.

The aim of this chapter is to investigate the effect of the resulting error from the channel estimation (CE) on the system performance. Next, a channel estimator for the WHT/OQAM is to be developed and assessed. The CFO effect is to be analysed and the sensitivity of the system is to be compared to the rivals. A simple approached to remove the CFO is to be considered.

This chapter is structured in the following manner, Section 5.2 provides an overview of the related work in the literature concerning channel and carrier frequency offset estimations. In Section 5.3 a preview to the basics of the pair of pilots channel estimation method. Section 5.4 presents the proposed channel estimation methods, in which Section 5.4.1 explains and discusses the enhanced pair of pilots' algorithm, while

Section 5.4.2 shows another variant known as the averaged enhanced pair of pilots. The performances of the two methods are studied in Section 5.4.3. In addition, Section 5.5 analyse the performance of the WHT/OQAM in the presence of the residual carrier frequency offset and evaluate its sensitivity. Moreover, a newly proposed method for the CFO is demonstrated in Section 5.6. Furthermore, Section 5.7 summaries the chapter.

5.2. Related Work

The channel estimation of the OQAM system was investigated firstly in [88], in which a scattered pilot aided estimation was introduced. The presented method focuses on the cancelation of the intrinsic interference from the neighbour subcarriers. This was obtained by modifying the values of the coefficients surrounding the pilots. Then, an interpolation process took place to estimate the channel response.

The same method of interference cancelation was utilised in [89] and applied to the preamble pilots scenario instead. Two preamble structures were presented stretched over three to five symbols duration. The work concluded that the first order neighbours are the main cause of the interference with well-localised pulse shapes such as the IOTA, so it is sufficient to consider them only in the interference calculation.

Later, an interference approximation method (IAM) for the preamble pilots was introduced in [60, 90]. The IAM focuses on utilising the interference terms to add their power constructively to the pilot term, which enhances the pilot power to reduce the noise presence in the estimated values of the channel coefficients. The IAM requires a preamble of length equal to three symbols. In addition, the estimation method by pair of pilots (POP) was commenced. The POP requires a preamble constructed of only two symbols to be executed, however, the performance of this technique is linked directly with the symbol power. An improved variant of the IAM was discussed in [91]. The improved technique replaces the real pilots with imaginary pilots in the IAM to achieve higher gain.

The scattered pilots technique for channel estimation was considered in [92]. The method is based on using orthogonal codes for the elements surrounding the pilots to eliminate the interference created by them. However, this method efficiency depends on the localisation of the prototype filter to attain usable results.

The theoretical framework for the IAM was developed in [93] and the selection for the optimal preamble configuration was analysed. The optimized configuration showed an improvement in the performance over the previous one. Nevertheless, the system still requires three symbols that equivalent to one and half complex OFDM symbol duration.

To reduce the number of real symbols required for CE, the POP scheme was improved in [94] by implementing an iterative method to remove the effect of the interference. The performance was improved with the increase of number of iterations. However, this technique involves high calculation cost. The same concept was applied for the scattered pilots case in [95]. In both scenarios, the receiver is considered to have full knowledge of the transmitted pilots including the intrinsic interference originated from the transmitter.

Another approach to avoid the interference, [96] investigated the effectiveness of adding guard symbols to the preamble in two ways: either on both sides or just before the preamble. The results of the two methods were similar; however, the encountered loss in the number of symbols was high.

Furthermore, the factor that affects the performance of the IAM was studied and specified in [97]. The power of the imaginary interference was regarded the main factor that can be utilised to enhance the efficiency of the IAM. Therefore, a system with two prototype filters was proposed. The first filter operates during the preamble transmission, while the second filter activated throughout the data part. Consequently, the complexity of the system is higher and it requires two different filters in operation, which limits the practicality of this method.

There are two main approaches to detect the CFO: blind and data aided estimators. A considerable amount of research has been done for both techniques for the OQAM system. The early research [98-99] investigated the robustness of the OQAM system and indicated an edge to the OQAM over the OFDM as a result to the implementation of pulse shapes.

A number of methods for blind carrier frequency estimation have been proposed in [100-106]. Theses algorithms depend on the conjugate and the un-conjugate second order cyclostationarity property of the transmitted OQAM signal to determine the CFO by exploiting the maximum likelihood or least squares estimators. However, this topic

is beyond the scope of this these and the interested reader can refer to the indicated references for further reading.

The data aided CFO estimation is also considered for the OQAM system. In [107-109] the joint symbol timing and CFO estimation were performed at the time domain by exploiting preamble signals. The proposed method requires two symbols with identical parts to achieve the estimation based on the least squares (LS) or the maximum likelihood (ML) approaches. This concept is extended in [110] by introducing a sliding window over a longer preamble signal to attain better timing and frequency synchronization. Nevertheless, the presented algorithm requires preamble of length of ten symbols to converge to an accurate estimation.

In addition, the scattered pilots were also employed to estimate the CFO in [111-112]. The technique is based on generating auxiliary pilots beside the original pilots to eliminate the intrinsic interference from the surrounding subcarriers, then the main pilots in the frequency domain is utilised to estimate the timing and the CFO. This method is conditioned by reliable estimation to the channel coefficients before estimating the CFO.

5.3. Pair of Pilots Preamble Channel Estimator

In the ideal case scenario, to estimate the channel coefficients perfectly the transmitted signal is known at the receiver and the noise term can be taken out of the calculations as presented in Figure 5.1. However, this is impossible in practice and there is always some error between the actual and the estimated values. The preamble constructed from pair of pilots is one of the methods that has some similarity with the basic method in the conventional CP-OFDM. In this section, the operation of this method is discussed and the weaknesses are highlighted.

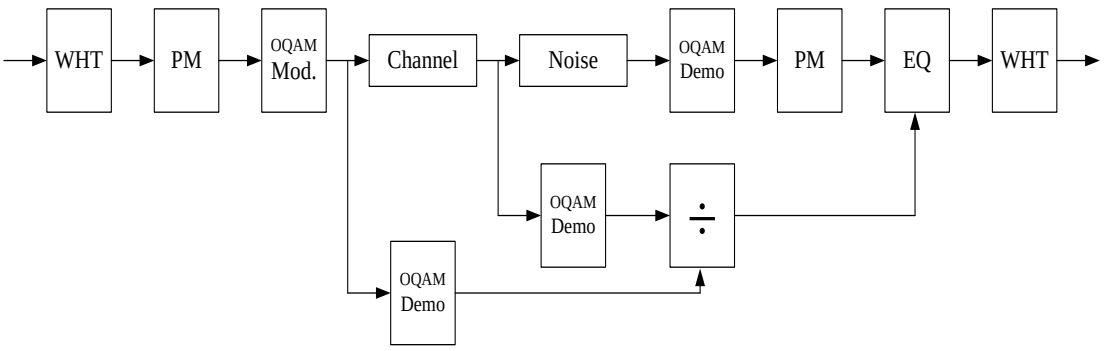

Figure 5.1 Ideal channel estimator for perfect CE

Recalling that the demodulated symbol of the WHT/OQAM after the FFT block with the noise term being removed is given by

$$y_{m_o,n_o} = H_{m_o,n_o} a_{m_o,n_o} + \sum_{m,n \neq m_o,n_o} a_{m,n}\, \Delta\theta\, e^{j\frac{\pi}{2}(m-m_o)(n+n_o)} H_{m,n} \times Ag\left[(n_o-n)\tau_o, (m-m_o)\frac{1}{M}\right] \quad (5.1)$$

Equation (5.1) can be written in a compact form as

$$y_{m_o,n_o} = H_{m_o,n_o}\left(a_{m_o,n_o} + j\frac{H_{m,n}}{H_{m_o,n_o}} J_{m_o,n_o}\right) \quad (5.2)$$

with J_{m_o,n_o} a real valued term that represents the intrinsic interference caused by the surrounding subcarriers to the one with index m_o,n_o.

The interference term, as discussed previously, is a pure imaginary term and for the well-localised prototype filters, it is limited to small zone surrounding that subcarrier, which can be expressed as

$$y_{m_o,n_o} = H_{m_o,n_o}\left(a_{m_o,n_o} + j\frac{H_{\Delta m,\Delta n}}{H_{m_o,n_o}} J^{\Delta m,\Delta n}_{m_o,n_o} + j\frac{H_{m,n}}{H_{m_o,n_o}} J^{m>\Delta m,n>\Delta n}_{m_o,n_o}\right) \quad (5.3)$$

where $J^{\Delta m,\Delta n}_{m_o,n_o}$ stands for the interference of in the effective zone which can be limited to Δm=1 and Δn=1 for the well localised pulse such as the IOTA. While $J^{m>\Delta m,n>\Delta n}_{m_o,n_o}$ indicates the interference accumulated from the elements outside that zone. The last term can be ignored as its level is well below the noise level [90, 97].

The remaining interference produced from the effective zone can be eliminated or reduced based on the selection of pilots' distribution. The pair of pilots' method utilises two real symbols, which is equivalent to one complex symbol compared to the standard OFDM system. Hence, there is no loss in the transmission rate efficiency compared to the IAM method.

In practice the POP are inserted at two successive symbols i.e. m_o=m_1 and n_1= n_o+1. In addition, by assuming the channel is quasi static over the two symbols i.e. $H_{m_o,n_o} = H_{m_1,n_1}$. Moreover, $J^{Im}_{\Delta m_o,\Delta n_o}$ denotes the compact form of $J^{\Delta m,\Delta n}_{m_o,n_o}$. Thus, the output of the FFT block can be written as [60, 90]

$$y_{m_o\,,\,n_o} = H_{m_o,\,n_o}\left(a_{m_o\,,\,n_o} + jJ^{Im}_{\Delta m_o\,,\,\Delta n_o}\right)$$
$$y_{m_1\,,\,n_1} = H_{m_1,\,n_1}\left(a_{m_1,\,n_1} + jJ^{Im}_{\Delta m_1\,,\,\Delta n_1}\right) \quad (5.4)$$

The terms $\frac{H_{\Delta m,\Delta n}}{H_{m_o,\,n_o}}$ and $\frac{H_{\Delta m,\Delta n}}{H_{m_1,\,n_1}}$ are taken out simply as the channel is invariant over the effective interference zone. By introducing a factor that represents the ratio between the real and imaginary parts of the complex channel coefficient, that is: $Q = \frac{H^{Im}_{m_o,\,n_o}}{H^{Re}_{m_o,\,n_o}}$. Then, by splitting the real and imaginary terms and rearranging equation (5.4):

$$y^{Re}_{m_o\,,\,n_o} = H^{Re}_{m_o,\,n_o}\,a_{m_o\,,\,n_o} - QH^{Re}_{m_o,\,n_o}J^{Im}_{\Delta m_o\,,\,\Delta n_o}$$
$$y^{Im}_{m_o\,,\,n_o} = QH^{Re}_{m_o,\,n_o}\,a_{m_o\,,\,n_o} + H^{Re}_{m_o,\,n_o}J^{Im}_{\Delta m_o\,,\,\Delta n_o}$$
$$y^{Re}_{m_1\,,\,n_1} = H^{Re}_{m_o,\,n_o}\,a_{m_1\,,\,n_1} - QH^{Re}_{m_o,\,n_o}J^{Im}_{\Delta m_1\,,\,\Delta n_1}$$
$$y^{Im}_{m_1\,,\,n_1} = QH^{Re}_{m_o,\,n_o}\,a_{m_1\,,\,n_1} + H^{Re}_{m_o,\,n_o}J^{Im}_{\Delta m_1\,,\,\Delta n_1} \quad (5.5)$$

Next, the real equations and imaginary equations are combined to produce two set of equations as the following:

$$\frac{y^{Re}_{m_o\,,\,n_o} + QH^{Re}_{m_o,\,n_o}J^{Im}_{\Delta m_o\,,\,\Delta n_o}}{a_{m_o\,,\,n_o}} = \frac{y^{Re}_{m_1\,,\,n_1} + QH^{Re}_{m_o,\,n_o}J^{Im}_{\Delta m_1\,,\,\Delta n_1}}{a_{m_1\,,\,n_1}}$$
$$\frac{y^{Im}_{m_o\,,\,n_o} - H^{Re}_{m_o,\,n_o}J^{Im}_{\Delta m_o\,,\,\Delta n_o}}{a_{m_o\,,\,n_o}} = \frac{y^{Im}_{m_1\,,\,n_1} - H^{Re}_{m_o,\,n_o}J^{Im}_{\Delta m_1\,,\,\Delta n_1}}{a_{m_1\,,\,n_1}} \quad (5.6)$$

This results in:

$$a_{m_1\,,\,n_1}y^{Re}_{m_o\,,\,n_o} - a_{m_o\,,\,n_o}y^{Re}_{m_1\,,\,n_1} = QH^{Re}_{m_o,\,n_o} \times \left(-a_{m_1\,,\,n_1}J^{Im}_{\Delta m_o\,,\,\Delta n_o} + a_{m_o\,,\,n_o}J^{Im}_{\Delta m_1\,,\,\Delta n_1}\right)$$
$$a_{m_1\,,\,n_1}y^{Im}_{m_o\,,\,n_o} - a_{m_o\,,\,n_o}y^{Im}_{m_1\,,\,n_1} = H^{Re}_{m_o,\,n_o} \times\left(a_{m_1\,,\,n_1}J^{Im}_{\Delta m_o\,,\,\Delta n_o} - a_{m_o\,,\,n_o}J^{Im}_{\Delta m_1\,,\,\Delta n_1}\right) \quad (5.7)$$

From (5.7) Q can be found as

$$Q = \frac{a_{m_1\,,\,n_1}y^{Re}_{m_o\,,\,n_o} - a_{m_o\,,\,n_o}y^{Re}_{m_1\,,\,n_1}}{a_{m_o\,,\,n_o}y^{Im}_{m_1\,,\,n_1} - a_{m_1\,,\,n_1}y^{Im}_{m_o\,,\,n_o}} \quad (5.8)$$

Now, to calculate the real part of the channel coefficient $H^{Re}_{m_o,\,n_o}$, the first two equation in (5.5) can be rewritten such as:

$$y^{Re}_{m_o\,,\,n_o} = H^{Re}_{m_o,\,n_o}\,a_{m_o\,,\,n_o} - QH^{Re}_{m_o,\,n_o}J^{Im}_{\Delta m_o\,,\,\Delta n_o}$$
$$Qy^{Im}_{m_o\,,\,n_o} = Q^2H^{Re}_{m_o,\,n_o}\,a_{m_o\,,\,n_o} + QH^{Re}_{m_o,\,n_o}J^{Im}_{\Delta m_o\,,\,\Delta n_o} \quad (5.9)$$

Then, by adding these equations, yielding:

$$H^{Re}_{m_o,\,n_o} = \frac{y^{Re}_{m_o\,,\,n_o} + Q y^{Im}_{m_o\,,\,n_o}}{a_{m_o\,,\,n_o}(1+Q^2)} \tag{5.10}$$

And the imaginary part can be calculated as

$$H^{Im}_{m_o,\,n_o} = Q H^{Re}_{m_o,\,n_o} \tag{5.11}$$

These equations indicate the possibility of estimating the channel coefficients without the need for prior knowledge of the transmitted signal and specifically the pulse shape filter.

All the previous derivation omits the effect of the noise; therefore, the relative noise term η can be included in equation (5.7) to become:

$$\begin{aligned} Z_1 &= Q H^{Re}_{m_o,\,n_o}\left(-a_{m_1\,,\,n_1} J^{Im}_{\Delta m_o\,,\,\Delta n_o} + a_{m_o\,,\,n_o} J^{Im}_{\Delta m_1\,,\,\Delta n_1}\right) + \eta_{m_o\,,\,n_o} \\ Z_2 &= H^{Re}_{m_o,\,n_o}\left(a_{m_1\,,\,n_1} J^{Im}_{\Delta m_o\,,\,\Delta n_o} - a_{m_o\,,\,n_o} J^{Im}_{\Delta m_1\,,\,\Delta n_1}\right) + \eta_{m_1\,,\,n_1} \end{aligned} \tag{5.12}$$

The ratio of Z_1/Z_2 indicates the effect of the noise on the CE accuracy, which can be expressed as the following:

$$\frac{Z_1}{Z_2} = Q\,\frac{1 + \dfrac{\eta_{m_o\,,\,n_o}}{H^{Re}_{m_o,\,n_o}\rho}}{1 - \dfrac{\eta_{m_1\,,\,n_1}}{H^{Re}_{m_o,\,n_o}\rho}} \tag{5.13}$$

with $\rho = \left(-a_{m_1\,,\,n_1} J^{Im}_{\Delta m_o\,,\,\Delta n_o} + a_{m_o\,,\,n_o} J^{Im}_{\Delta m_1\,,\,\Delta n_1}\right)$.

The power of the term ρ affects the quality of the CE directly, as with the increase of the value of ρ the effect of the noise is suppressed. However, if the power of ρ drops close to zero, then the noise enhancement causes degradation in the CE. Moreover, the value of ρ depends on the interference power beside the pilot power. This interference is a random value created from the elements around the pilots. Consequently, this approach of POP is not reliable enough because of these unpredicted parameters values.

5.4. Enhanced Pair of Pilots (EPOP) Channel Estimator

The aim of this section is to design a CE technique that suits the WHT/OQAM and to investigate the effect of CE errors on the performance of the system. Due to the presence of the WHT in the system, which spreads the input coefficients over all subcarrier, the WHT/OQAM requires different pattern of pilots. In fact, this spreading effect makes the scattered pilots requires more hardware to be achieved (an extra

WHT), but for the preamble method, it can be implemented directly as depicted in Figure 5.2.

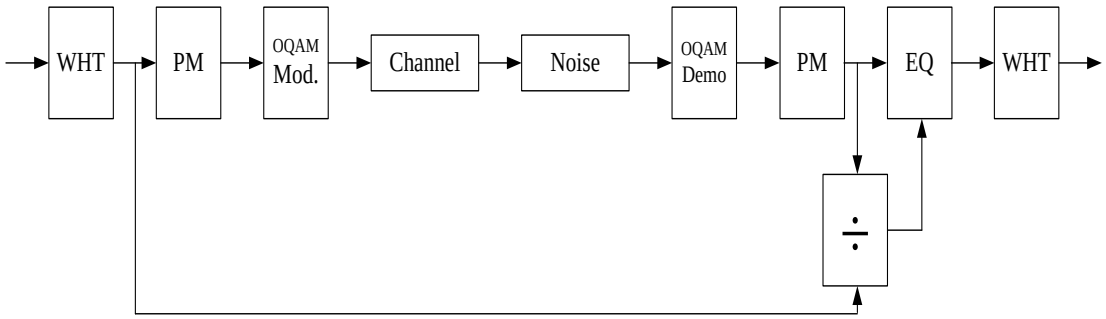

Figure 5.2 Block diagram of the channel estimation for the WHT/OQAM

As the POP discussion concluded, the power of the transmitted signal needs to be maximized and the interference power has to be cancelled. Consequently, in order to gain more control on the behaviour of the interference and to enhance the performance of the POP, a new enhanced pair of pilots (EPOP) is proposed. The new method is based on a different pilot distribution and enhanced pilots power.

5.4.1. EPOP algorithm

Before considering the preamble structure, the system operating environments required to be set. As for the WiMAX system in the last standard for the IEEE which is 802.16m [113-115], before each preamble there is a gap of no transmission followed by the preamble. This gap is known as receive time / transition gap (RTG). This gap lasts sufficient time depending on the general system parameters that can be utilized for the benefit of the preamble of the WHT/OQAM without actually transmitting anything. Consequently, this no transmission gap represents a virtual symbol that holds zero elements.

There are two symbols in the EPOP same as the POP. The first symbol contains the pilots, which normally utilizes binary phase shift keying (BPSK) mapping. The second symbol is set to zero aiming to reduce the interference (ISI in this case) to the minimum.

The structure of the first symbol can have one of two options: either cancelling the ICI interference produced from the neighbour subcarriers, or produce a constructive addition to boost the pilots by the means of the interference. The former option is illustrated in Figure 5.3 (A), while the later is shown in Figure 5.3 (B). These preambles

then processed by the WHT and the relative output is depicted in Figure 5.4 for both structures [60].

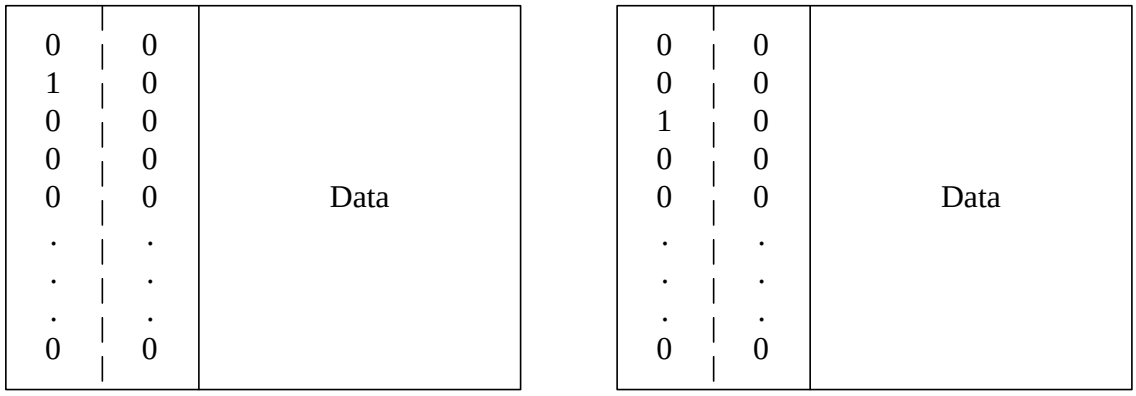

(A) (B)

Figure 5.3 The EPOP preamble structure at the input of the WHT/OQAM

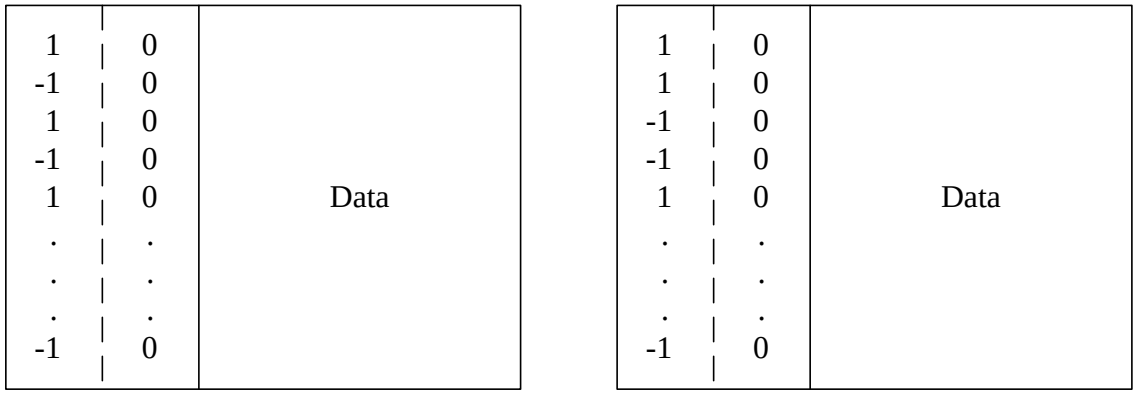

(A) (B)

Figure 5.4 The preamble at the input of the phase mapping (PM) block

The second preamble arrangement adds constructively the surrounding terms though it only contains interference of ICI type as a result of eliminating the ISI by the virtual symbol of zeros and the following symbol of zeros. As a result, the received pilot at m_o,n_o location in the first symbol over an ideal channel can be expressed as:

$$y_{m_o\,,\,n_o} = a_{m_o\,,\,n_o} + j2a_{m_o+1,\,n_o}Ag[0,1] \tag{5.14}$$

And by assuming that the pulse shape is real and even function, the value of the ambiguity function $Ag[0,1]$ equals to:

$$Ag[0,1] = \sum_{k=0}^{L-1} g^2\,[k]\, e^{j\frac{2\pi k}{M}} = \sum_{k=0}^{L-1} g^2\,[k] \cos\left(\frac{2\pi k}{M}\right) \quad (5.15)$$

The result of the last equation depends on the localisation of the filter. For example, the MIA4 with M=128 has $Ag[0,1] = 0.0054$ and the SRRC4 has $Ag[0,1] = 0.0013$, while the TFL1 has different localisation which leads to higher value of $Ag[0,1] = 0.5357$. Therefore, the contribution expected form the interference term is limited with some filters.

As explained in the previous section, by increasing the signal power, the noise effect is reduced. By assuming the receiver knows the preamble signal; the estimated channel coefficient $H_{m_o\,,\,n_o,\ ES}$ in the presence of noise can be expressed as

$$H_{m_o\,,\,n_o\,,\ ES} = H_{m_o\,,\,n_o} + \frac{\eta_{m_o\,,\,n_o}}{a_{m_o\,,\,n_o} + j2a_{m_o+1,\,n_o} Ag[0,1]} \quad (5.16)$$

Consequently, the noise term that affects the accuracy of the estimation can be contained by increasing the value of the denominator in (5.16). This is the drive for selecting the preamble structure of Figure 5.4 (B). Furthermore, in [97], the authors suggested utilising two different filters: one for the preamble transmission phase and a different one for the data phase.

In the discussion of the theoretical BER of the WHT/OQAM in Chapter 3, the real symbol is assumed to be uncorrelated Gaussian random variables with variance equals to σ_x^2. The same assumption can be applied here for the $a_{m,n}$ variables. In contrast, the OFDM system employs complex symbols with equal variance for the real and imaginary parts, this means that OFDM signal has variance equals to $2\sigma_x^2$. Thus, by comparing the power of the preamble in both systems, the WHT/OQAM preamble carries half the power of the OFDM signal. Although, the WHT/OQAM symbol power can still be boosted by including the interference power as the second preamble scheme, the interference power is reduced by setting the second symbol in the EPOP to zero and the virtual symbol of zeros. Therefore, to overcome this short in the transmitted preamble power, the EPOP proposal suggests a boost to the preamble power to become $2\sigma_x^2$ to attain an equivalent power to the OFDM system. This increase in the power of the first symbol of the preamble is compensated by the zero power of the second symbol. Thus, the average power for one complex symbol transmission is not affected.

In addition, both systems preambles are boosted eight times (9dB) in practice for the WiMAX system [114-115].

Unlike the IAM method that requires $3\tau_o$ or three real symbols to attain the CE, the EPOP employs only two symbols and a virtual symbol to estimate the channel coefficients. Moreover, the EPOP has higher level of signal power to suppress the effect of the noise as compared with POP technique.

5.4.2. Averaged EPOP algorithm

In the circumstances with more freedom to set the number of symbols to be implemented in the preamble, the EPOP can be enhanced by increasing the number of symbols to four instead of two, and then the resulting estimation represents the average to the estimation at each preamble. This proposed algorithm is known as the average EPOP (AEPOP) and the preamble structure is illustrated in Figure 5.5. This scheme is still viable compared to the CP-OFDM channel estimator even with the loss of one complex symbol, because there is no cyclic prefix with WHT/OQAM (and the OQAM). Hence, the WHT/OQAM can recover and achieve the same amount of data transmission after few symbols.

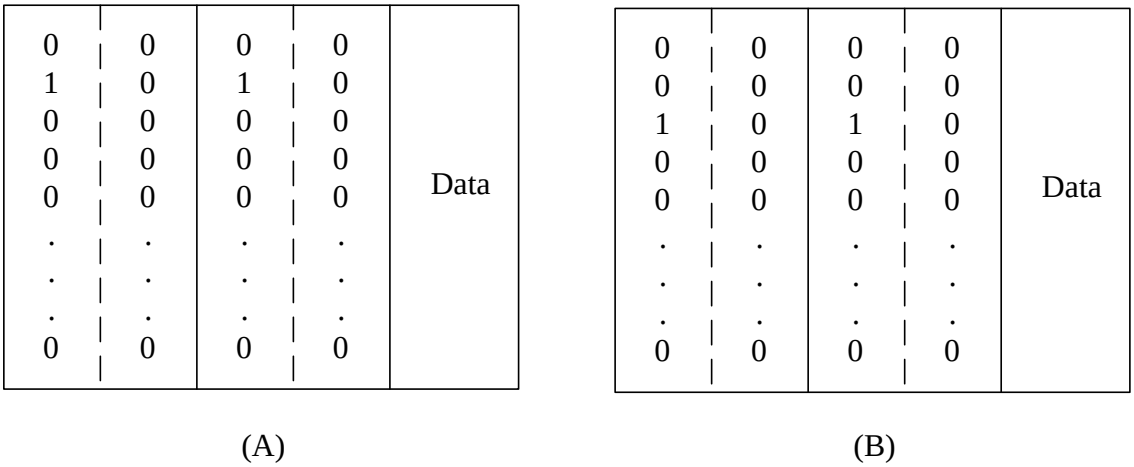

Figure 5.5 The AEPOP preamble structure at the input of the WHT/OQAM

5.4.3. EPOP and AEPOP performance

To assess the reliability of the proposed EPOP and AEPOP algorithms, the method is applied to both the WHT/OQAM and the OQAM systems over quasi-static channel in computer simulations. The number of subcarriers is set to 128 and the filter is the IOTA4. The 16QAM is the chosen mapping for the input data. The channel is the ITU-

Pedestrian type B with speed set to 6 km / hr. the frame length is set to 43 symbols [113]. The performance of both systems exploiting EPOP and AEPOP are demonstrated in Figure 5.6 and Figure 5.7.

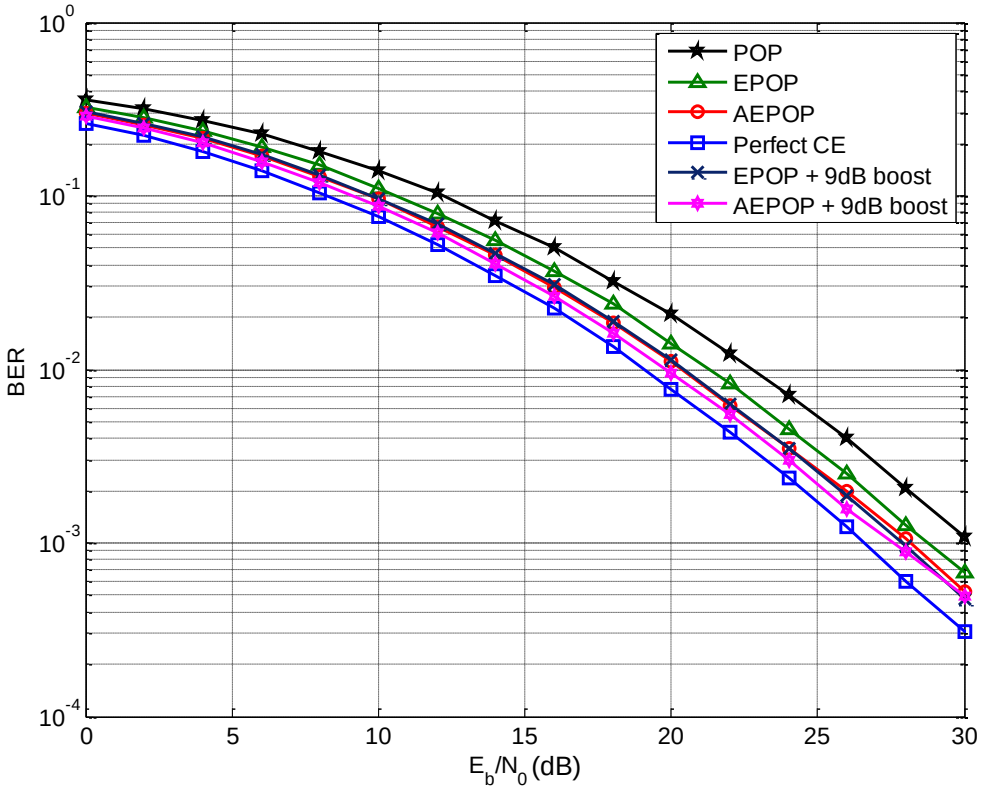

Figure 5.6 The EPOP and AEPOP algorithms performance with OQAM

The EPOP has advantage of 1.5 dB at BER of 10^{-3} over the POP method with the OQAM system without any boost. This improvement increases to 2.25 dB with 9 dB boost the power of the preamble. While the more symbols-demanding algorithm, the AEPOP, has a gain of 2 dB at 10^{-3} raises to 2.75 dB with power boost. In fact, the AEPOP with the boost is only 0.5 dB less than the perfect channel estimation performance.

The WHT/OQAM remains performing better than OQAM in term of BER even with the POP. However, the EPOP demonstrate an improvement of 2.5 dB at BER of 10^{-4} increases to 3.25 dB when the input power is 9 dB boosted. The AEPOP, as expected, achieves higher gain as a result of the noise averaging to obtain 4 dB over the POP when the preambles are enhanced. The performance of the WHT/OQAM indicates a higher sensitivity to any distortion or noise enhancement as a result of the spreading effect of the WHT. Nevertheless, the gain attained by adding the WHT is higher than

the deterioration caused by noise enhancement, which keeps the system ahead of the competitors in all cases.

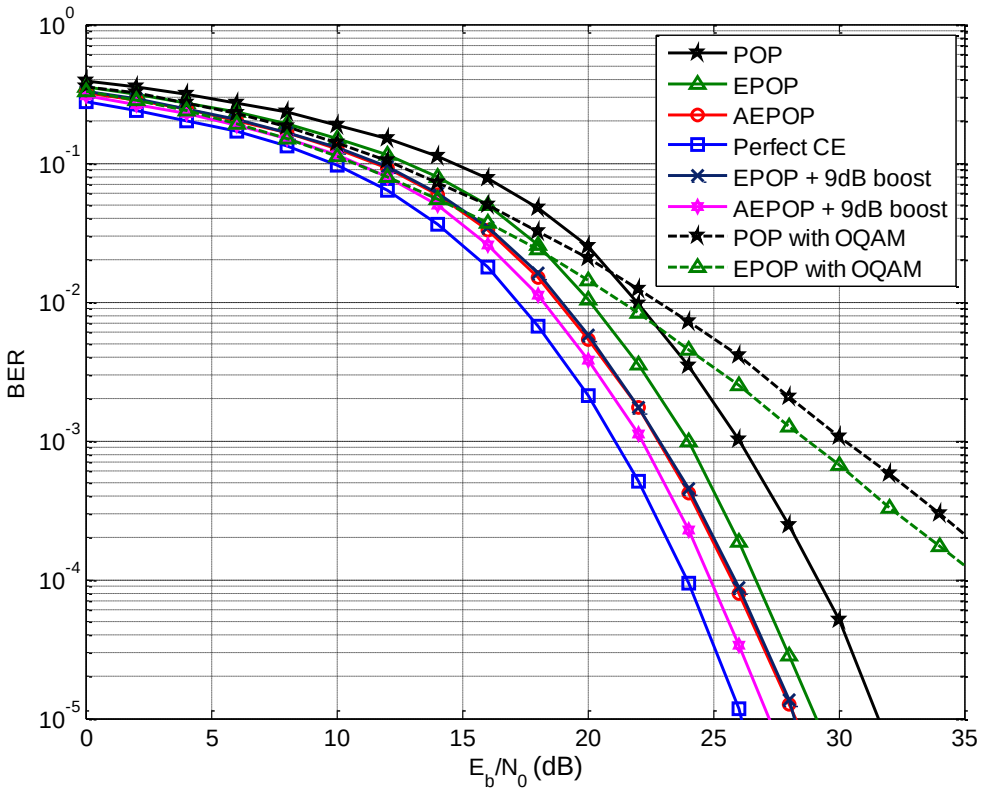

Figure 5.7 The EPOP and AEPOP algorithms performance with WHT/OQAM

5.5. WHT/OQAM Sensitivity Analysis to CFO

This section studies the influence of the CFO on the performance of the WHT/OQAM system. The OQAM system is more robust to the CFO than the OFDM system due to the utilization of well-localised filters in the filterbanks [61, 116-118]. Hence, it is important to investigate the effect of integrating the WHT on the performance of the system.

The CFO is one of the common impairments in wireless communication systems. It is originated from the difference between the local oscillators' frequencies at both ends of the system that convert the signals between baseband and the RF stages. This mismatch between the oscillators causes a deterioration in amplitude of the received signal plus increasing the level of the ICI, which destroys the orthogonality between subcarriers and halt the demodulation process [119].

For better understanding of the CFO effect, a graphical illustration for the OQAM spectrum can be used, as in Figure 5.8. The IOTA1 is chosen to emphasise the case of a pulse shape with bad localisation that causes higher levels of interference. Hence, in Figure 5.8(A), the subcarriers suffer from small interference from the neighbour subcarriers even with normalised carrier frequency offset ε (the ratio of the CFO to the subcarrier spacing) equals to zero.

Then, by increasing the CFO to ε = 0.25, as in Figure 5.8 (B), the received signal is composed from reduced signal amplitude and increased interference level especially for the neighbour subcarrier. It is clear how the CFO destroys the orthogonality and impairs the performance of the system.

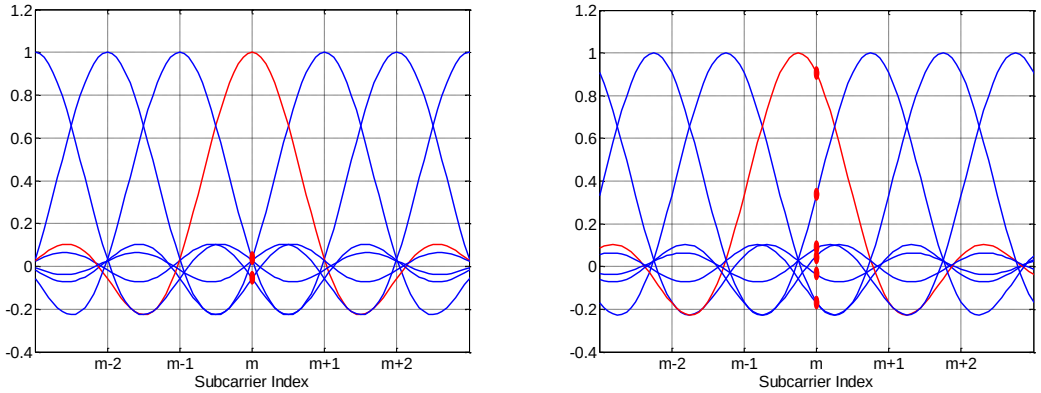

(A) ε = 0 (B) ε = 0.25

Figure 5.8 The effect of CFO on the subcarrier frequency spectrum for IOTA1

The baseband equivalent system of the WHT/OQAM is demonstrated in Figure 5.9, which includes the CFO term $e^{j(2\pi\varepsilon t+\varphi)}$ with φ represents a constant phase offset. To study the effect of the CFO on the performance, the coarse CFO and the timing offset is assumed to be compensated previously. Consequently, the residual CFO is small value and has limited effect on the performance. Therefore, taking out the noise effect, the received signal can be written as the following:

$$\begin{aligned} r(t) &= \left(s(t) \otimes h(t)\right)e^{j\left(\frac{2\pi\varepsilon t}{M}+\varphi\right)} \\ &= \left(\sum_{d=0}^{D-1} h(t,\tau_d)s(t-\tau_d)\right)e^{j\left(\frac{2\pi\varepsilon t}{M}+\varphi\right)} \\ &= e^{j\varphi}\sum_{d=0}^{D-1} h_d \sum_{n=-\infty}^{\infty}\sum_{m=0}^{M-1} a_{m,n}g(t-\tau_d-n\tau_o)\theta_{m,n}e^{j2\pi m(t-\tau_d)/M}e^{j\frac{2\pi\varepsilon t}{M}} \end{aligned} \quad (5.17)$$

The CFO term causes a constant phase rotation with time. By carrying out with the same method and assumptions conducted in chapter 3, the demodulated received signal at subcarrier m_o and time index n_o can be expressed as

$$y_{m_o\,,\,n_o} = e^{j\varphi} \sum_{n=-\infty}^{\infty} \sum_{m=0}^{M-1} a_{m,n}\, \Delta\theta e^{j\frac{\pi}{2}(m-m_o)(n+n_o)} e^{j\frac{\pi}{2}\varepsilon(n+n_o)} \underbrace{\sum_{d=0}^{D-1} h_d e^{-\frac{j2\pi\, m\, \tau_d}{M}}}_{H_m}$$

$$\times\; Ag\left[(n_o - n)\tau_o\,, \frac{(m - m_o + \varepsilon)}{M}\right] \tag{5.18}$$

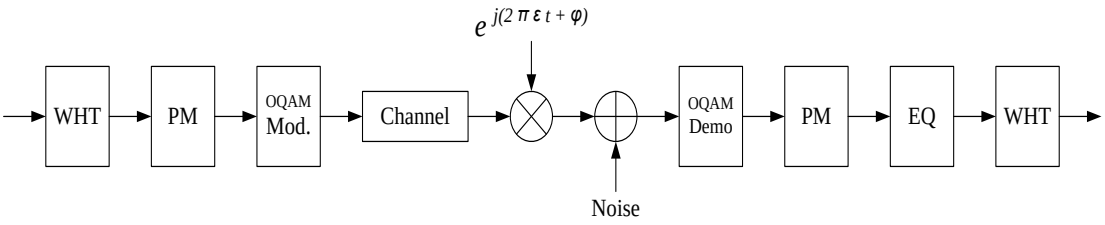

Figure 5.9 System model including the CFO term

Next, by splitting the received signal between the effective part with $m,n = m_o,n_o$ and the interference part with $m,n \neq m_o,n_o$, the previous equation can be written as

$$\begin{aligned} y_{m_o\,,\,n_o} &= e^{j\varphi} e^{j\pi\varepsilon n_o} H_{m_o} Ag\left[0, \frac{\varepsilon}{M}\right] a_{m_o\,,\,n_o} \\ &+ e^{j\varphi} \sum_{m,n\,\neq\, m_o\,,\,n_o} a_{m,n}\, \Delta\theta e^{j\frac{\pi}{2}(m-m_o)(n+n_o)} e^{j\frac{\pi}{2}\varepsilon(n+n_o)} H_m \\ &\times\; Ag\left[(n_o - n)\tau_o\,, \frac{(m - m_o + \varepsilon)}{M}\right] \end{aligned} \tag{5.19}$$

The ambiguity function term $Ag\left[0, \frac{\varepsilon}{M}\right]$, here indicates attenuation in the amplitude of the specified subcarrier compared to the case of $Ag[0,0] = 1$ for the case of zero CFO. Nevertheless, this term is very close to one for the small values of ε (residual COF) and can be assumed $Ag\left[0, \frac{\varepsilon}{M}\right] \approx 1$. While the term $Ag\left[(n_o - n)\tau_o\,, \frac{(m-m_o+\varepsilon)}{M}\right]$ reflects the produced ICI as a result of the CFO shift.

By assuming a perfect phase estimation and setting the equalization stage to equal $e^{j\pi\varepsilon n_o M} H_{m_o}$, the equalized symbol can be written as

$$\hat{a}_{m_o\,,\,n_o} = a_{m_o\,,\,n_o} \tag{5.20}$$

$$+ \underbrace{\sum_{m,n \neq m_o\,,\,n_o} a_{m,n}\,\Theta_{m,n} e^{j\frac{\pi}{2}\varepsilon(n-n_o)}\,\frac{H_m}{H_{m_o}}\,Ag\left[(n_o-n)\tau_o\,,\frac{(m-m_o+\varepsilon)}{M}\right]}_{I^{\varepsilon}_{m_o\,,\,n_o}}$$

$$= a_{m_o\,,\,n_o} + I^{\varepsilon}_{m_o\,,\,n_o}$$

The outcome of (3.22) then processed by the WHT to reconstruct the distributed symbol, which results in:

$$\hat{x}_{q\,,n_o} = x_{q,\,n_o} + \underbrace{\sum_{m=0}^{M-1} WH_{q,m}\,I^{\varepsilon}_{m\,,\,n_o}}_{CI^{\varepsilon}_{m\,,\,n_o}} \tag{5.21}$$

The last equation shows the resulting effect of the interference for each subcarrier, which equals to the average value of the interference of all subcarriers. Hence, this is a random variable and depends on the individual subcarriers levels. Consequently, the slight increase in the CFO level is more pronounced on the performance than the ordinary OQAM as the WHT distributes the effect on all subcarriers.

To compare between the performance of the WHT/OQAM and the conventional systems, a computer simulation was utilised to evaluate these systems over two situations: AWGN channel and ITU-Pedestrian type B multipath channel. The number of subcarriers is set to 256. The primary filter is the IOTA with length of 4*M*. The length of the CP is chosen to be *M*/4. The mapping of the systems are fixed to 16-QAM. Perfect channel equalization and timing synchronization are assumed.

The BER of the WHT/OQAM with E_b/N_o=10dB over AWGN channel as a function of the CFO is illustrated in Figure 5.10. The impact of the CFO on the OFDM is higher than the other systems that employ filterbanks in the system. The WHT/OQAM and the OQAM showed similar behaviour, as expected, because the WHT has no effect on the system performance over AWGN channels due to the lack of deep fade on any subcarrier.

The WHT/OQAM sustained superior performance over the other systems for $0 \leq \varepsilon \leq 0.06$ in case of the multipath channel for E_b/N_o=25dB as depicted in Figure 5.11. While the OFDM comes the last in term of the immunity to the CFO. The performance of the system is also considered by utilizing different types of pulse shapes. Also from the graph, it is clear that IOTA4 has better localization in the frequency domain followed by the SRRC4 then the MIA4, which demonstrated more sensitivity to the CFO.

To have an insight view of the performance of the systems over a wider range of SNR, the responses of the three systems are compared over a different values of residual CFO as shown in Figure 5.12 and Figure 5.13. In all these results, the filterbanks based systems have more room for the error in the CFO estimation than the case of the OFDM.

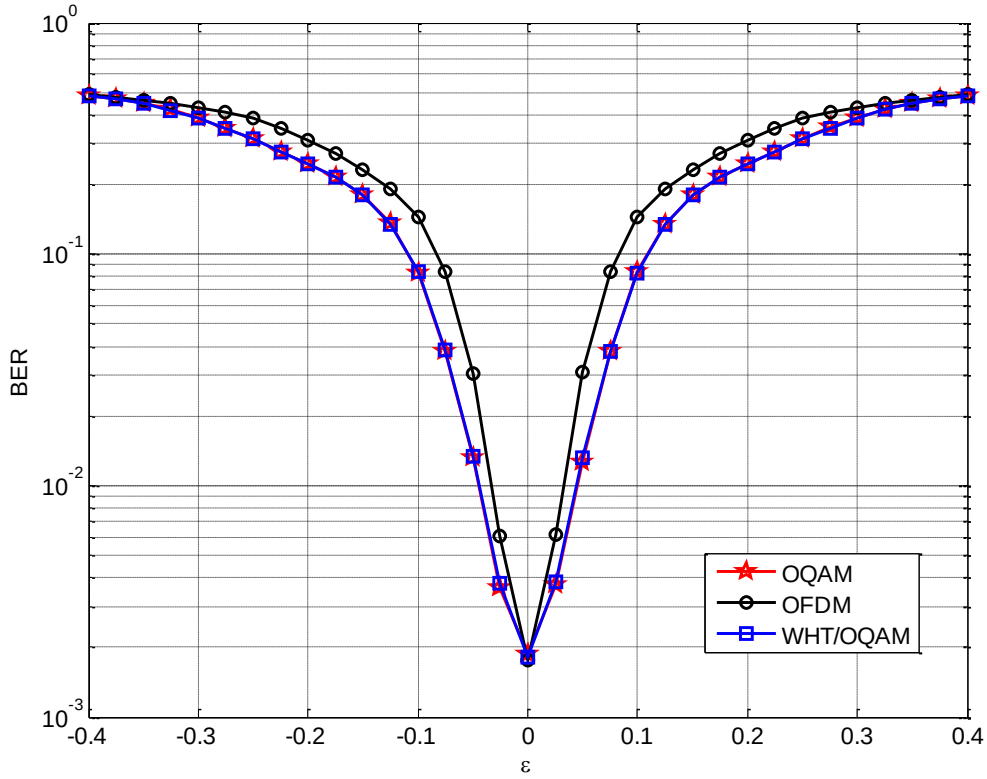

Figure 5.10 BER as a fuction of the CFO over the AWGN channel with E_b/N_o=10dB

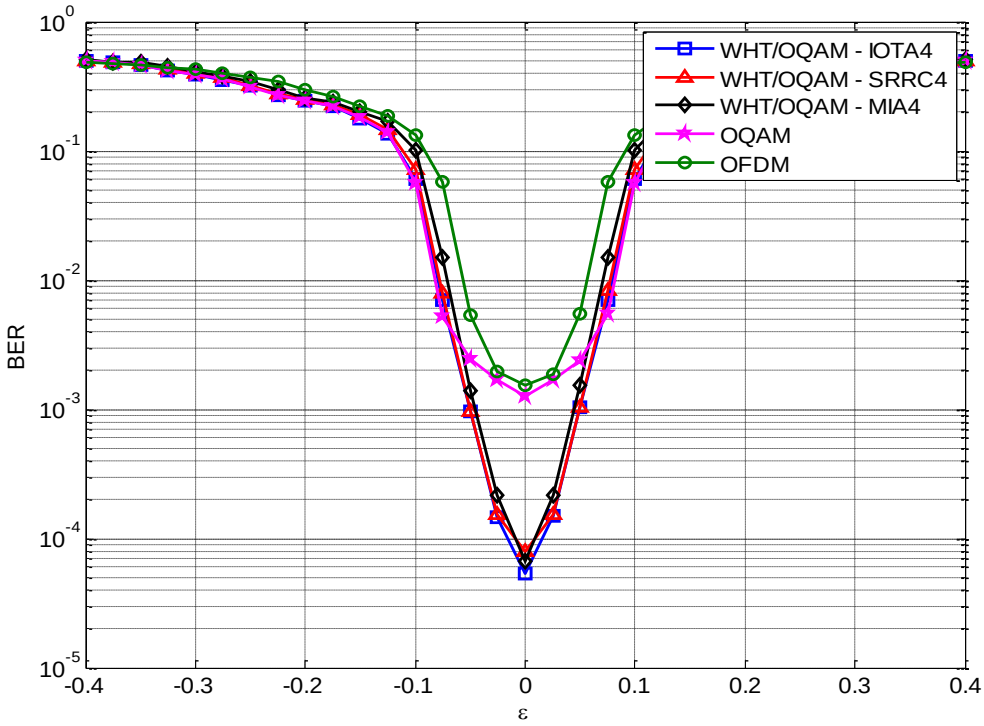

Figure 5.11 BER as a fuction of the CFO over the ITU-Pedestrian type B multipath channel with E_b/N_o=25dB

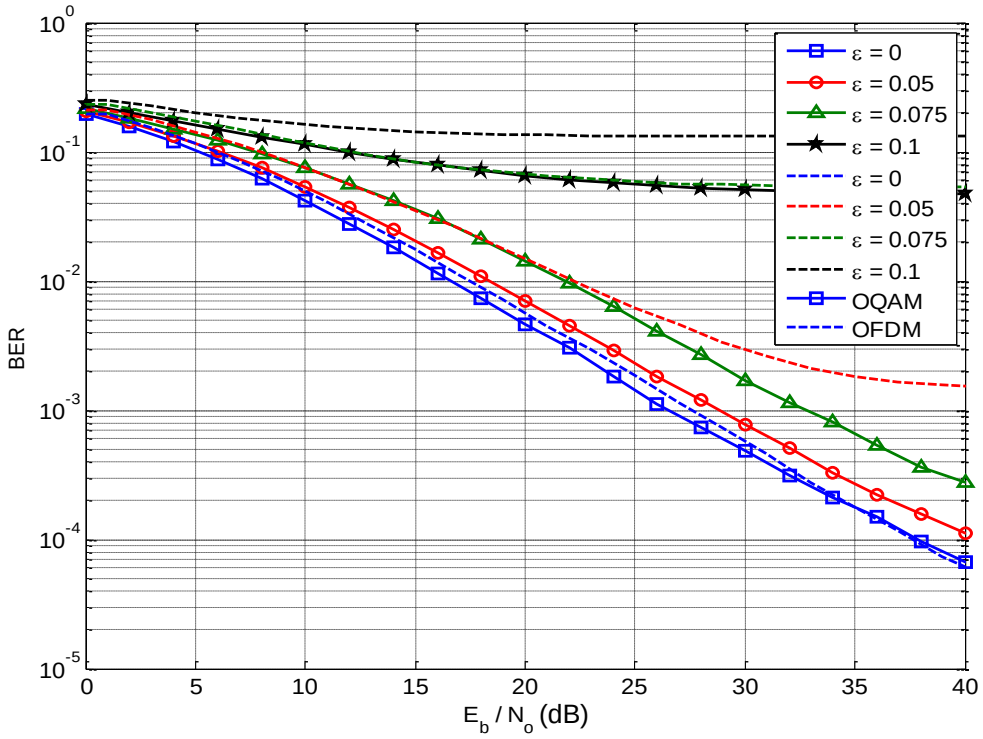

Figure 5.12 OQAM and OFDM systems sensitivity to the CFO over a multipath channel

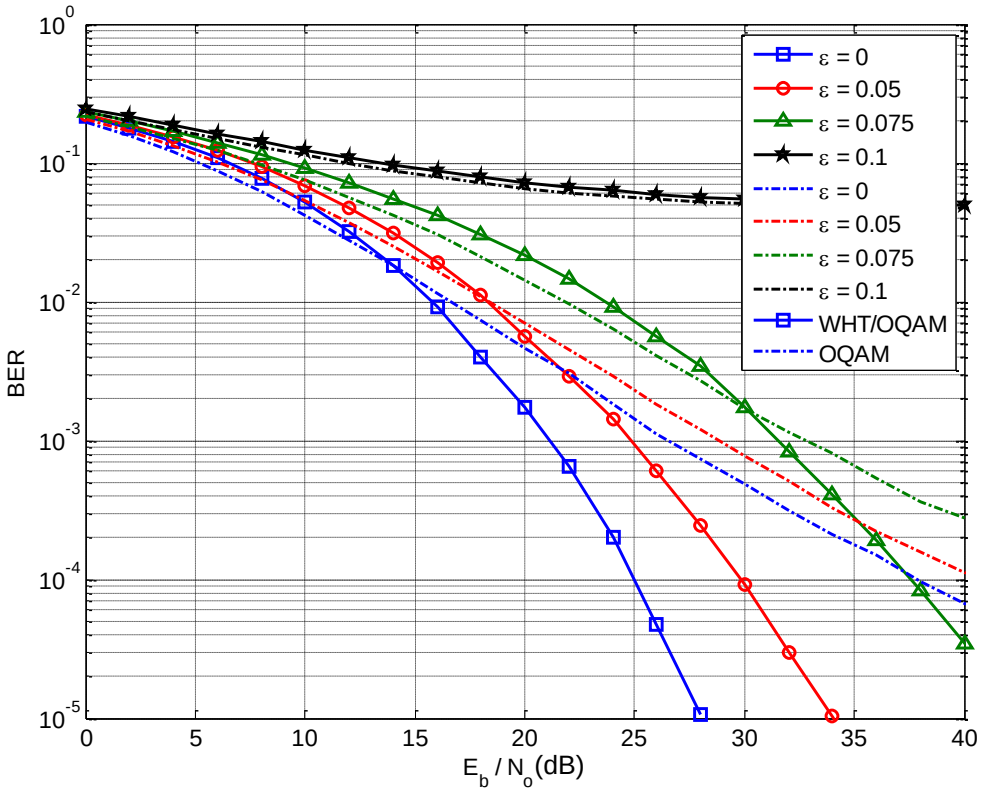

Figure 5.13 WHT/OQAM and OQAM systems sensitivity to the CFO over a multipath channel

5.6. CFO Estimation for WHT/OQAM

The estimation of the CFO is one of the stages that performs its task before the modulation process of the data starts. This stage is inevitable in any MCM to overcome the consequences of the CFO. The data aided CFO estimation relies on the preamble signals or the scattered pilots to execute the estimation process. This section aims to investigate the level of error encountered in the CFO estimators. Two methods are considered for the estimation: frequency domain (FD) estimation and time domain (TD) estimation.

The proposed CFO estimation conducted in the frequency domain is based on the approach originally proposed in [120]. The algorithm is based on the difference between the phases of the subcarriers of consecutive preamble symbols. It requires similar blocks of data to be transmitted so that the same phase values of the modulation held constant at each subcarrier, assuming slow fading channel. This approach differs from the method reported in [111-112] by executing the estimation at the preamble stage not the scattered pilots. In addition, this technique has no extra calculation overhead over the

TD approach, as the preamble signals required to be processed by the receiver filterbank for the channel estimation purposes.

By considering the preamble designs produced in the previous section, the POP or the EPOP preamble are not suitable options. This is because, in both techniques, the second symbol carries no data that can be utilised in the correlation process. Therefore, the possible options are either to utilise two POP preambles or the proposed AEPOP scheme.

In equation (5.17), the CFO produces a linear time varying phase rotation of $2\pi\varepsilon/M$. This rotation is transferred to frequency shift after the receiver filterbank equals to $\pi\varepsilon$ radians as a result of the symbol duration of $\tau_o = T/2$. Consequently, if two pilots at the same subcarrier index m_o, and at two different symbols after Δn samples, then the phase rotation relation between these two symbols can be expressed as [111-112]

$$\Delta\phi = \pi\varepsilon\,\Delta n \tag{5.22}$$

Hence, the normalised CFO can be estimated as the following:

$$\begin{aligned}\hat{\varepsilon} &= \frac{\Delta\phi}{\pi\,\Delta n} \\ &= \frac{1}{\pi\,\Delta n}\tan^{-1}\frac{\sum_{m=0}^{M-1} Im\left(j^{-\Delta n} y_{m_o,\,n_o+\Delta n}\, y^*_{m_o,\,n_o}\right)}{\sum_{m=0}^{M-1} Re\left(j^{-\Delta n} y_{m_o,\,n_o+\Delta n}\, y^*_{m_o,\,n_o}\right)}\end{aligned} \tag{5.23}$$

The same principle applies for the time domain estimation with signals being compared prior to the receiver filterbank, so the estimated ε can be written as [108]

$$\hat{\varepsilon} = \frac{1}{\pi\,\Delta n}\tan^{-1}\frac{\sum_{k=0}^{M-1} Im\left(r\left(k+\frac{\Delta nM}{2}\right)r^*(k)\right)}{\sum_{k=0}^{M-1} Im\left(r\left(k+\frac{\Delta nM}{2}\right)r^*(k)\right)} \tag{5.24}$$

To evaluate the performance of the two approaches, a system with 128 subcarriers is considered. The filter is set to IOTA4, while the channel is taken first as the AWGN then as the ITU-Pedestrian type B channel to simulate the slow fade. The normalised CFO is randomly generated with values varied in the range $-0.45 \le \varepsilon \le 0.45$. Two types of preamble signals: two consecutive POP and AEPOP are utilised with both estimation methods.

The resulting root mean square error (RMSE) for the FD and TD are depicted in Figure 5.14. It can be noted that the TD algorithm demonstrated gain of around 1 dB over the

FD in all the evaluations. This is because of the reconstruction error produced by the NPR filter utilised at the receiver filterbank. As expected, the AEPOP produces better results compared to the case of two POP preambles as a result of the enhanced signal to noise ratio. Although FD method loses some performance over TD, it is still within the acceptable error margin of the system. It is worth noting that this method can be applied for the WHT/OQAM as well as the OQAM systems without any restriction.

Based on the sensitivity analysis to the CFO, clearly the WHT/OQAM can sustain superior performance over the OQAM system at any signal levels over the 10 dB in the case of multipath channel in which the RMSE level is less than the 0.05%.

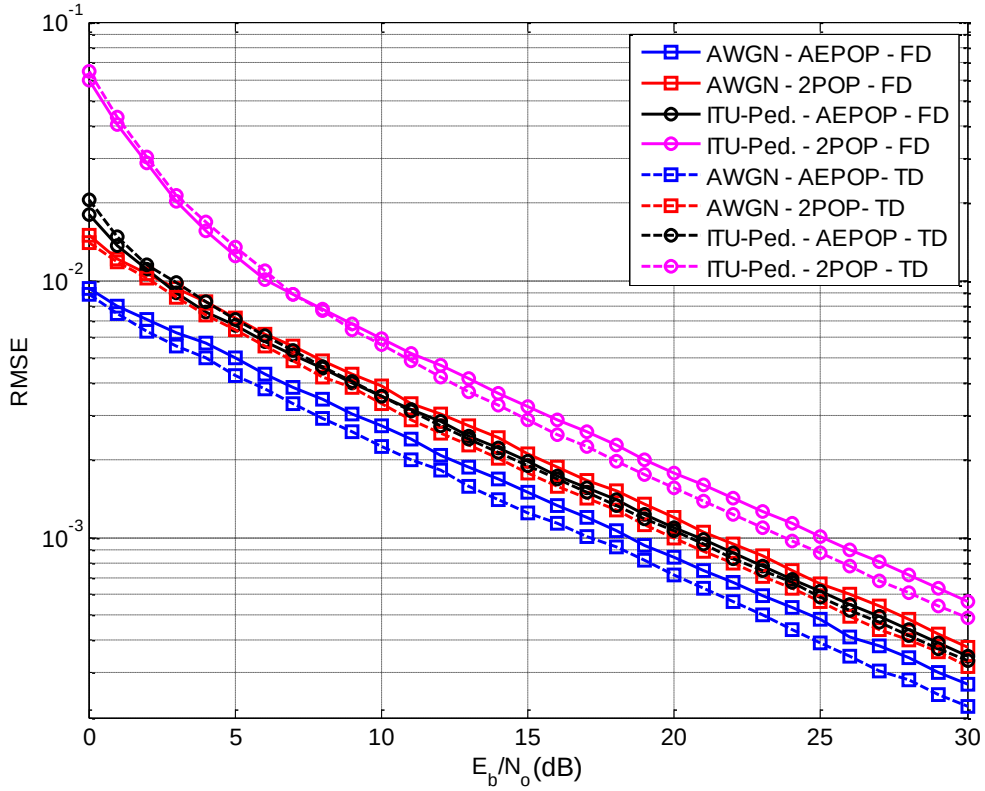

Figure 5.14 RMSE of the CFO estimation by the FD and TD approaches

5.7. Conclusion and Summary

In this chapter, channel estimation stage was investigated. A new enhanced method to estimate channel coefficients was proposed and investigated. This method utilises the practical environments to attain more compact design while enhancing the pilots power to match them with the standards to gain better performance. Two variations of the preambles were suggested and analysed. The proposed techniques are verified and

compared with the existing ones via computer simulation to confirm the validity and the efficiency of the methods.

Taking into the consideration the practical environments, the carrier frequency offset impairment was also studied. System sensitivity to the residual CFO was analysed and evaluated. Computer simulations results indicate better immunity to the CFO than the standard OFDM. Although the system is less sensitive to the CFO, it must have a CFO estimation stage prior to the modulation stage with higher degree of freedom over the OFDM. A simple approach to estimate the CFO in the frequency domain was proposed and combined with the preamble schemes previously suggested to the system. Furthermore, the proposed method was compared with time domain estimation technique through simulations to show close match in the accuracy.

Chapter 6. Conclusion and Further Work

6.1. Conclusion

The current revolution in mobile communications like never before, increased the demand on more efficient and more reliable systems that can satisfy the rich multimedia contents requirements. Multicarrier modulation systems are the leaders in this filed represented by the well-known OFDM technique. Unfortunately, this technique has some drawbacks that impair its performance. The main one is the loss in the transmission efficiency due to the utilization of the cyclic prefix that can take up 25% of the transmission bandwidth in severely distorted channels.

The motivation behind this thesis was to create an alternative multicarrier modulation system that can achieve better performance and provide better transmission rate. Besides that, this system must have acceptable computational complexity compared with OFDM. All these factors are taken into account in the proposal for the new system.

The main contribution of this thesis was to present a novel system based on the combination of the OFDM with offset QAM and Walsh-Hadamard transform. The OFDM/OQAM is multicarrier system that exploits filterbanks and real coefficients to attain full transmission bandwidth. The Walsh-Hadamard transform is a unitary matrix exploited to spread the data uniformly. The combination of the WHT as a precoder and the OFDM/OQAM as a modulator produced a system, named WHT/OFDM/OQAM that has a superior BER performance over multipath fading channels compared to the conventional systems. The analytical model of the system was provided and the theoretical BER with closed form equations was derived. Computer simulations confirmed the validity of the proposal and the acceptable accuracy of the theoretical calculations.

Due to the importance of the low computational complexity in mobile communications, the complexity of the proposed system was investigated and a new fast algorithm was developed. Computational complexity of the system with the new V-transform was derived and formulated. A remarkable reduction in the computational complexity was achieved by utilising V-transform.

As a result of utilising filterbank in the construction of the modulator, the system benefit of having higher attenuation in the stopband compared to the OFDM. The theoretical

power spectral density (PSD) of the WHT/OFDM/OQAM was derived and a closed form solution was produced. Computer simulation provided a comparison between different types of filters and the standard OFDM.

As with the other multicarrier modulation systems that suffer from the large dynamic range in their signal envelop, the problem of the high peak to average power ratio (PAPR) was studied. Three algorithms to reduce PAPR level based state of art techniques were proposed. The WOSLM technique provides high level of PAPR reduction while SSLM and WPTS both provide reasonable PAPR reduction but with high reduction in the implementation complexity. All of the three methods were evaluated and compared by computer simulations to the existing approaches. The computational complexity was also calculated and formulated.

Furthermore, system performance was studied in the presence of high power amplifiers. The assessment indicates the ability of the system to restore its superiority over the conventional systems in the presence of the previously developed PAPR reduction techniques.

The channel estimation process for the WHT/OFDM/OQAM was researched. Two schemes (EPOP and AEPOP) of preamble pilots featuring the current standard in WiMAX and enhanced pilot power were proposed to attain better channel estimation results. Computer simulations confirmed the validity and the efficiency of the suggested pilots' patterns.

Finally, WHT/OFDM/OQAM performance was evaluated in the presence of the carrier frequency offset (CFO). System sensitivity to the residual CFO was analysed and evaluated by the means of computer simulations. A simple approach based on EPOP and AEPOP to estimate the CFO in frequency domain was developed and assessed via computer simulations.

6.2. Further Work

This research project concentrated primarily on developing WHT/OFDM/OQAM system; however, there is still a room for improvement that can be considered in future work. In this work, the WHT is considered as the spreading matrix due to its real values, unitary property and very low computational complexity; however, future work should consider another real transforms such as the discrete Hartley transform (DHT) or even the DFT to achieve lower complexity. Although the system benefits from the precoding

of the WHT, it would be interesting to compare the performance in the presence of the channel coding.

While this thesis covered constellation of the mapping stage of orders no more than 16 for the QAM, extending the work to higher constellation order is worthwhile to be investigated. As the increase in the level of inherited interference might require advance equalization stage.

Accurate BER closed form solutions were derived for the system in AWGN and multipath fading channels environments. This work can be extended to consider HPA nonlinearity and CFO effects.

Furthermore, the effect of the maximum Doppler shift and timing offset were not considered in this study based on the assumption of perfect phase and timing synchronisation. The research would benefit form including user speed and timing synchronization errors in the system performance assessments. It could be useful to consider joint timing and CFO estimation methods besides the CFO estimation presented in this study.

This thesis proposed different algorithms to reduce the computational complexity, these algorithms can benefit from implementing them in hardware by exploiting field programmable gate array (FPGA) and digital signal processing (DSP) units. This could show the potential of such algorithms and reveal their efficiency in practice.

Further work should consider a compound of the WHT/OQAM and, the other diversity technique, the multiple-input-multiple-output (MIMO) system in order to take this system to the practical level of the mobile communication systems.

References

[1] U. Madhow, *Fundamentals of Digital Communication*. Cambridge: Cambridge University Press, 2008.

[2] I. Gohberg and S. Goldberg, *Basic Operator Theory*. Boston, MA: Birkhäuser, 1981.

[3] M. Vetterli and J. Kovaˇcevi´c, *Wavelets and Subband Coding*. New Jersey: Prentice Hall PTR, 2007.

[4] N. Benvenuto and G. Cherubini, *Algorithms for Communications Systems and their Applications*. Sussex, England: John Wiley & Sons, Ltd., 2002.

[5] R. J. Duffin and A. C. Schaeffer, "A class of nonharmonic Fourier series," *Transactions of the American Mathematical Society*, vol. 72, pp. 341-366, 1952.

[6] D. Gabor, "Theory of communication. Part 1: The analysis of information," *Electrical Engineers - Part III: Radio and Communication Engineering, Journal of the Institution of,* vol. 93, pp. 429-441, 1946.

[7] I. Daubechies, "The wavelet transform, time-frequency localization and signal analysis," *Information Theory, IEEE Transactions on,* vol. 36, pp. 961-1005, 1990.

[8] M. A. Rieffel, "Von Neumann algebras associated with pairs of lattices in Lie groups," *Mathematische Annalen*, vol. 257, pp. 403-418, 1981.

[9] J. Ramanathan and T. Steger, "Incompleteness of Sparse Coherent States," *Applied and Computational Harmonic Analysis*, vol. 2, pp. 148-153, April 1995.

[10] S. Mallat, *A Wavelet Tour of Signal Processing*. San Diego, Ca: Academic Press, 1999.

[11] R. Balian, "Un principe d'incertitude fort en th´eorie du signal ou enm´ecanique quantique," *C. R. Acad. Sci. Paris S´er. IIM´ec. Phys. Chim. Sci. Univers Sci. Terre*, vol. 20, pp. 1357–1362, 1981.

[12] F. Low, "Complete sets of wave packets," *A passion for physics - essays in honor of Geoffrey Chew (C.DeTar, et al., Eds.), World Scientific,* pp. 17-22, 1985.

[13] J. J. Benedetto, C. Heil, and D. F. Walnut, "Differentiation And The Balian-Low Theorem," *Journal of Fourier Analysis and Applications,* vol. 1, pp. 355-402, 1995.

[14] J.-P. Gabardo and D. Han, "Balian–Low phenomenon for subspace Gabor frames," *Journal of Mathematical Physics,* vol. 45, pp. 3362-3378, Aug. 2004.

[15] W. Kozek and A. F. Molisch, "Nonorthogonal pulseshapes for multicarrier communications in doubly dispersive channels," *Selected Areas in Communications, IEEE Journal on,* vol. 16, pp. 1579-1589, 1998.

[16] R. Haas and J.-C. Belfiore, "A Time-Frequency Well-localized Pulse for Multiple Carrier Transmission," *Wirel. Pers. Commun.,* vol. 5, pp. 1-18, 1997.

[17] M. I. Doroslovacki, "Product of second moments in time and frequency for discrete-time signals and the uncertainty limit," *Signal Processing,* vol. 67, pp. 59-76, 1998.

[18] P. Siohan, C. Siclet, and N. Lacaille, "Analysis and design of OFDM/OQAM systems based on filterbank theory," *Signal Processing, IEEE Transactions on,* vol. 50, pp. 1170-1183, 2002.

[19] M. Ibnkahla, *Signal processing for mobile communications handbook*. Washington, DC.: CRC Press LLC, 2005.

[20] R. W. Chang, "Synthesis of band-limited orthogonal signals for multichannel data transmission," *Bell Systems Tech. Journal,* vol. 45, pp. 1775–1796, Dec. 1966.

[21] S. B. Weinstein, "The history of orthogonal frequency-division multiplexing [History of Communications]," *Communications Magazine, IEEE,* vol. 47, pp. 26-35, 2009.

[22] N. LaSorte, W. J. Barnes, and H. H. Refai, "The History of Orthogonal Frequency Division Multiplexing," in *Global Telecommunications Conference, 2008. IEEE GLOBECOM 2008. IEEE,* 2008, pp. 1-5.

[23] S. Weinstein and P. Ebert, "Data Transmission by Frequency-Division Multiplexing Using the Discrete Fourier Transform," *Communication Technology, IEEE Transactions on,* vol. 19, pp. 628-634, 1971.

[24] A. Peled and A. Ruiz, "Frequency domain data transmission using reduced computational complexity algorithms," in *Acoustics, Speech, and Signal Processing, IEEE International Conference on ICASSP '80.*, 1980, pp. 964-967.

[25] G. Cherubini, E. Eleftheriou, and S. Olcer, "Filtered multitone modulation for very high-speed digital subscriber lines," *Selected Areas in Communications, IEEE Journal on,* vol. 20, pp. 1016-1028, 2002.

[26] H. Bolcskei, F. Hlawatsch, and H. G. Feichtinger, "Frame-theoretic analysis of oversampled filter banks," *Signal Processing, IEEE Transactions on*, vol. 46, pp. 3256-3268, 1998.

[27] Z. Cvetkovic and M. Vetterli, "Oversampled filter banks," *Signal Processing, IEEE Transactions on*, vol. 46, pp. 1245-1255, 1998.

[28] B. Saltzberg, "Performance of an Efficient Parallel Data Transmission System," *Communication Technology, IEEE Transactions on*, vol. 15, pp. 805-811, 1967.

[29] B. Hirosaki, "An Orthogonally Multiplexed QAM System Using the Discrete Fourier Transform," *Communications, IEEE Transactions on*, vol. 29, pp. 982-989, 1981.

[30] M. Bellanger and J. Daguet, "TDM-FDM Transmultiplexer: Digital Polyphase and FFT," *Communications, IEEE Transactions on*, vol. 22, pp. 1199-1205, 1974.

[31] H. Schulze and C. Luders, *Theory and Applications of OFDM and CDMA*. Sussex, England: John Wiley & Sons Ltd, 2005.

[32] S. Hara and R. Prasad, *Multicarrier techniques for 4G mobile communications*. Boston: Artech House, 2003.

[33] M.-O. Pun, M. Morelli, and C.-C. J. Kuo, *Multi-Carrier Techniques for Broadband Wireless Communications: A Signal Processing Perspective*. London: Imperial College Press, 2007.

[34] B. Le Floch, M. Alard, and C. Berrou, "Coded orthogonal frequency division multiplex [TV broadcasting]," *Proceedings of the IEEE*, vol. 83, pp. 982-996, 1995.

[35] J. W. Cooley and J. W. Tukey, "An algorithm for the machine calculation of complex Fourier series," *Math. Comp.*, vol. 19, pp. 297-301, 1965.

[36] Z. Wang and G. B. Giannakis, "Wireless Multicarrier Communications: Where Fourier Meets Shannon," *IEEE Signal Processing Magazine* vol. 17, pp. 29-48, May 2000.

[37] T. Ihalainen, A. Viholainen, T. H. Stitz, and M. Renfors, "Generation of Filter Bank-Based Multicarrier Waveform Using Partial Synthesis and Time Domain Interpolation," *Circuits and Systems I: Regular Papers, IEEE Transactions on*, vol. 57, pp. 1767-1778, 2010.

[38] P. P. Vaidyanathan, *Multirate Systems and Filter Banks*. Englewood Cliffs, NJ: Prentice Hall Inc., 1993.

[39] N. J. Fliege, *Multirate Digital Signal processing: Multirate Systems, Filter Banks, Wavelets*. Sussex, England: John Wiley & Sons, 1994.

[40] P. Siohan and C. Roche, "Cosine-modulated filterbanks based on extended Gaussian functions," *Signal Processing, IEEE Transactions on,* vol. 48, pp. 3052-3061, 2000.

[41] D. Pinchon, R. Siohan, and C. Sidet, "A fast design method for orthogonal modulated filter banks," in *Acoustics, Speech, and Signal Processing, 2002. Proceedings. (ICASSP '02). IEEE International Conference on*, 2002, pp. 1177-1180.

[42] D. Pinchon, P. Siohan, and C. Siclet, "Design techniques for orthogonal Modulated filterbanks based on a compact representation," *Signal Processing, IEEE Transactions on*, vol. 52, pp. 1682-1692, 2004.

[43] L. Lin and B. Farhang-Boroujeny, "Cosine-modulated multitone for very-high-speed digital subscriber lines," *EURASIP Journal on Applied Signal Processing*, vol. 2006, pp. 1-16, 2006.

[44] Z. Dlugaszewski and K. Wesolowski, "WHT/OFDM - an improved OFDM transmission method for selective fading channels," in *Communications and Vehicular Technology, 2000. SCVT-200. Symposium on*, 2000, pp. 144-149.

[45] M. S. Ahmed, S. Boussakta, B. Sharif, and C. C. Tsimenidis, "OFDM Based New Transform with BER Performance Improvement across Multipath Transmission," in *Communications (ICC), 2010 IEEE International Conference on*, 2010, pp. 1-5.

[46] M. S. Ahmed, S. Boussakta, B. S. Sharif, and C. C. Tsimenidis, "OFDM Based on Low Complexity Transform to Increase Multipath Resilience and Reduce PAPR," *Signal Processing, IEEE Transactions on*, vol. 59, pp. 5994-6007, 2011.

[47] W. Yan, H. Chin Keong, and S. Sumei, "On some properties of Walsh-Hadamard transformed OFDM," in *Vehicular Technology Conference, 2002. Proceedings. VTC 2002-Fall. 2002 IEEE 56th*, 2002, pp. 2096-2100 vol.4.

[48] P. Myonghee, J. Heeyoung, C. Jaehee, C. Namshin, H. Daesik, and K. Changeun, "PAPR reduction in OFDM transmission using Hadamard transform," in *Communications, 2000. ICC 2000. 2000 IEEE International Conference on*, 2000, pp. 430-433 vol.1.

[49] R. Merched, "On OFDM and single-carrier frequency-domain systems based on trigonometric transforms," *Signal Processing Letters, IEEE*, vol. 13, pp. 473-476, 2006.

[50] D. D. Falconer, "Linear Precoding of OFDMA Signals to Minimize Their Instantaneous Power Variance," *Communications, IEEE Transactions on,* vol. 59, pp. 1154-1162, 2011.

[51] L. Zihuai, X. Pei, B. Vucetic, and M. Sellathurai, "Analysis of receiver algorithms for lte LTE SC-FDMA based uplink MIMO systems," *Wireless Communications, IEEE Transactions on,* vol. 9, pp. 60-65, 2010.

[52] L. Zhongding, W. Yan, H. Chin Keong, S. Sumei, H. Ping, and L. Yuan, "Iterative detection for Walsh-Hadamard transformed OFDM," in *Vehicular Technology Conference, 2003. VTC 2003-Spring. The 57th IEEE Semiannual*, 2003, pp. 637-640 vol.1.

[53] C. Lélé, P. Siohan, R. Legouable, and M. Bellanger, "OFDM/OQAM for Spread-Spectrum Transmission," in *Multi-Carrier Spread Spectrum 2007*. vol. 1, ed: Springer Netherlands, 2007, pp. 157-166.

[54] C. Lélé, P. Siohan, R. Legouable, and Maurice Bellanger, "CDMA Transmission with Complex OFDM/OQAM," *EURASIP Journal on Wireless Communications and Networking,* 2008.

[55] K. J. Horadam, *Hadamard matrices and their applications*. New Jersey, Oxford: Princeton University Press, 2007.

[56] H. Schulze and C. L¨uders, *Theory and Applications of OFDM and CDMA*. Chichester, Sussex: John Wiley & Sons Ltd, 2005.

[57] H. Bölcskei, "Orthogonal frequency division multiplexing based on offset QAM," in *Advances in Gabor Analysis*, H. G. Feichtinger and T. Strohmer, Eds., ed: Birkhäuser Boston, 2003, pp. 321-352.

[58] W. Shaopeng, Z. Shihua, and Z. Guomei, "A Walsh-Hadamard coded spectral efficient full frequency diversity OFDM system," *Communications, IEEE Transactions on,* vol. 58, pp. 28-34, Jan. 2010.

[59] H. Lin, P. Siohan, P. Tanguy, and J.-P. Javaudin, "An Analysis of the EIC Method for OFDM/OQAM Systems," *Journal of Communications,* vol. 4, pp. 52-60, February 2009.

[60] C. Lele, P. Siohan, R. Legouable, and J. P. Javaudin, "Preamble-based channel estimation techniques for OFDM/OQAM over the powerline," in *Power Line Communications and Its Applications, 2007. ISPLC '07. IEEE International Symposium on*, 2007, pp. 59-64.

[61] H. Saeedi-Sourck, Y. Wu, J. W. M. Bergmans, S. Sadri, and B. Farhang-Boroujeny, "Sensitivity analysis of offset QAM multicarrier systems to residual

carrier frequency and timing offsets," *Signal Processing,* vol. 91, pp. 1604-1612, 2011.

[62] T. H. Stitz, T. Ihalainen, A. Viholainen, and M. Renfors, "Pilot-Based Synchronization and Equalization in Filter Bank Multicarrier Communications " *EURASIP Journal on Advances in Signal Process.*, p. 18, 2010.

[63] L. Yuan-Pei and P. See-May, "BER minimized OFDM systems with channel independent precoders," *Signal Processing, IEEE Transactions on,* vol. 51, pp. 2369-2380, 2003.

[64] S. Askar and H. S. Al-Raweshidy, "Performance evaluation of IEEE802.16-2004 Wimax with fixed high fading channels," in *Wireless and Microwave Technology Conference (WAMICON), 2011 IEEE 12th Annual*, 2011, pp. 1-6.

[65] IEEE, "Channel Models for Fixed Wireless Applications," in *IEEE 802.16 Broadband Wireless Access Working Group*, ed, 2001.

[66] ITU, "Guidelines for the evaluation of radio transmission technologies for IMT-2000," in *Recommendation ITU-R M.1225*, ed, 1997.

[67] S. Boussakta and A. G. J. Holt, "Fast algorithm for calculation of both Walsh-Hadamard and Fourier transforms (FWFTs)," *Electronics Letters,* vol. 25, pp. 1352-1354, 1989.

[68] M. T. Hamood and S. Boussakta, "Fast Walsh-Hadamard-Fourier Transform Algorithm," *Signal Processing, IEEE Transactions on,* vol. 59, pp. 5627-5631, 2011.

[69] A. Skrzypczak, P. Siohan, N. Chotkan, and M. Djoko-Kouam, "OFDM/OQAM: An appropriate modulation scheme for an optimal use of the spectrum," in *Communications, Control and Signal Processing, 2008. ISCCSP 2008. 3rd International Symposium on*, 2008, pp. 405-410.

[70] S. Alexandre, S. Pierre, and J. Jean-Philippe, "Power Spectral Density and Cubic Metric for the OFDM/OQAM Modulation," in *Signal Processing and Information Technology, 2006 IEEE International Symposium on*, 2006, pp. 846-850.

[71] H. Seung Hee and L. Jae Hong, "An overview of peak-to-average power ratio reduction techniques for multicarrier transmission," *Wireless Communications, IEEE,* vol. 12, pp. 56-65, 2005.

[72] J. Tao and W. Yiyan, "An Overview: Peak-to-Average Power Ratio Reduction Techniques for OFDM Signals," *Broadcasting, IEEE Transactions on,* vol. 54, pp. 257-268, 2008.

[73] A. Skrzypczak, P. Siohan, and J. P. Javaudin, "Analysis of the Peak-To-Average Power Ratio for OFDM/OQAM," in *Signal Processing Advances in Wireless Communications, 2006. SPAWC '06. IEEE 7th Workshop on*, 2006, pp. 1-5.

[74] A. Skrzypczak, J. P. Javaudin, and P. Siohan, "Overlapped Selective Mapping for Pulse-Shaped Multi-Carrier Modulations," in *Vehicular Technology Conference, 2006. VTC-2006 Fall. 2006 IEEE 64th*, 2006, pp. 1-5.

[75] A. Skrzypczak, J. P. Javaudin, and P. Siohan, "Reduction of the Peak-to-Average Power Ratio for the OFDM/OQAM Modulation," in *Vehicular Technology Conference, 2006. VTC 2006-Spring. IEEE 63rd*, 2006, pp. 2018-2022.

[76] R. van Nee and A. de Wild, "Reducing the peak-to-average power ratio of OFDM," in *Vehicular Technology Conference, 1998. VTC 98. 48th IEEE*, 1998, pp. 2072-2076 vol.3.

[77] V. Ahirwar and S. Rajan, "Tradeoff between PAPR reduction and decoding complexity in transformed OFDM systems," in *Information Theory, 2005. ISIT 2005. Proceedings. International Symposium on*, 2005, pp. 1256-1260.

[78] C. Tellambura, "Upper bound on peak factor of N-multiple carriers," *Electronics Letters*, vol. 33, pp. 1608-1609, 1997.

[79] H. Ochiai and H. Imai, "Performance of the deliberate clipping with adaptive symbol selection for strictly band-limited OFDM systems," *Selected Areas in Communications, IEEE Journal on*, vol. 18, pp. 2270-2277, 2000.

[80] L. Xiaodong and L. J. Cimini, Jr., "Effects of clipping and filtering on the performance of OFDM," *Communications Letters, IEEE*, vol. 2, pp. 131-133, 1998.

[81] A. E. Jones and T. A. Wilkinson, "Combined coding for error control and increased robustness to system nonlinearities in OFDM," in *Vehicular Technology Conference, 1996. 'Mobile Technology for the Human Race'., IEEE 46th*, 1996, pp. 904-908 vol.2.

[82] S. H. Muller and J. B. Huber, "OFDM with reduced peak-to-average power ratio by optimum combination of partial transmit sequences," *Electronics Letters*, vol. 33, pp. 368-369, 1997.

[83] H. Nikookar and K. S. Lidsheim, "Random phase updating algorithm for OFDM transmission with low PAPR," *Broadcasting, IEEE Transactions on*, vol. 48, pp. 123-128, 2002.

[84] R. W. Bauml, R. F. H. Fischer, and J. B. Huber, "Reducing the peak-to-average power ratio of multicarrier modulation by selected mapping," *Electronics Letters*, vol. 32, pp. 2056-2057, 1996.

[85] R. J. Baxley and G. T. Zhou, "Comparing Selected Mapping and Partial Transmit Sequence for PAR Reduction," *Broadcasting, IEEE Transactions on*, vol. 53, pp. 797-803, 2007.

[86] P. Banelli, G. Baruffa, and S. Cacopardi, "Effects of HPA nonlinearity on frequency multiplexed OFDM signals," *Broadcasting, IEEE Transactions on*, vol. 47, pp. 123-136, 2001.

[87] C. A. R. Fernandes, J. C. M. Mota, and G. Favier, "Analysis and Power Diversity-Based Cancellation of Nonlinear Distortions in OFDM Systems," *Signal Processing, IEEE Transactions on*, vol. 60, pp. 3520-3531, 2012.

[88] J. P. Javaudin, D. Lacroix, and A. Rouxel, "Pilot-aided channel estimation for OFDM/OQAM," in *Vehicular Technology Conference, 2003. VTC 2003-Spring. The 57th IEEE Semiannual*, 2003, pp. 1581-1585 vol.3.

[89] K. SeungWon, H. Joo, and C. KyungHi, "Robust Channel Estimation Scheme to the Intrinsic Interference of IOTA Function in OFDM/OQAM-IOTA System," in *Vehicular Technology Conference, 2006. VTC-2006 Fall. 2006 IEEE 64th*, 2006, pp. 1-5.

[90] C. Lélé, J. P. Javaudin, R. Legouable, A. Skrzypczak, and P. Siohan, "Channel estimation methods for preamble-based OFDM/OQAM modulations," *European Transactions on Telecommunications*, vol. 19, pp. 741-750, 2008.

[91] C. Lele, P. Siohan, and R. Legouable, "2 dB Better Than CP-OFDM with OFDM/OQAM for Preamble-Based Channel Estimation," in *Communications, 2008. ICC '08. IEEE International Conference on*, 2008, pp. 1302-1306.

[92] C. Lele, R. Legouable, and P. Siohan, "Channel estimation with scattered pilots in OFDM/OQAM," in *Signal Processing Advances in Wireless Communications, 2008. SPAWC 2008. IEEE 9th Workshop on*, 2008, pp. 286-290.

[93] D. Jinfeng and S. Signell, "Novel Preamble-Based Channel Estimation for OFDM/OQAM Systems," in *Communications, 2009. ICC '09. IEEE International Conference on*, 2009, pp. 1-6.

[94] S. Hu, G. Wu, and S. Li, "Preamble Design and Iterative Channel Estimation for OFDM/Offset QAM System," *Journal of Networks*, vol. 4, pp. 1050-1057, December 2009.

[95] C. Lele, R. Legouable, and P. Siohan, "Iterative scattered pilot channel estimation in OFDM/OQAM," in *Signal Processing Advances in Wireless Communications, 2009. SPAWC '09. IEEE 10th Workshop on*, 2009, pp. 176-180.

[96] H. Su, W. Gang, Y. Gang, L. Shaoqian, and G. Bo, "Effectiveness of Preamble Based Channel Estimation for OFDM/OQAM System," in *Networks Security, Wireless Communications and Trusted Computing, 2009. NSWCTC '09. International Conference on*, 2009, pp. 34-37.

[97] L. Hao and P. Siohan, "Robust channel estimation for OFDM/OQAM," *Communications Letters, IEEE*, vol. 13, pp. 724-726, 2009.

[98] P. K. Remvik and N. Holte, "Carrier frequency offset robustness for OFDM systems with different pulse shaping filters," in *Global Telecommunications Conference, 1997. GLOBECOM '97., IEEE*, 1997, pp. 11-15 vol.1.

[99] P. K. Remvik, N. Holte, and A. Vahlin, "Fading and carrier frequency offset robustness for different pulse shaping filters in OFDM," in *Vehicular Technology Conference, 1998. VTC 98. 48th IEEE*, 1998, pp. 777-781 vol.2.

[100] H. Bölcskei, "Blind estimation of symbol timing and carrier frequency offset in wireless OFDM systems," *IEEE Transactions on Communications*, vol. 49, pp. 988-999, June 2001.

[101] P. Ciblat and E. Serpedin, "A fine blind frequency offset estimator for OFDM/OQAM systems," *Signal Processing, IEEE Transactions on*, vol. 52, pp. 291-296, 2004.

[102] L. Gang, L. Lundheim, and N. Holte, "New Methods for Blind Fine Estimation of Carrier Frequency Offset in OFDM/OQAM Systems," in *Signal Processing Advances in Wireless Communications, 2006. SPAWC '06. IEEE 7th Workshop on*, 2006, pp. 1-5.

[103] L. Gang, L. Lundheim, and N. Holte, "Blind Carrier Frequency Offset Estimation for OFDM/OQAM Systems Based on Subchannel Signals," in *Global Telecommunications Conference, 2006. GLOBECOM '06. IEEE*, 2006, pp. 1-6.

[104] T. Fusco and M. Tanda, "Blind Cfo Estimation for OFDM/OQAM Systems," in *Acoustics, Speech and Signal Processing, 2006. ICASSP 2006 Proceedings. 2006 IEEE International Conference on*, 2006, pp. IV-IV.

[105] T. Fusco and M. Tanda, "Blind Frequency-Offset Estimation for OFDM/OQAM Systems," *Signal Processing, IEEE Transactions on,* vol. 55, pp. 1828-1838, 2007.

[106] T. Fusco, A. Petrella, and M. Tanda, "Blind carrier-frequency offset estimation for pulse shaping OFDM/OQAM systems," in *Communications, Control and Signal Processing, 2008. ISCCSP 2008. 3rd International Symposium on*, 2008, pp. 942-947.

[107] T. Fusco, A. Petrella, and M. Tanda, "Joint symbol timing and CFO estimation in multiuser OFDM/OQAM systems," in *Signal Processing Advances in Wireless Communications, 2009. SPAWC '09. IEEE 10th Workshop on*, 2009, pp. 613-617.

[108] T. Fusco, A. Petrella, and M. Tanda, "Data-aided symbol timing and CFO synchronization for filter bank multicarrier systems," *Wireless Communications, IEEE Transactions on*, vol. 8, pp. 2705-2715, 2009.

[109] T. Fusco, A. Petrella, and M. Tanda, "Joint Symbol Timing and CFO Estimation for OFDM/OQAM Systems in Multipath Channels," *EURASIP Journal on Advances in Signal Processing*, p. 11, 2010.

[110] Y. Gang, C. Hao, H. Su, W. Gang, and L. Shaoqian, "Data-aided joint symbol timing and CFO estimation for OFDM/OQAM systems," in *Information, Communications and Signal Processing (ICICS) 2011 8th International Conference on*, 2011, pp. 1-5.

[111] T. H. Stitz, A. Viholainen, T. Ihalainen, and M. Renfors, "CFO estimation and correction in a WiMAX-like FBMC system," in *Signal Processing Advances in Wireless Communications, 2009. SPAWC '09. IEEE 10th Workshop on*, 2009, pp. 633-637.

[112] T. Stitz, T. Ihalainen, A. Viholainen, and M. Renfors, "Pilot-Based Synchronization and Equalization in Filter Bank Multicarrier Communications," *EURASIP Journal on Advances in Signal Processing*, vol. 2010, 2010.

[113] IEEE, "Part 16: Air Interface for Broadband Wireless Access Systems, Amendment 3: Advanced Air Interface," in *IEEE Std 802.16m™-2011(Amendment to IEEE Std 802.16™-2009)* ed. New York: The Institute of Electrical and Electronics Engineers, Inc., 2011.

[114] Y. Xiao, *WiMAX/MobileFi Advanced Research and Technology*. New York Auerbach Publications, 2008.

[115] Y. Zhang and H.-H. Chen, *MOBILE WiMAX: Toward Broadband Wireless Metropolitan Area Networks*. New York: Auerbach Publications, 2008.

[116] H. S. Sourck, W. Yan, J. Bergmans, S. Sadri, and B. Farhang-Boroujeny, "Effect of Carrier Frequency Offset on Offset QAM Multicarrier Filter Bank Systems over Frequency-Selective Channels," in *Wireless Communications and Networking Conference (WCNC), 2010 IEEE*, 2010, pp. 1-6.

[117] H. Saeedi-Sourck, S. Sadri, and B. Farhang-Boroujeny, "Sensitivity analysis of the multiuser offset QAM multicarrier systems to carrier frequency and timing offsets," in *Telecommunications (IST), 2010 5th International Symposium on*, 2010, pp. 48-52.

[118] H. Saeedi-Sourck, W. Yan, J. W. M. Bergmans, S. Sadri, and B. Farhang-Boroujeny, "Complexity and Performance Comparison of Filter Bank Multicarrier and OFDM in Uplink of Multicarrier Multiple Access Networks," *Signal Processing, IEEE Transactions on*, vol. 59, pp. 1907-1912, 2011.

[119] M. Morelli, C. C. J. Kuo, and M. O. Pun, "Synchronization Techniques for Orthogonal Frequency Division Multiple Access (OFDMA): A Tutorial Review," *Proceedings of the IEEE*, vol. 95, pp. 1394-1427, 2007.

[120] P. H. Moose, "A technique for orthogonal frequency division multiplexing frequency offset correction," *Communications, IEEE Transactions on*, vol. 42, pp. 2908-2914, 1994.